BIOFIZYKA DOŚWIADCZALNA

III semestr studiów II stopnia

Zastosowania fizyki w biologii i medycynie
specjalność: Biofizyka molekularna

i

Fizyka doświadczalna
specjalność: Biofizyka

(*60 godz.; wykłady 1 – 15*)

www.biogeo.uw.edu.pl/Biofizyka_doswiadczalna

2. PLAN WYKŁADU - ZAGADNIENIA

1. Biofizyka i jej miejsce w badaniach z zakresu fizyki i nauk biomedycznych; kluczowe zagadnienia współczesnej BIOFIZYKI MOLEKULARNEJ *(**1 wykład**)*
2. **Struktura chemiczna**, metabolizm i biologiczna rola biopolimerów: kwasy nukleinowe DNA i RNA, białka, lipidy i polisacharydy (*przegląd i uzupełnienie wiadomości*; ***3 wykłady***)
3. **Oddziaływania elektrostatyczne** i **hydrofobowe** stabilizujące struktury makrocząsteczek i kompleksów molekularnych; rola rozpuszczalnika *(**1 wykład**)*
4. Przegląd zaawansowanych TECHNIK badania struktur i dynamiki biopolimerów i ich kompleksów z **rozdzielczością atomową**, techniki **mikroskopowe;** manipulacja **pojedynczymi** cząsteczkami *(**1 wykład**)*
5. GENOMIKA i **sekwencjonowanie DNA**; budowa chromosomu, **mutageneza**, **kancerogeneza** i systemy naprawcze **nano**struktury DNA *(**3 wykłady**)*
6. PROTEOMIKA: zastosowanie spektrometrii mas (MS); **przestrzenne struktury** białek: dyfrakcja rentgenowska i magnetyczny rezonans jądrowy NMR, **dynamika** ruchów molekularnych, interactom *(**6 wykładów**)*
7. ZWIJANIE BIAŁEK (*PROTEIN FOLDING*): **mechanizmy zwijania** *in vitro* i *i n vivo:* badania doświadczalne i teoretyczne, „błędne" zwijanie i agregacja (formy amyloidalne) *(**3 wykłady**)*
8. **Struktury przestrzenne** i zwijanie **RNA**; TRANSKRYPTOMIKA: mikromacierze, profile ekspresji, biosensory (***2 wykłady**)*
9. **Kompleksy** biomolekularne: kinetyka i **dynamika** asocjacji *(**1 wykład**)*
10. SPECYFICZNE ODDZIAŁYWANIA biopolimerów: w kompleksach: białko - ligand; białko - DNA i białko - RNA; projektowanie leków (*DRUG DESIGN*); struktury subkomórkowe - **motory molekularne** *(**2 wykłady**)*
11. BŁON Y BIOLOGICZNE i PROCESY BIOENERGETYCZNE w komórce: transfer elektronów i protonów *(**2 wykłady**)*
12. Biopolimery w „żywej komórce" (*in vivo* NMR, in cell NMR) *(**1 wykład**)*
13. **Obrazowanie NMR** w DIAGNOSTYCE MEDYCZNEJ (*MRI* i *fMRI*); porównanie z tomografią komputerową (*X-ray CT*) i pozytonową (*PET*) *(**1 wykład**)*
14. „Niekonwencjonalne" wykorzystanie polimerów biologicznych *(**1 wykład**)*

LITERATURA

1. W. Saenger „Principles of nucleic acid structures"
2. T.E. Creighton „Proteins. Structures and molecular properties"
3. I.N. Serdyuk, N.R. Zaccai i J. Zaccai „Methods in Molecular Biophysics"
4. Aktualne odnośniki literaturowe (***podawane na wykładzie***)

3. WHAT IS BIOPHYSICS ?

Biophysics exploits the methods of physics, chemistry, biology, mathematics, and (bio)informatics to investigate biological objects

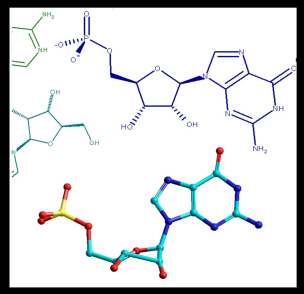
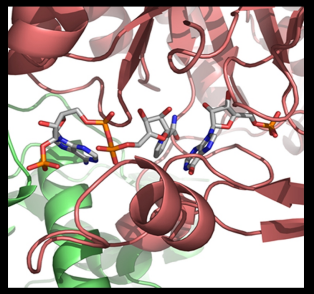
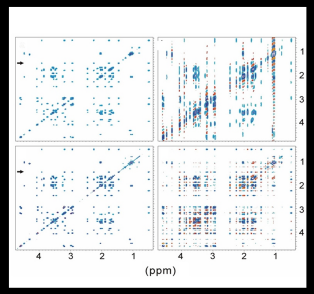


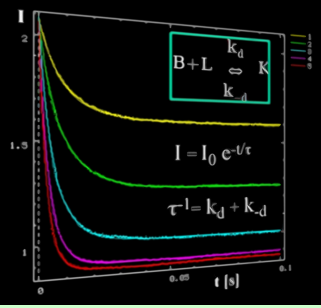



4. Molecular biophysics deals with structure, dynamics and interactions of biological macromolecules:

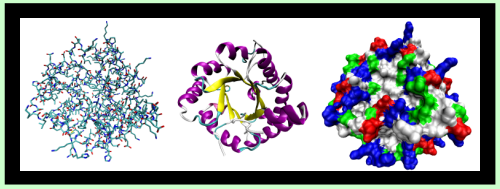

proteins

nucleic acids DNA

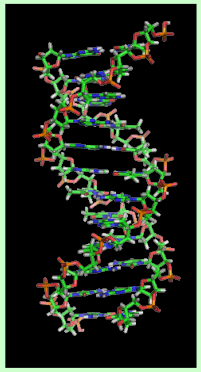

and RNA

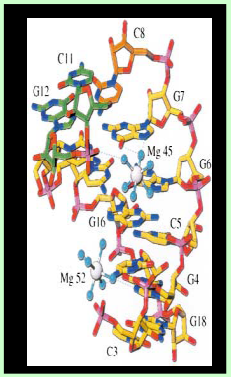

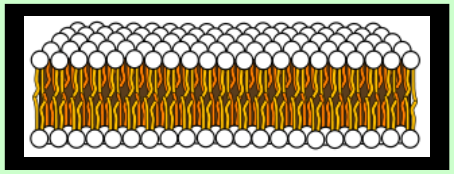

lipids

polysaccharides

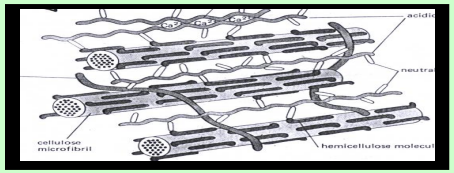

molecular complexes

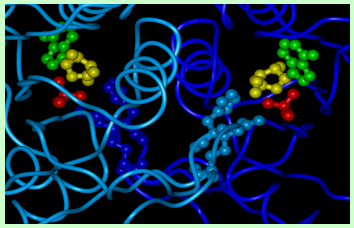

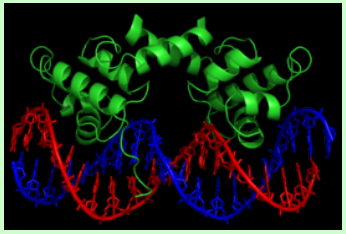



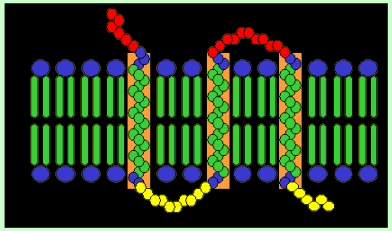

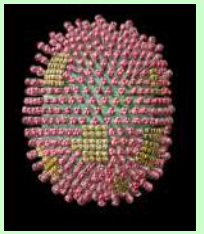

5. BIOPOLYMERS - NUCLEIC ACIDS, PROTEINS, LIPIDS

Genome:
all genes in the chromosomes

Transkryptome:
all RNAs transcribed in the cell

Proteome:
all proteins in the cell

Genomics
DNA sequencing and gene identification

Transcryptomics
expression level and profiles

Proteomics
whole proteome characteristics

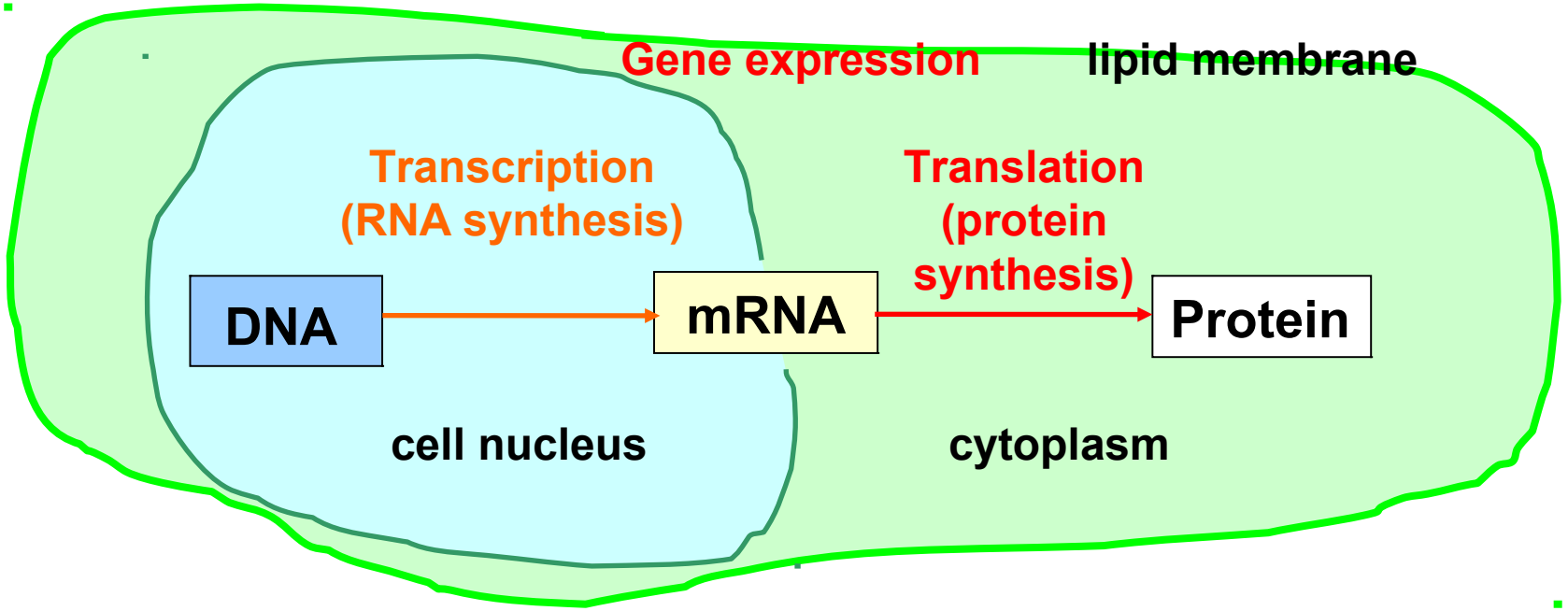

Metabolome: **all biochemical processes;** ***Metabolomics***

6. KEY PROBLEMS OF CONTEMPORARY MOLECULAR BIOPHYSICS

Spatial structures of biopolymers and their complexes: X-ray diffraction, nuclear magnetic resonance NMR, molecular modelling, STRUCTURAL PROTEOMICS: biopolymers in cell metabolism - molecular mechanisms, DRUG DESIGN

PROTEIN and RNA FOLDING: structure prediction and determination of the mechanisms (folding pathways); misfolding (amyloid fibryls, prions)

Electron and proton transfer in cell ENERGETICS (photosynthesis)

Probing and imaging of SINGLE BIOMOLECULES and their complexes, single molecule spectroscopy (SMS), atomic force microscopy (AFM), electron microscopy (cryoEM), optical and magnetic tweezers

„NANO" systems: from molecular motors to microarrays

Noninvasive imaging of tissues in MEDICAL DIAGNOSTICS: magnetic resonance imaging (MRI), computer tomography (X-ray CT), positron emission tomography (PET); living cell metabolism (fMRI, *in vivo* NMR, in cell NMR)

7. DNA STRUCTURE; COMPLEMENTARY BASE PAIRING

L. Stryer Biochemistry Freeman & Co. 1988

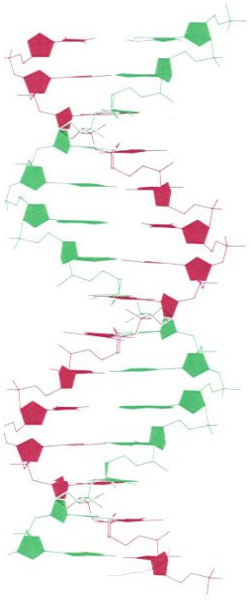

Figure 4-7
Skeletal model of double-helical DNA. The structure repeats at intervals of 34 Å, which corresponds to ten residues on each chain.

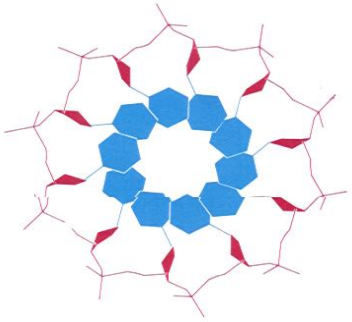

Figure 4-8
Diagram of one of the strands of a DNA double helix, viewed down the helix axis. The bases (all pyrimidines here) are inside, whereas the sugar-phosphate backbone is outside. The tenfold symmetry is evident. The bases are shown in blue and the sugars in red.

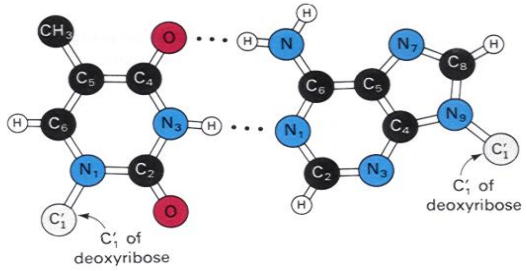

Figure 4-9
Model of an adenine-thymine base pair.

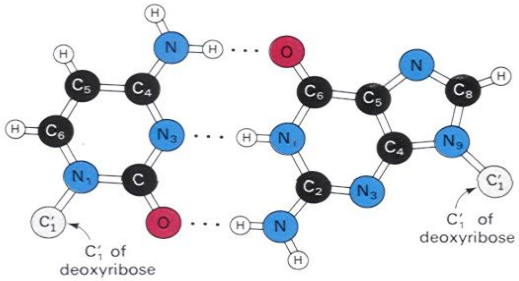

Figure 4-10
Model of a guanine-cytosine base pair.

DNA REPLICATION

L. Stryer Biochemistry Freeman & Co. 1988

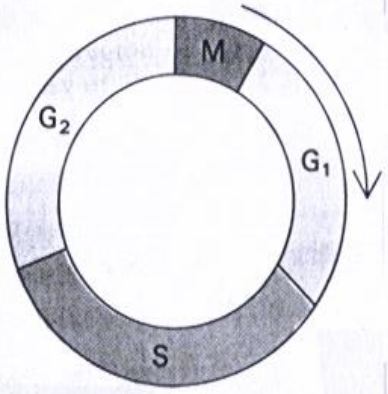

Phases in the life cycle of a eucaryotic cell: M (mitosis); G_1 (gap 1, prior to DNA synthesis); S (period of DNA synthesis); and G_2 (gap 2, between DNA synthesis and mitosis). The length of these periods depends on the cell type and conditions of growth. Mitosis is usually the shortest phase.

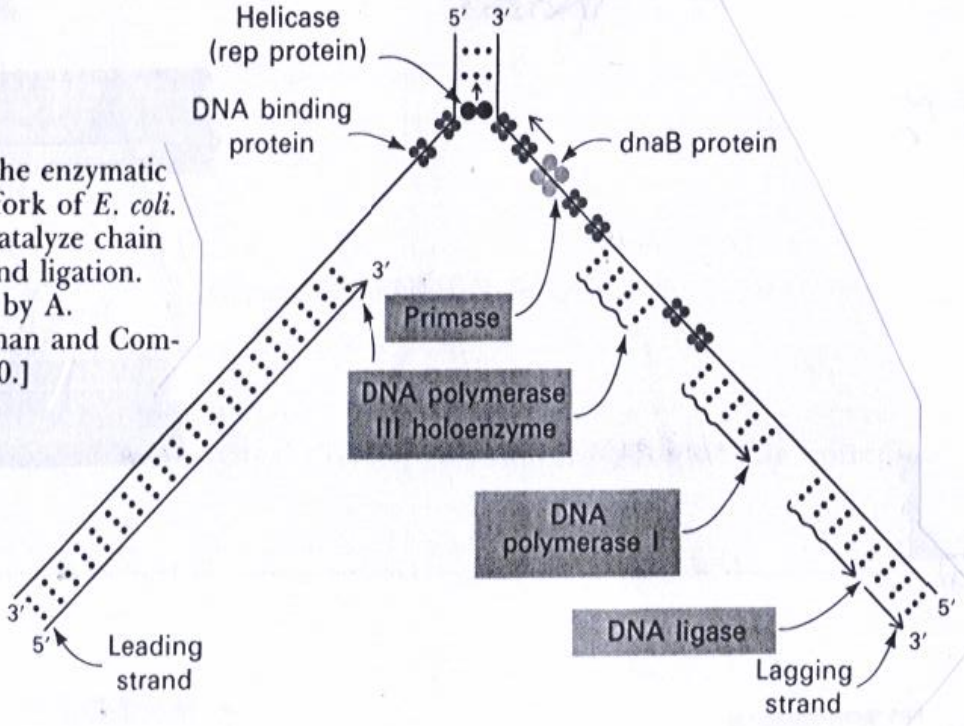

Schematic diagram of the enzymatic events at a replication fork of *E. coli*. Enzymes shaded blue catalyze chain initiation, elongation, and ligation. [After *DNA Replication*, by A. Kornberg. W. H. Freeman and Company. Copyright © 1980.]

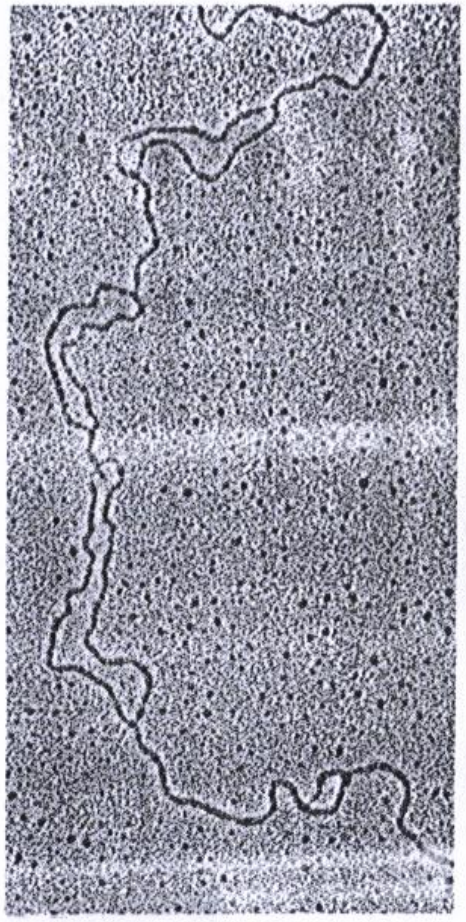

Electron micrograph of replicating chromosomal DNA from cleavage nuclei of *Drosophila*. The eye forms are the newly replicated regions. [Courtesy of Dr. David Hogness.]

9. POINT MUTATIONS

Topal & Fresco. Nature 263, 283, 1976

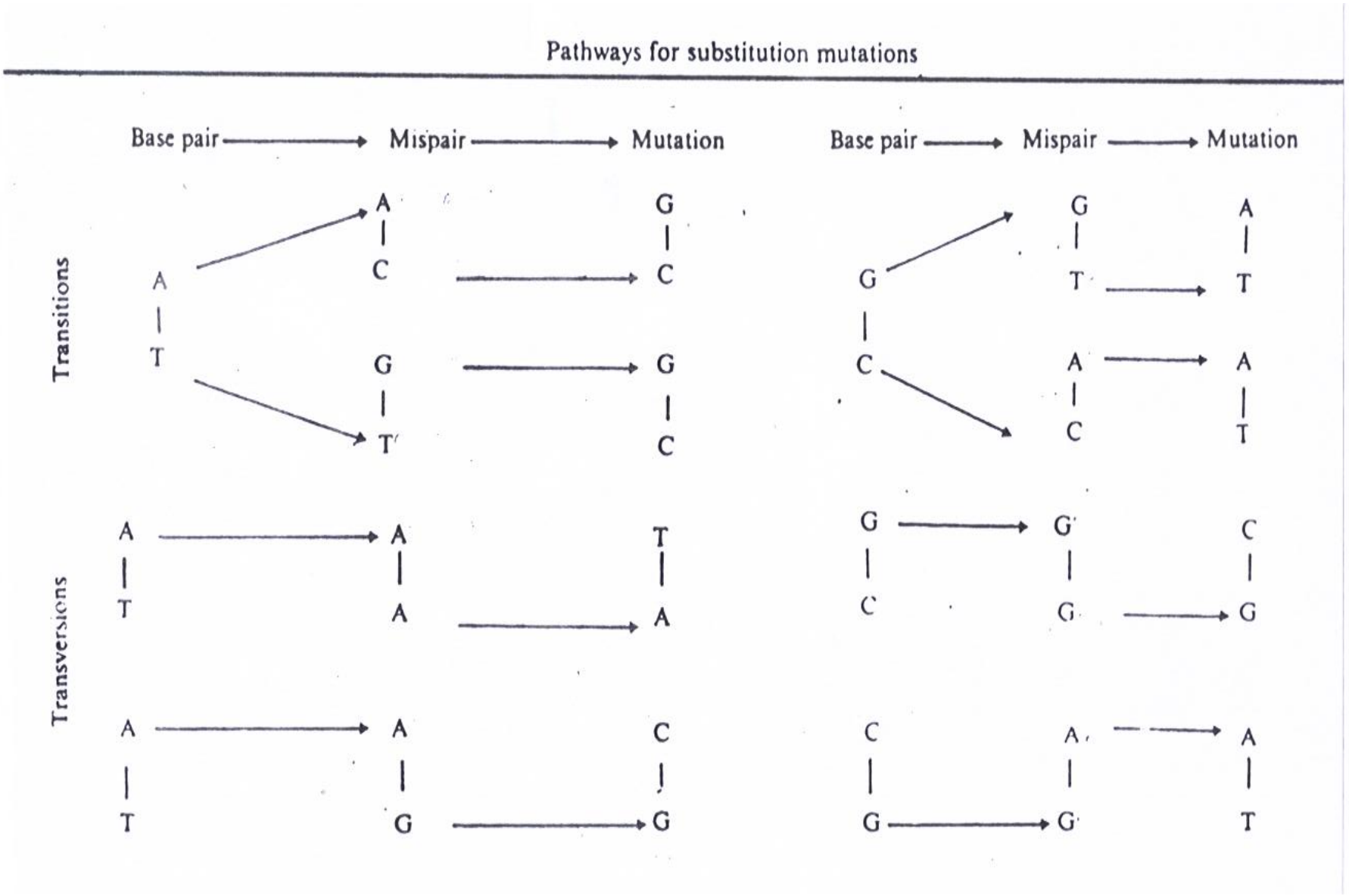

10. NUCLEOSIDE STRUCTURES, TAUTOMERISM AND PROTONATION/DISSOCIATION SITES

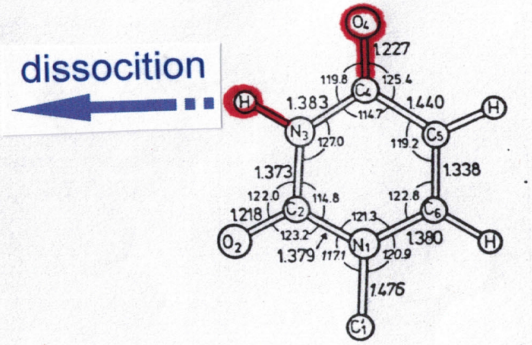

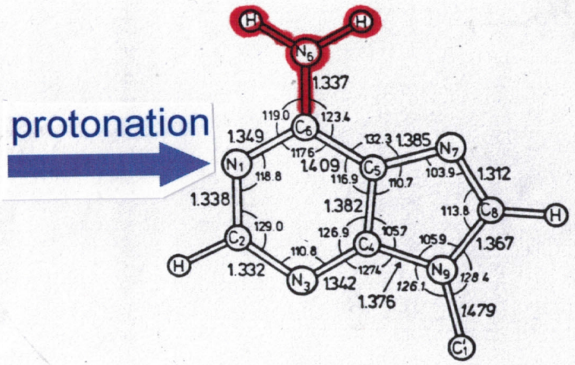

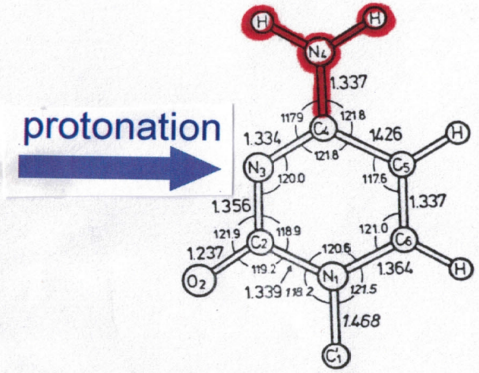

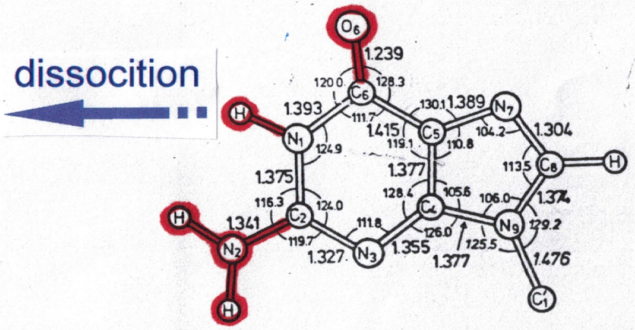

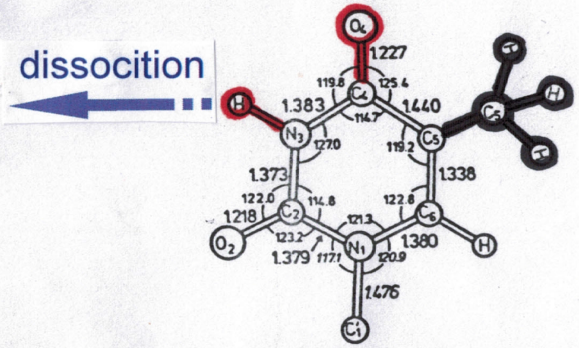

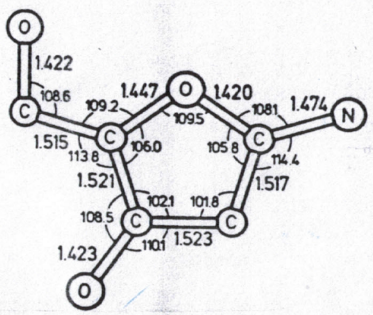

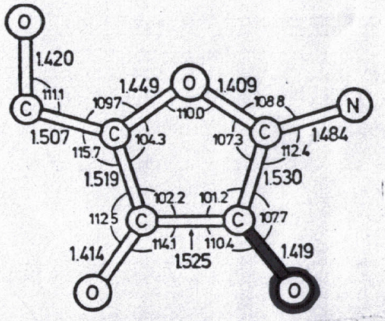

11. UV ABSORPTION OF NUCLEOTIDES

Sprecher & Johnson Jr. Biopolymers 16, 2243, 1977

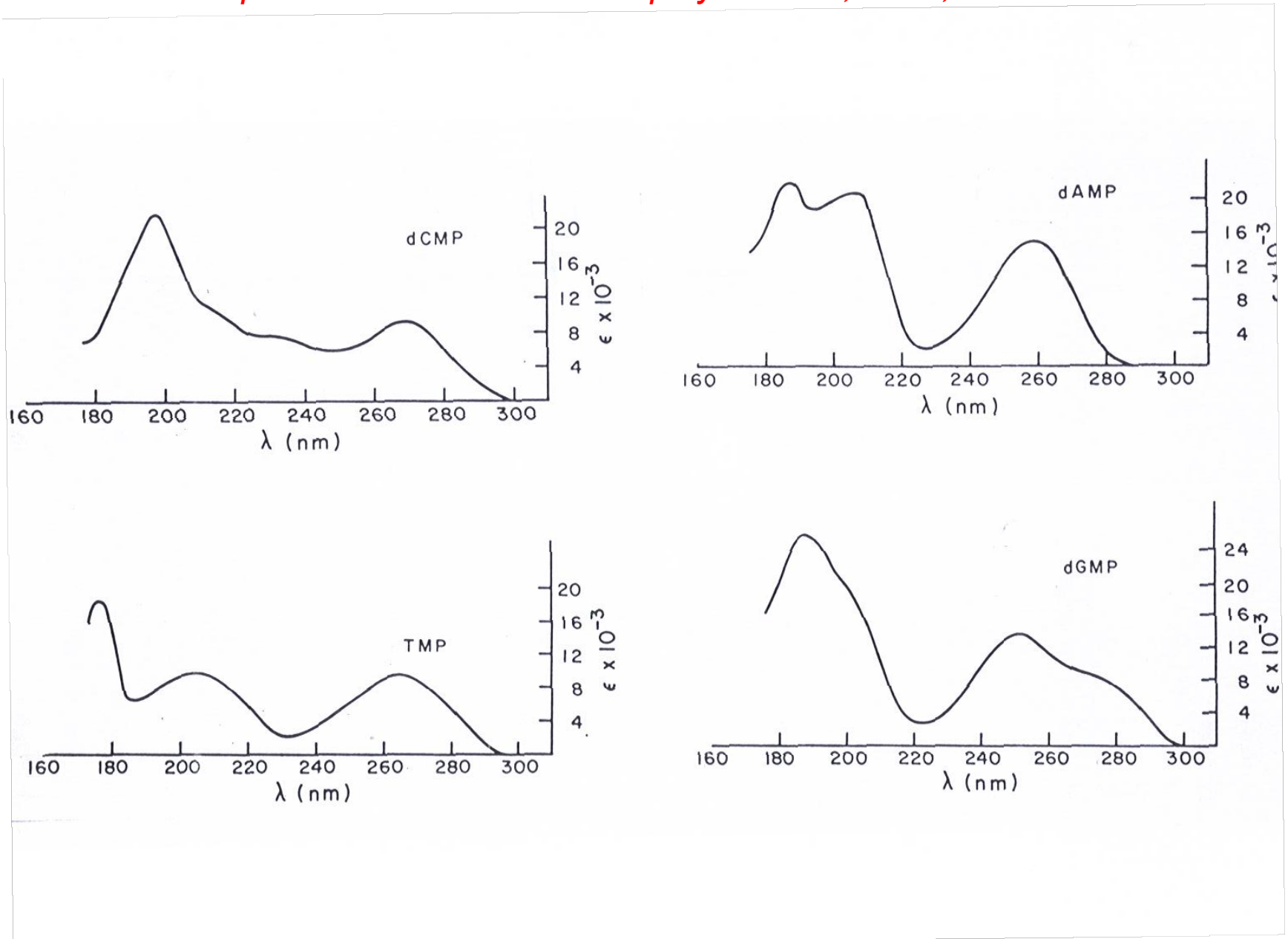

12. CONFORMATIONAL PARAMETERS OF THE POLYNUCLEOTIDE CHAIN AND THE BASE

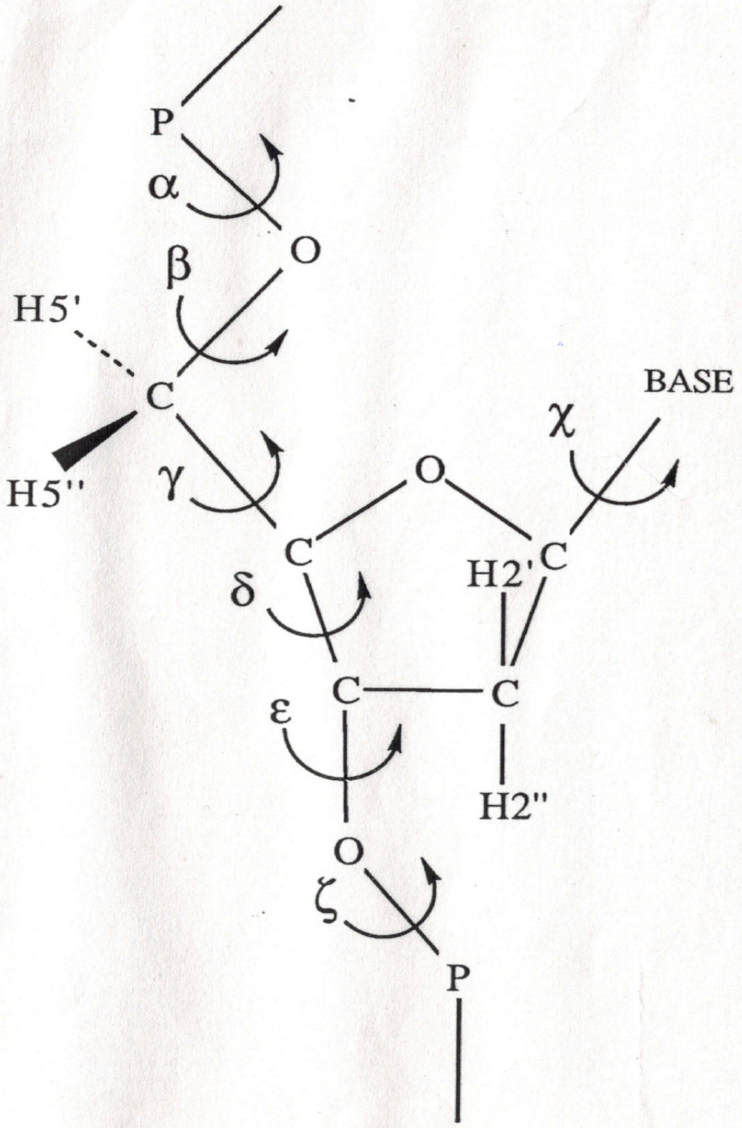

PURINE NUCLEOTIDES

χ: O4' – C1' – N9 – C4

PYRIMIDINE NUCLEOTIDES

χ: O4' – C1' – N1 – C2

13. PSEUDOROTATION CYCLE OF THE FURANOSE RING

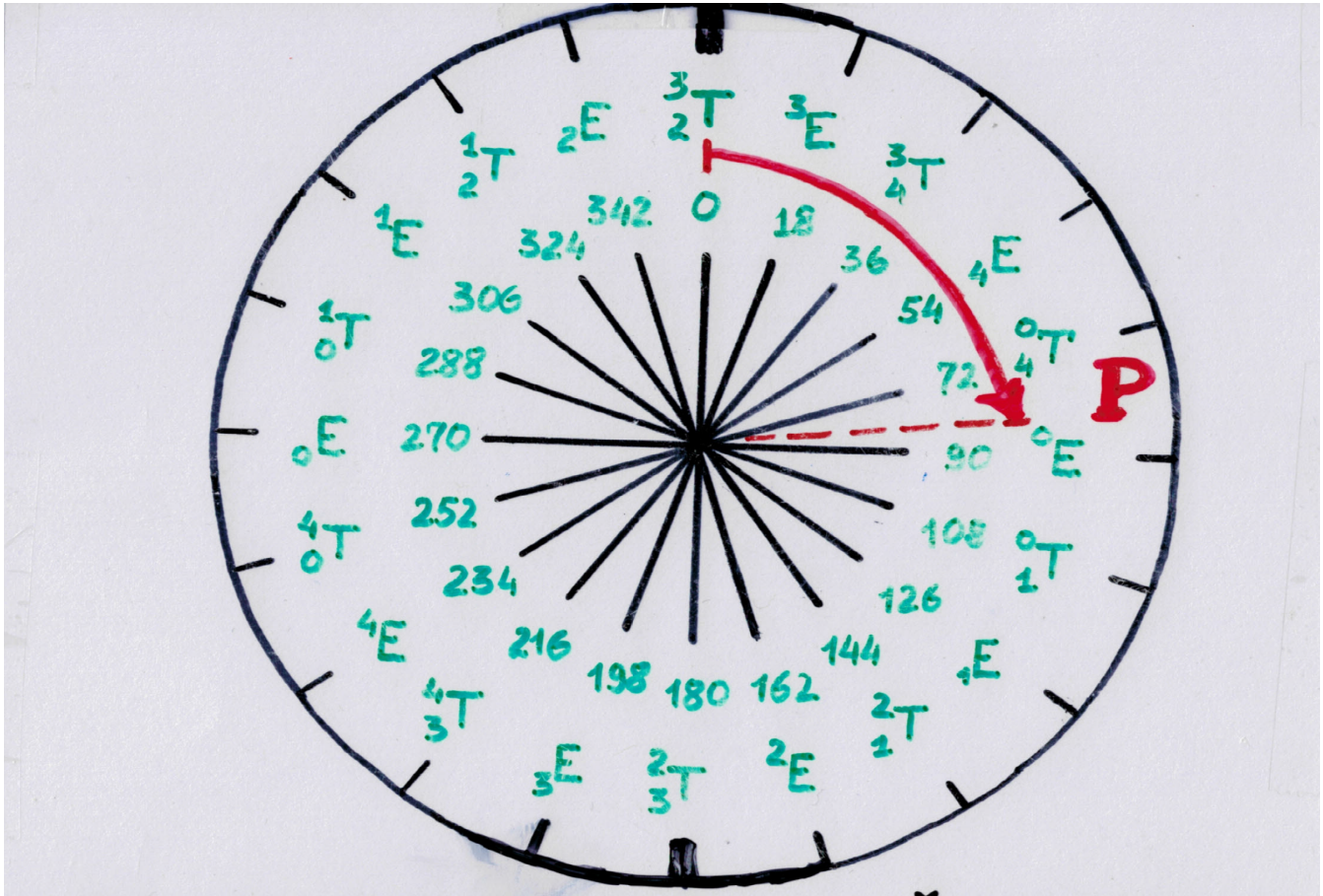

^{x}E C(x) endo or O endo

$_{x}^{}E$ C(x) exo or O exo

$^{x}_{y}T$ C(x) endo - C(y) exo

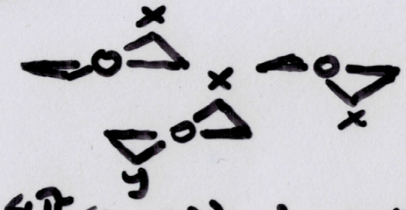

$$\nu_j = \nu_{max} \cos\left(P + \frac{4\pi}{5}(j-2)\right) \quad j=0,1,2,3,4$$

$$tgP = \frac{\nu_4 + \nu_1 - \nu_3 - \nu_0}{2\nu_2(\sin 36° + \sin 72°)}$$

$$\nu_{max} = \nu_0 / \cos P$$

$$\sum_{j=0}^{4} \nu_j = 0$$

14. CONFORMATIONS OF NUCLEOTIDES

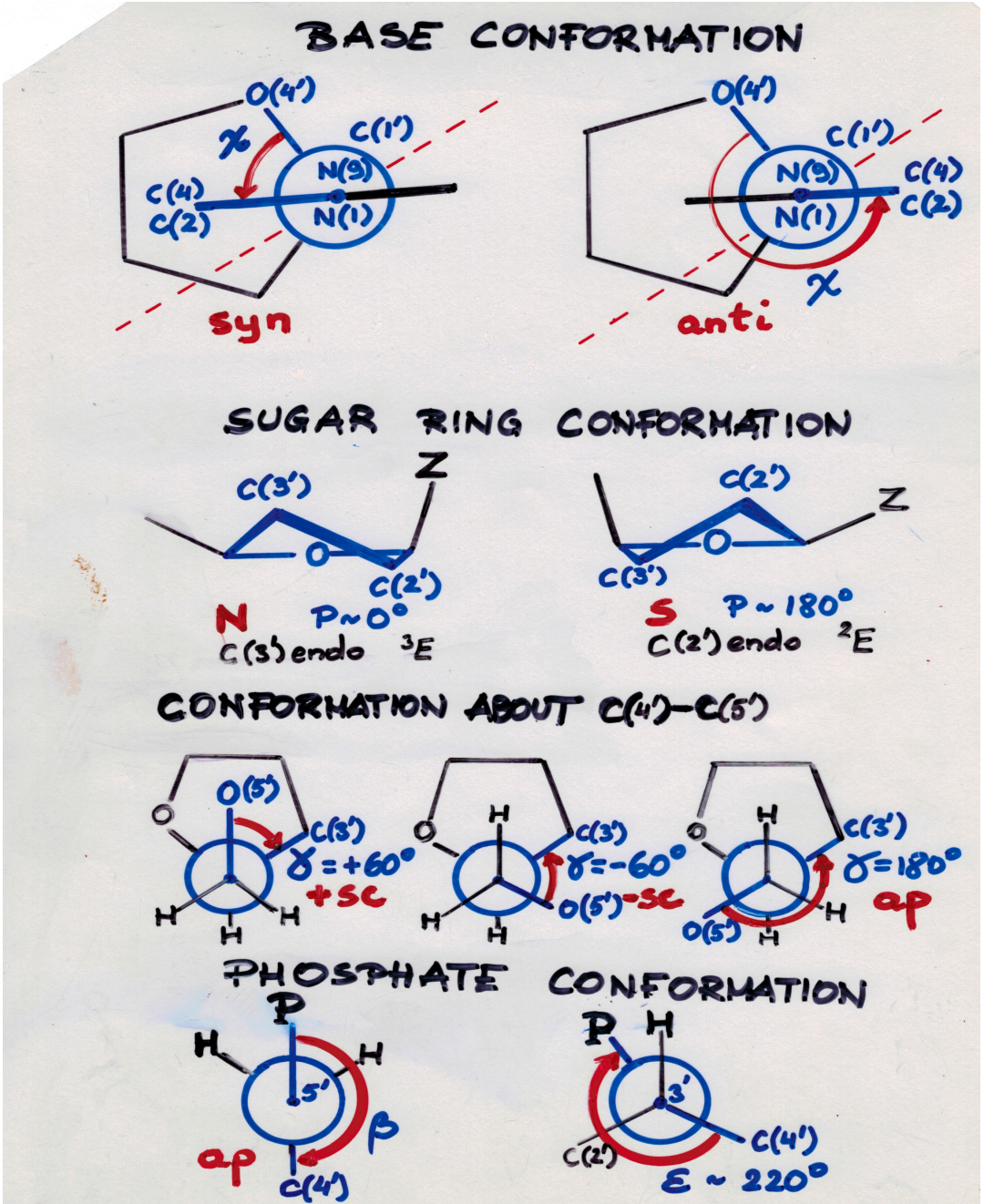

15. RIBONUCLEIC ACIDS RNA (*Tetrahymena* INTRON)

Batey et. al. Angew. Chem. Int. Ed. Engl. 38, 2326, 1999

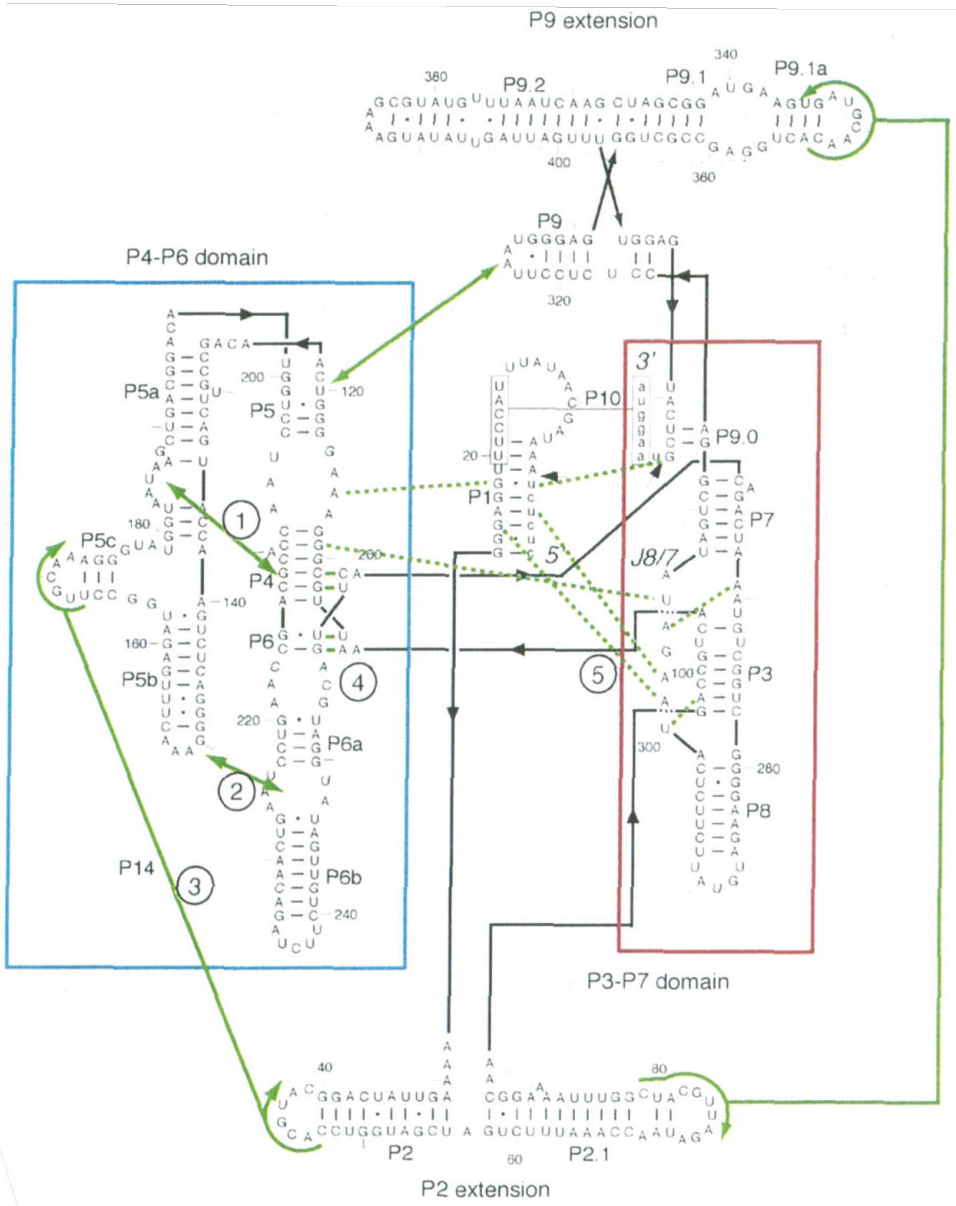

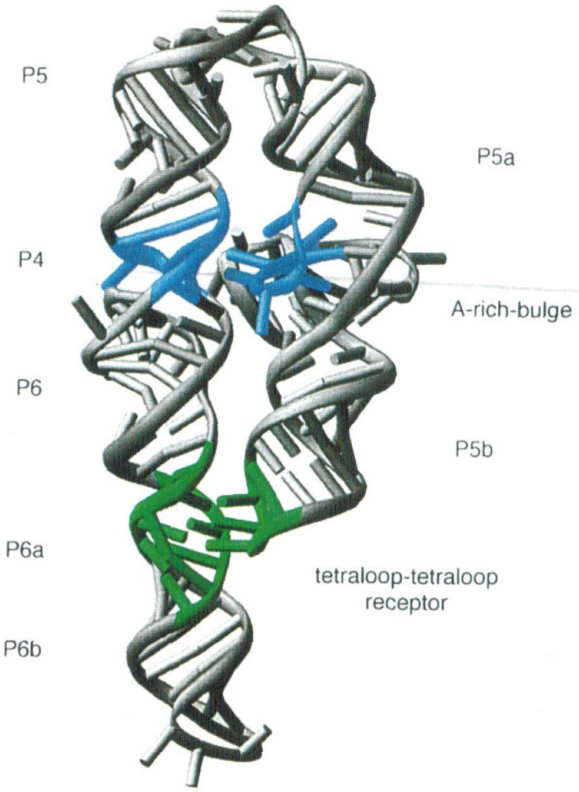

16. PSEUDOKNOT TERTIARY MOTIF (tRNA MIMICRY)

Bierley et al. Nature Rev. Microbiol. 5, 598, 2007

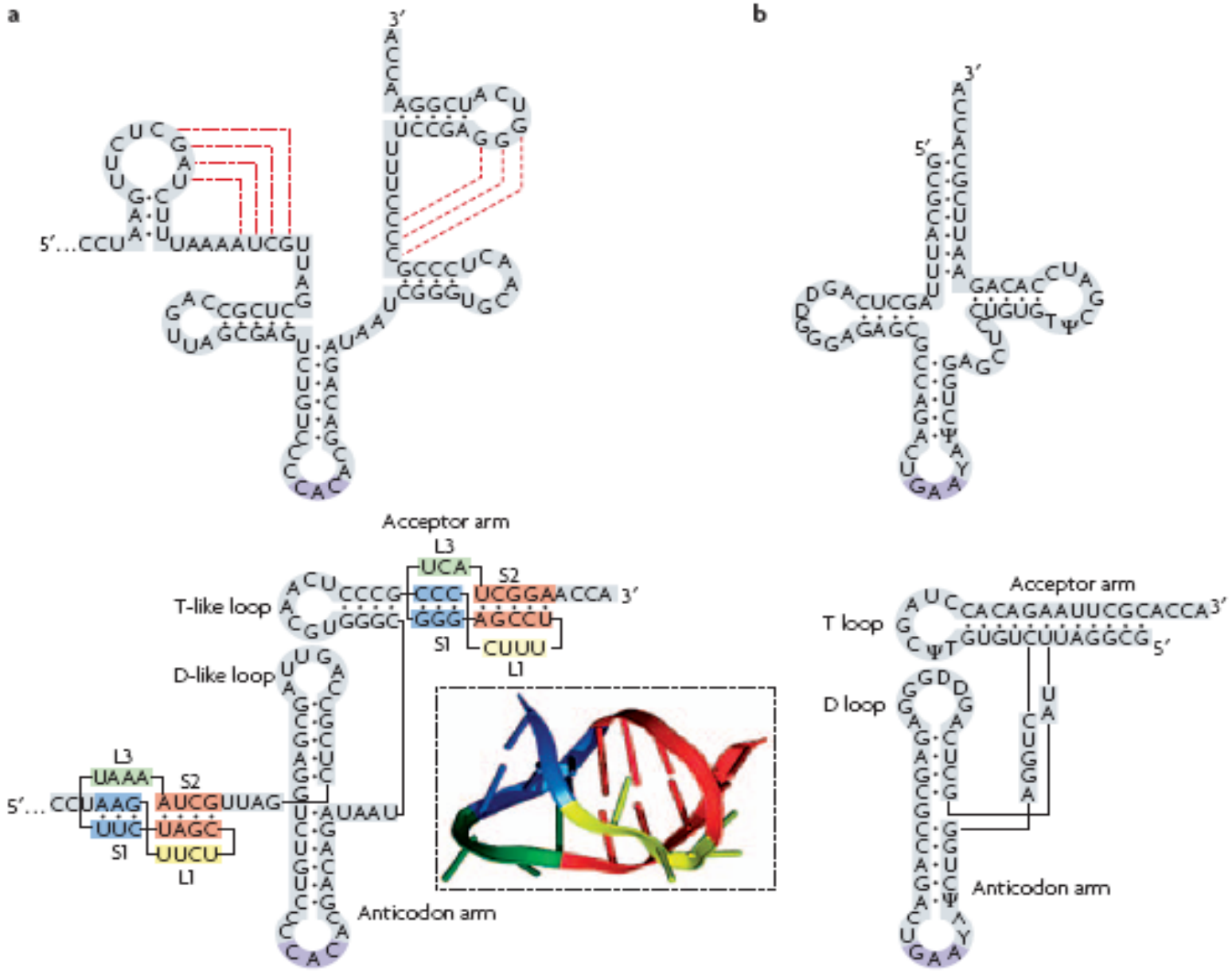

17. ACTIVE CHROMATIN STRUCTURE

Cockerill FEBS J. 278, 2182, 2011

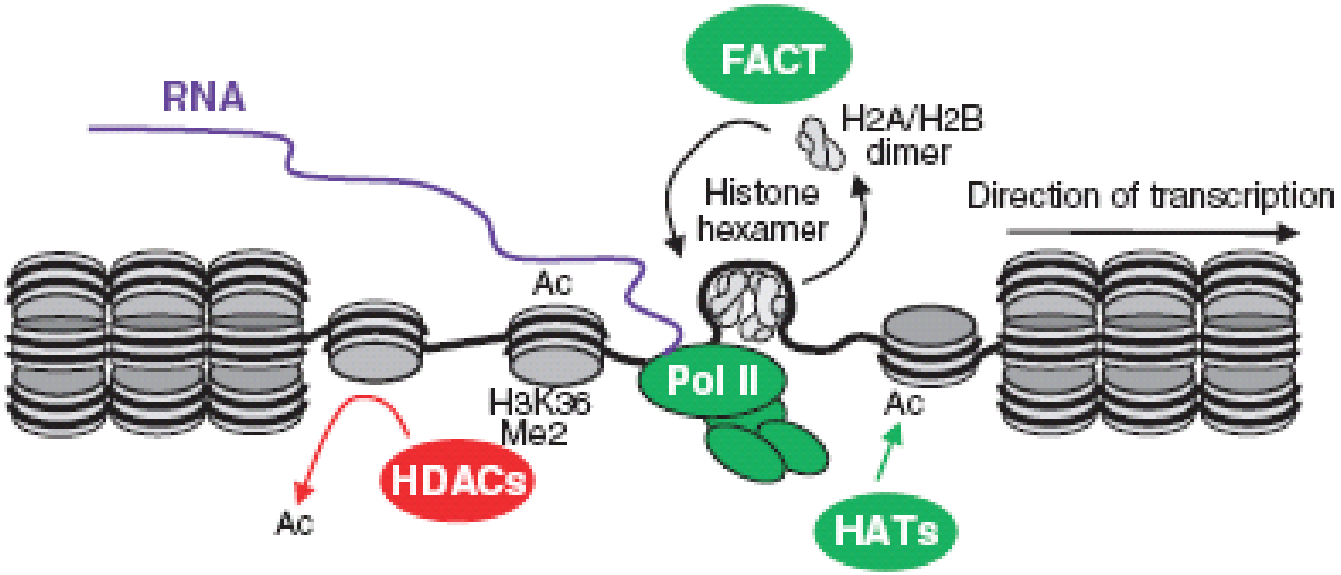

Fig. 5. Model of the chromatin structure in the vicinity of an elongating Pol II complex. Histone acetylation in advance of polymerases is likely to create an open chromatin structure. The advancing polymerase recruits FACT which partially disassembles the nucleosome, allowing Pol II to pass this barrier. Once Pol II has passed, HDACs such as Rpd3S can be recruited via dimethylated or trimethylated H3-K36 and act to return chromatin to the condensed state.

18. mRNA TRANSLATION

B. Alberts et al. Molecular Biology of the Cell Garland Publish. 1989

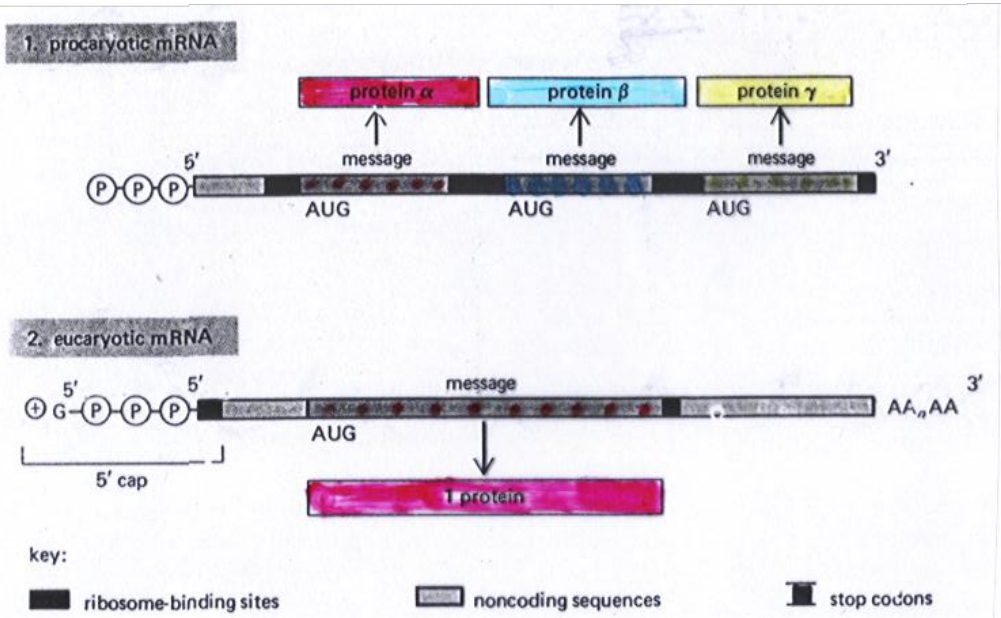

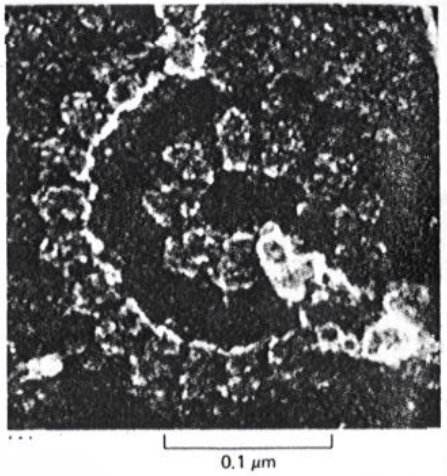

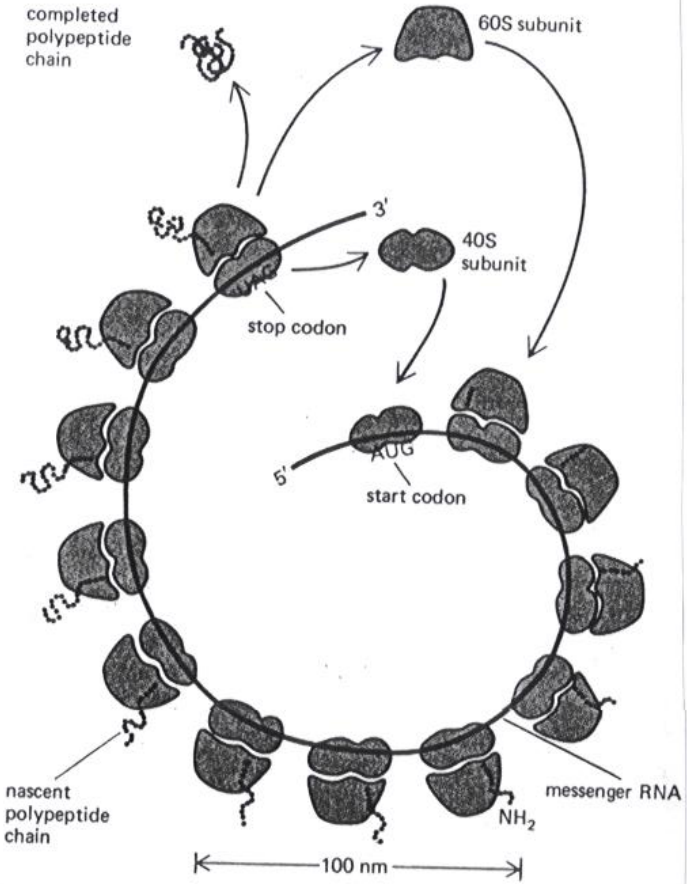

Schematic drawing of a polyribosome showing that a series of ribosomes simultaneously translates the same mRNA molecule.

19. GLOBULAR PROTEIN eIF4E

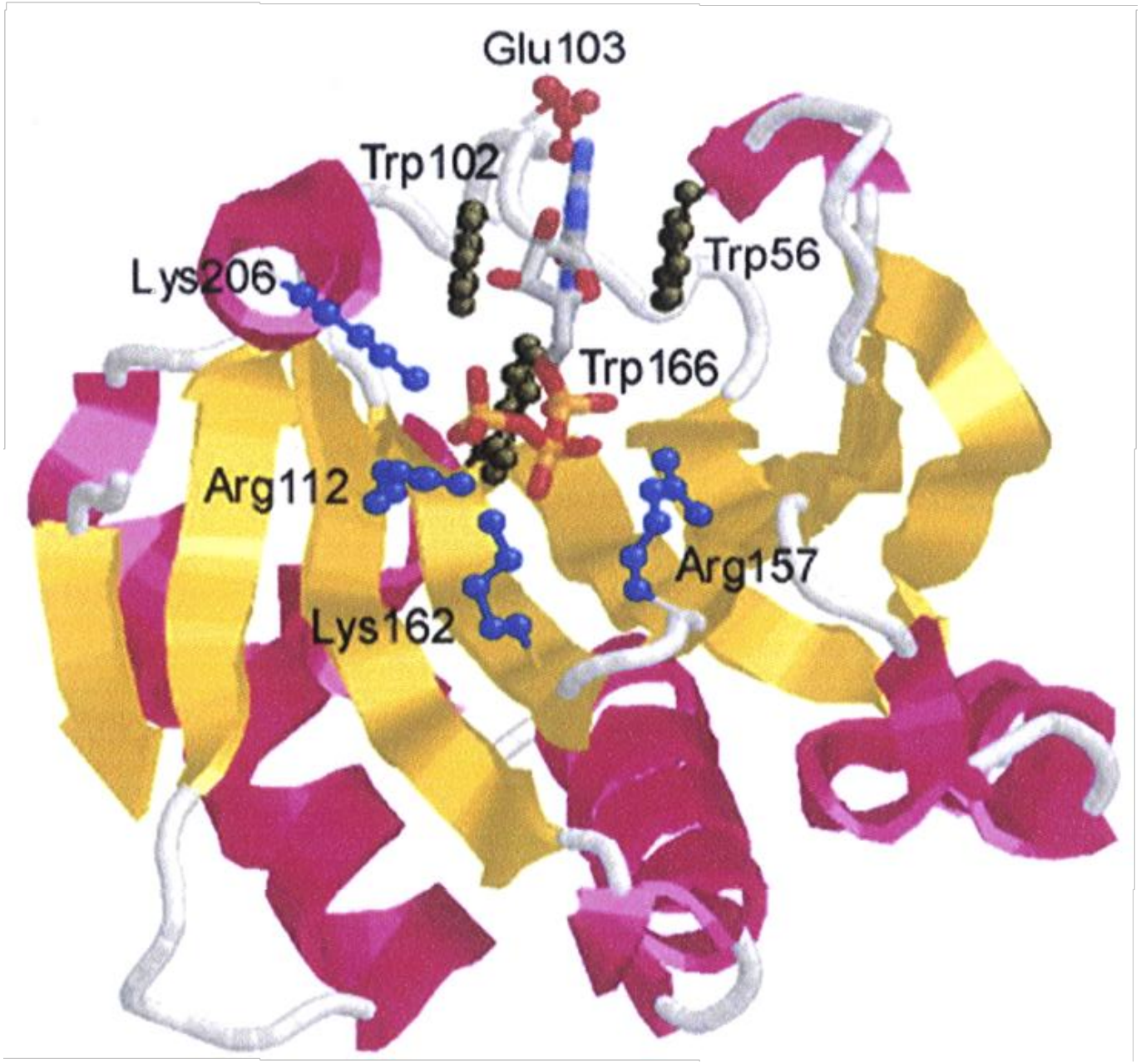

20. FIBROUS PROTEIN: COLLAGEN

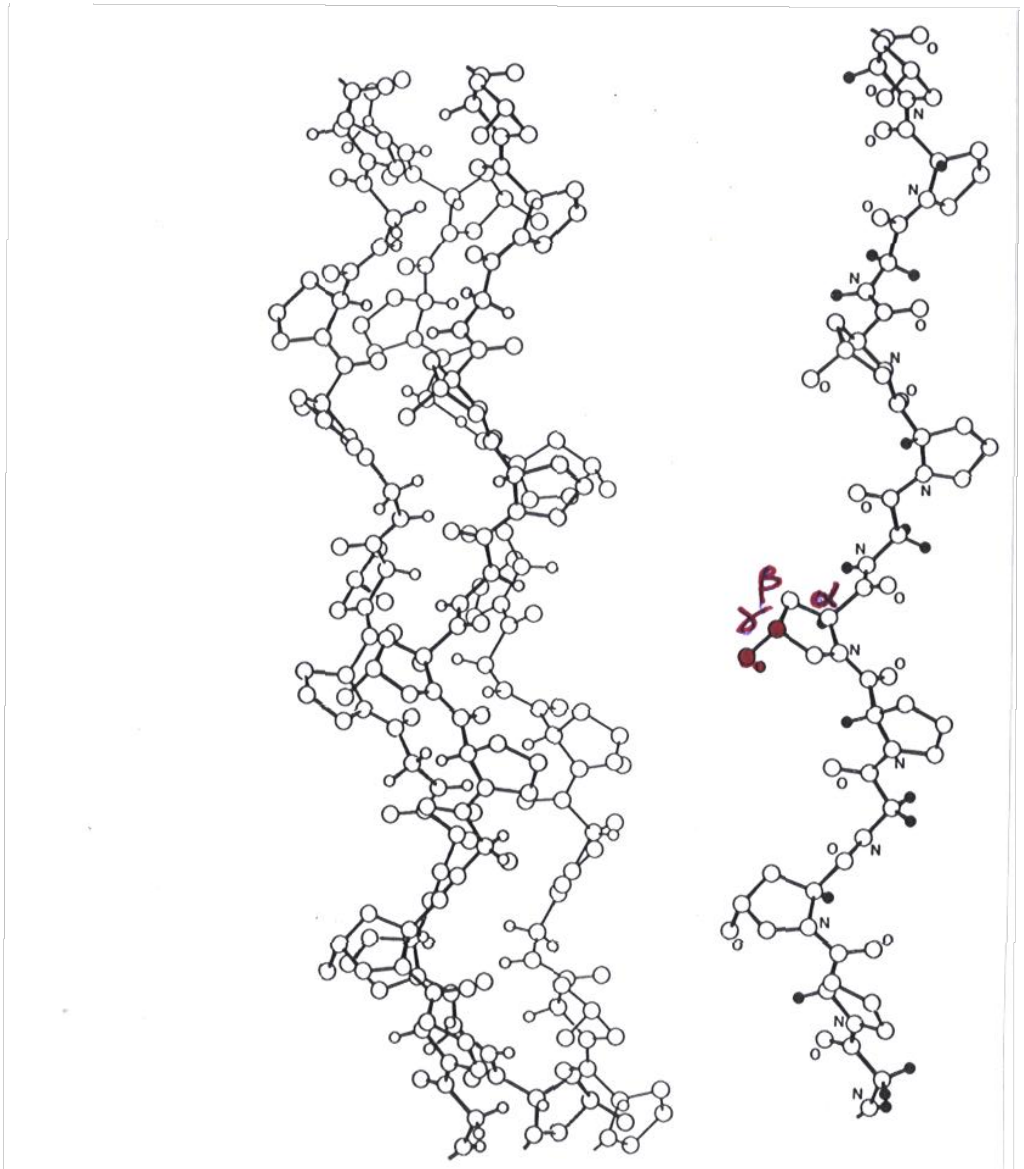

Model for the three-stranded collagen structure, represented as the repeating sequence -Gly-Pro-γOH Pro-. The three-stranded structure is on the *left*, a single strand on the *right*. (From R. D. B. Fraser et al., *J. Mol. Biol.* 129:463–481, 1979.)

21. MEMBRANE PROTEINS

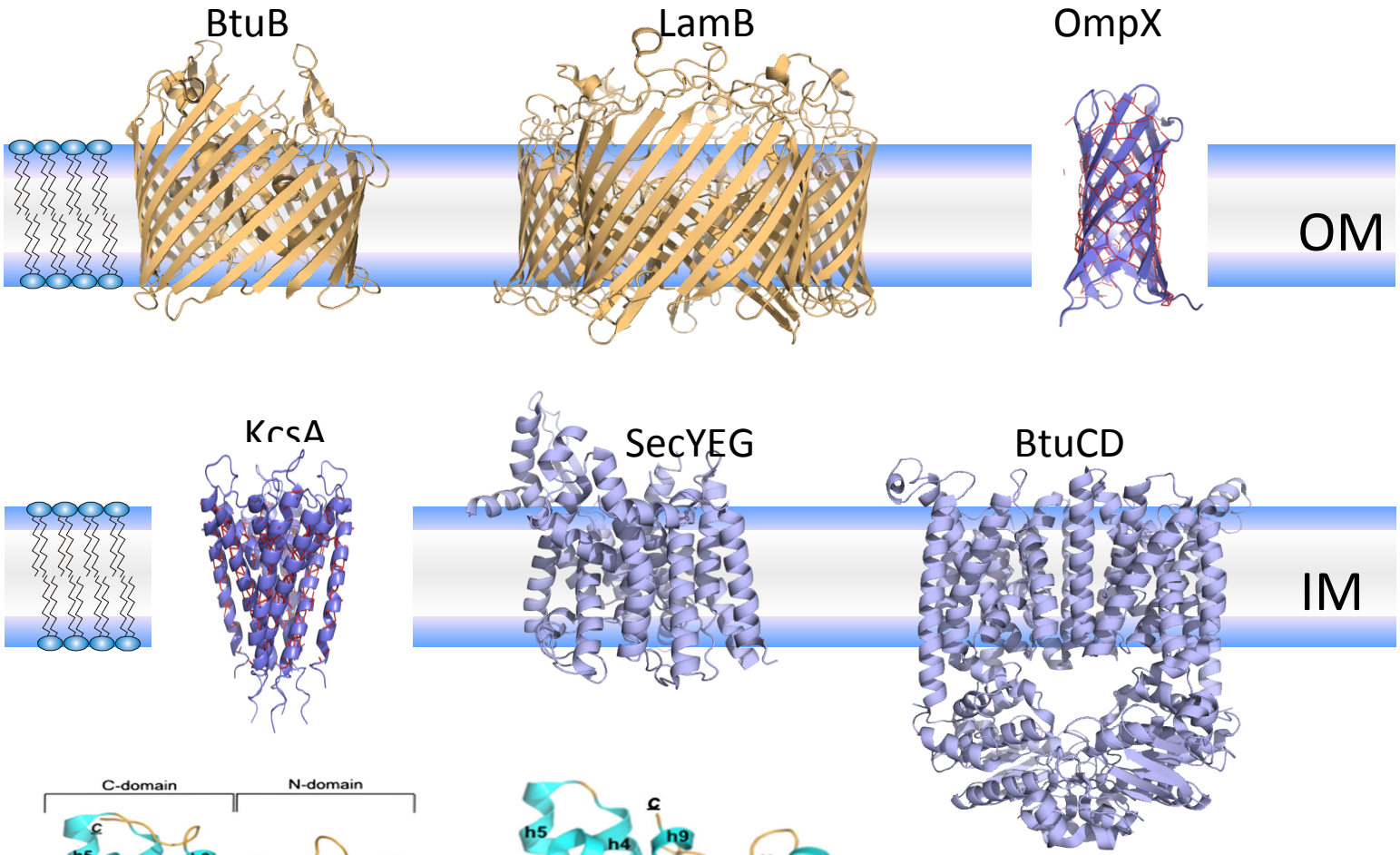

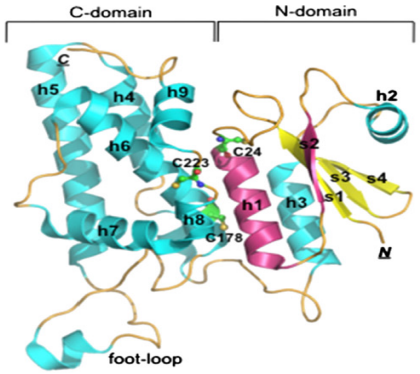

monomer (reduced)

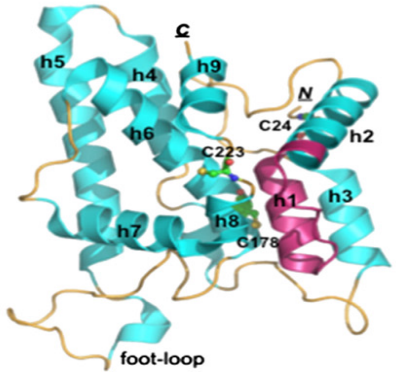

half-dimer (oxidised)

CLIC1

Jiang et al. Biochim. Biophys. Acta 1838, 643, 2014

22. CHEMICAL STRUCTURE OF α - AMINO ACID

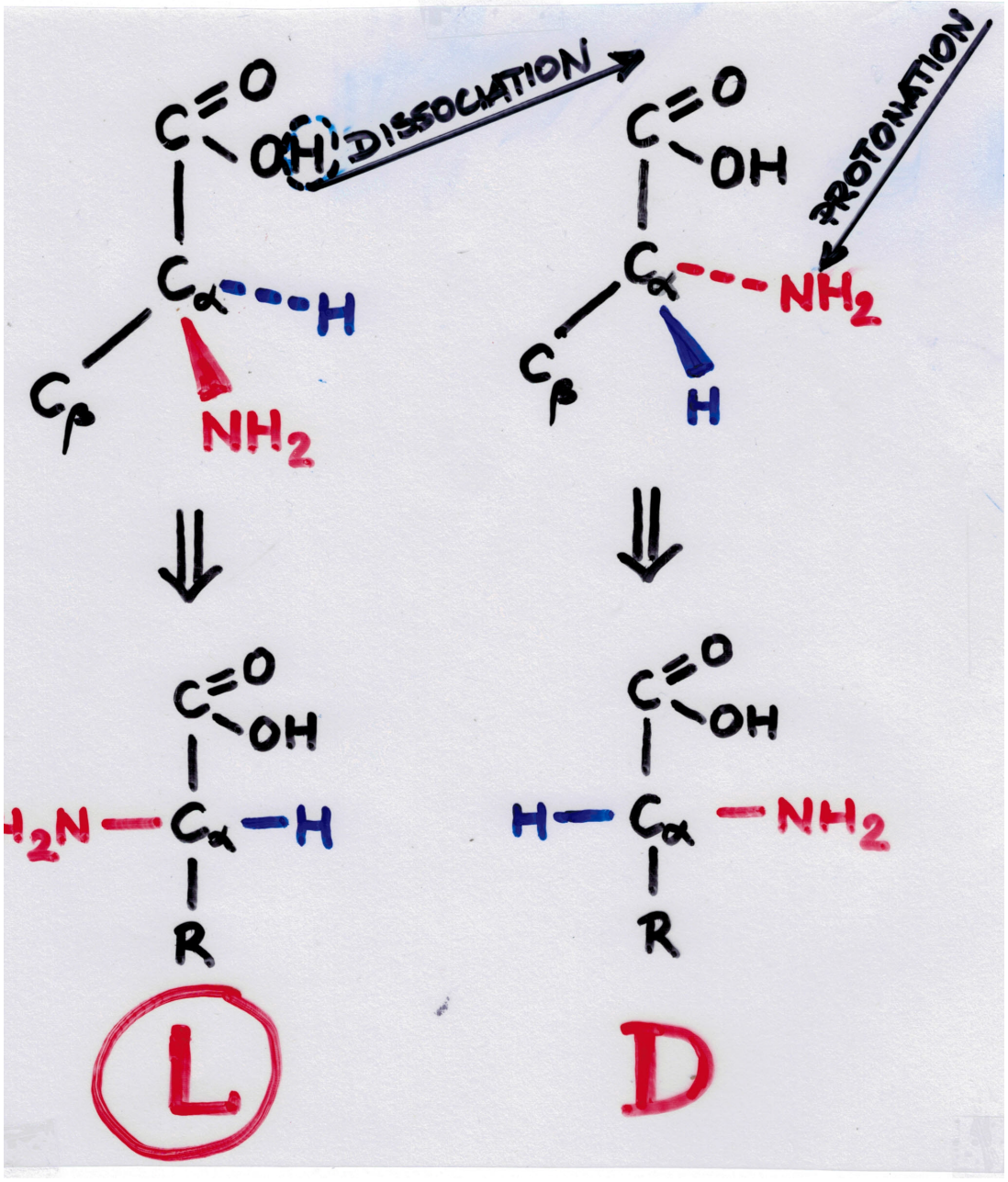

23. AMINO ACIDS

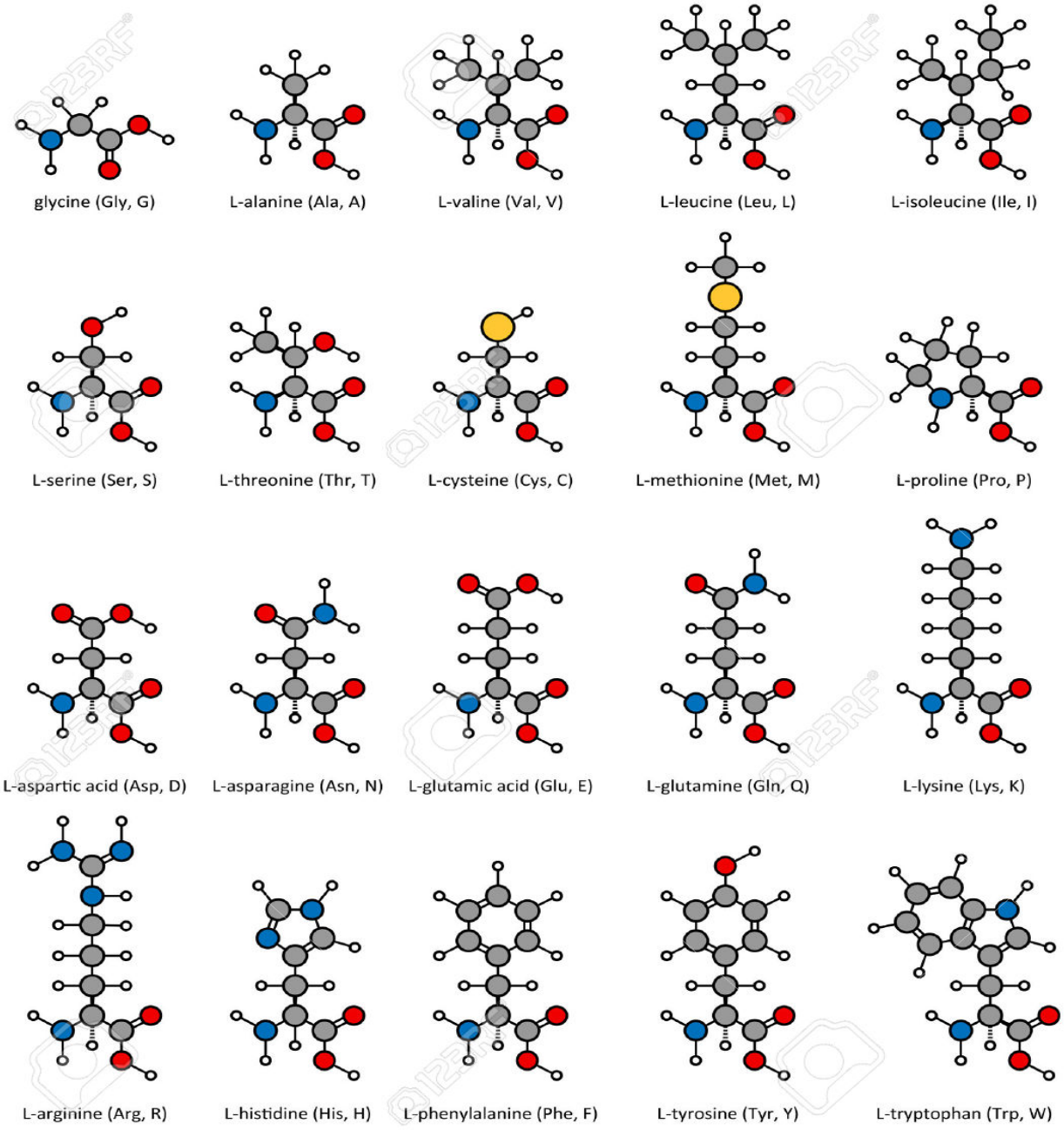

24. UV AND FLUORESCENCE SPECTRA OF AMINO ACIDS

T. Creighton Proteins Freeman & Co. 1993

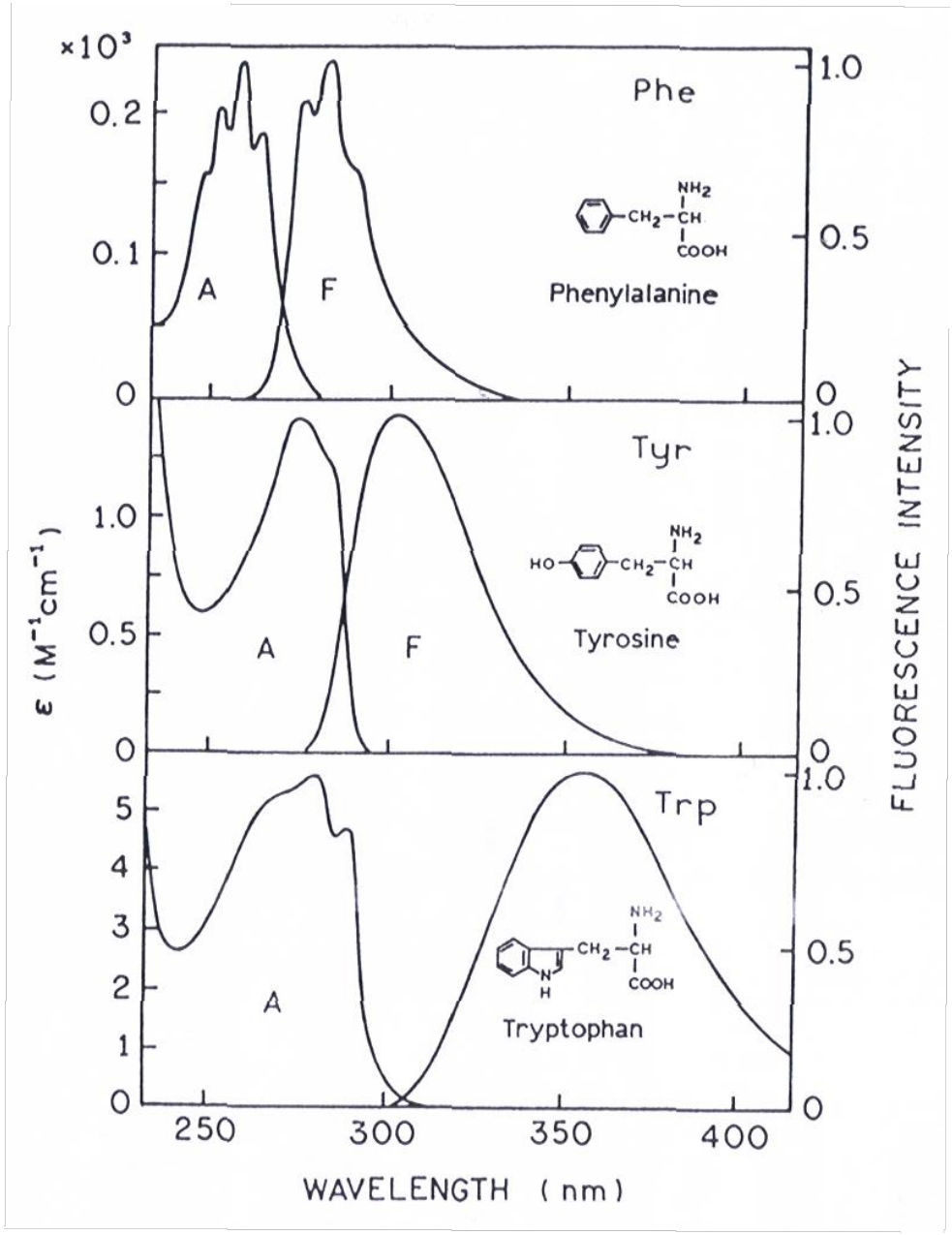

25. PEPTIDE BOND

T. Creighton Proteins Freeman & Co. 1993

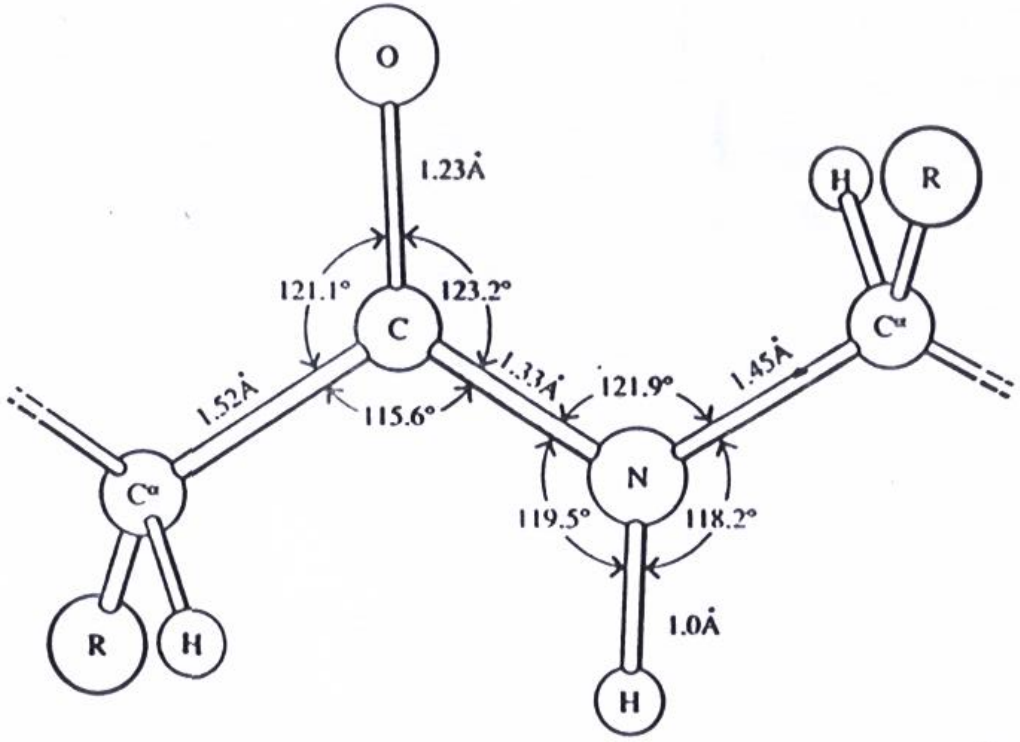

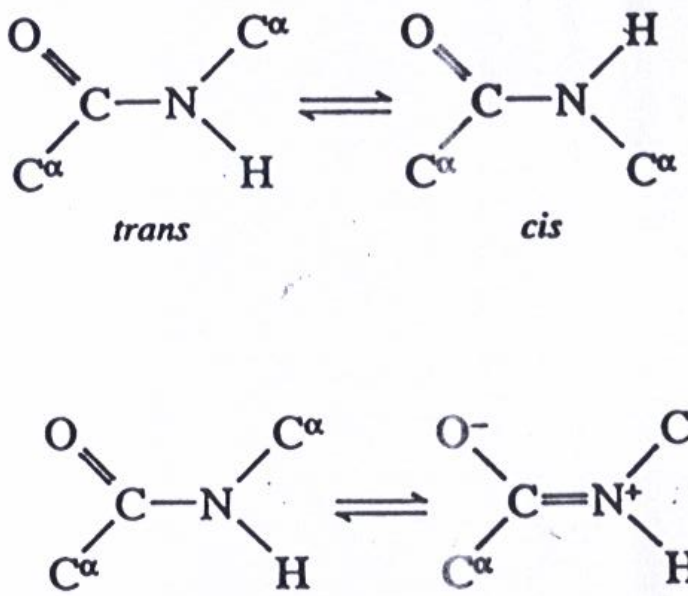

FIGURE 1.2

The geometry of the peptide backbone, with a *trans* peptide bond, showing all the atoms between two C^{α} atoms of adjacent residues. The peptide bond is stippled. The dimensions given are the averages observed crystallographically in amino acids and small peptides. (G. N. Ramachandran et al., *Biochim. Biophys. Acta* 359:298–302, 1974.)

26. GENETIC CODE

L. Stryer Biochemistry Freeman & Co. 1988

Amino Acids and Their Symbols			Codons					
A	Ala	Alanine	GCA	GCC	GCG	GCU		
C	Cys	Cysteine	UGC	UGU				
D	Asp	Aspartic acid	GAC	GAU				
E	Glu	Glutamic acid	GAA	GAG				
F	Phe	Phenylalanine	UUC	UUU				
G	Gly	Glycine	GGA	GGC	GGG	GGU		
H	His	Histidine	CAC	CAU				
I	Ile	Isoleucine	AUA	AUC	AUU			
K	Lys	Lysine	AAA	AAG				
L	Leu	Leucine	UUA	UUG	CUA	CUC	CUG	CUU
M	Met	Methionine	AUG					
N	Asn	Asparagine	AAC	AAU				
P	Pro	Proline	CCA	CCC	CCG	CCU		
Q	Gln	Glutamine	CAA	CAG				
R	Arg	Arginine	AGA	AGG	CGA	CGC	CGG	CGU
S	Ser	Serine	AGC	AGU	UCA	UCC	UCG	UCU
T	Thr	Threonine	ACA	ACC	ACG	ACU		
V	Val	Valine	GUA	GUC	GUG	GUU		
W	Trp	Tryptophan	UGG					
Y	Tyr	Tyrosine	UAC	UAU				

27. „NON-TYPICAL” AMINO ACIDS (*ARCHEA, EUBACTERIA*)

PYRROLYSINE (Pyl, O)
kodon: UAG

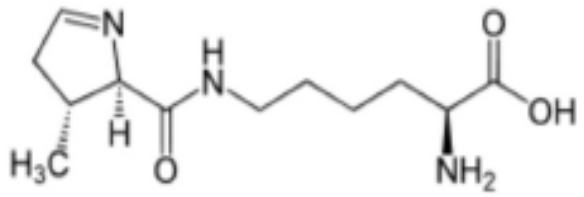

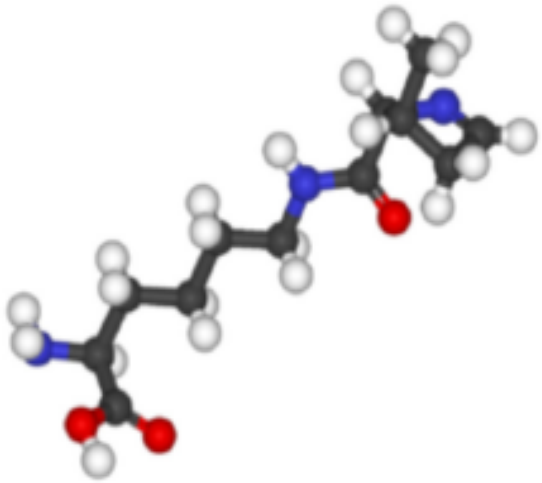

SELENOCYSTEINE (Sec, U)
kodon: UGA

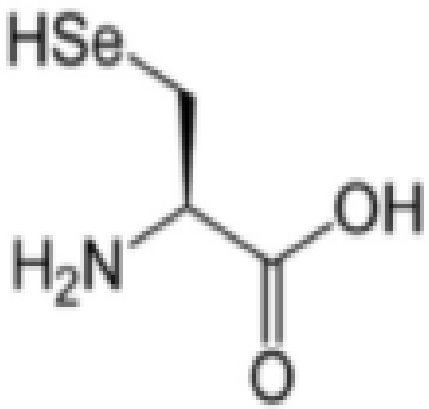

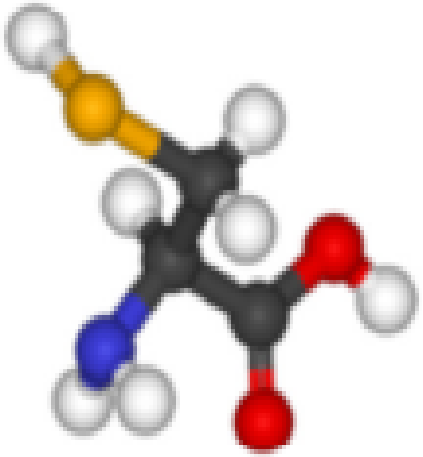

Atkins & Gesteland Science 296, 1409, 2002

28.

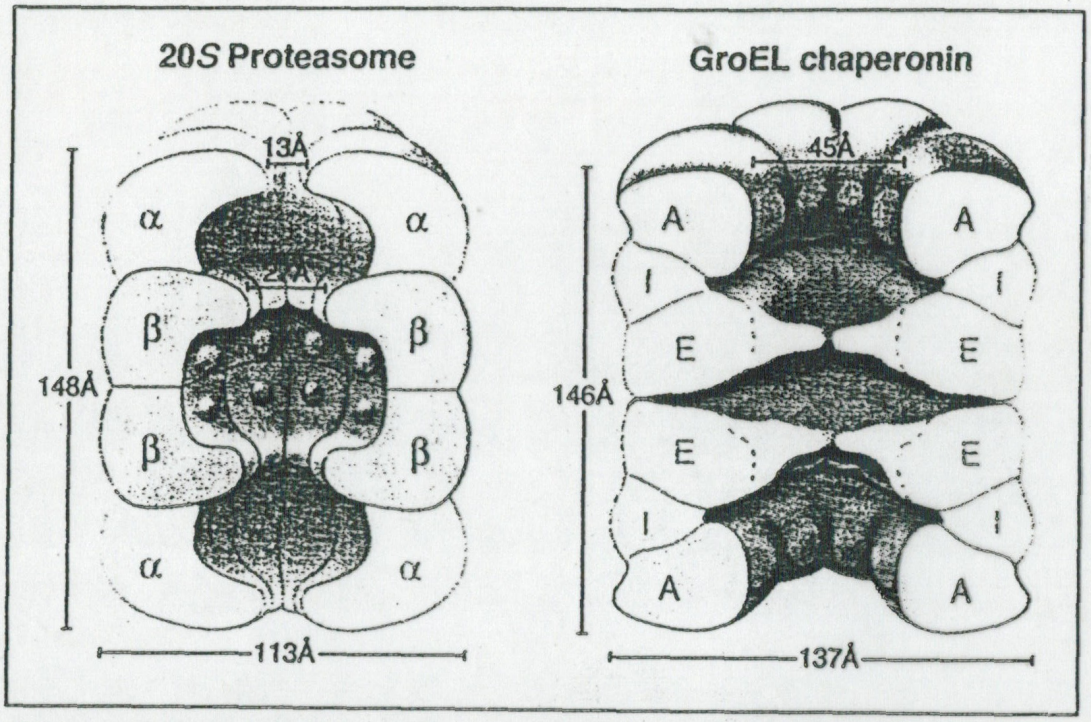

Ring complexes: The 20*S* proteasome and GroEL. (Left) The 20*S* proteasome is composed of four stacked, seven-membered rings. In the 20*S* proteasome from *T. acidophilum* (*7*), the two outer rings comprise seven copies of a 25.9-kilodalton α subunit, and the two inner rings comprise seven copies of a 22.3-kilodalton β subunit. These rings form a central channel with three chambers: Two antechambers flank an inside chamber that houses the catalytic sites (yellow spheres). **(Right)** The GroEL chaperonin is a homo-oligomer formed by two seven-membered rings of 57-kilodalton subunits stacked back to back. The GroEL rings form a wide channel open at either end of the cylinder but likely to be blocked at the equator (*2*). The GroEL subunit is composed of an apical (A), intermediate (I), and equatorial (E) region. The putative polypeptide binding sites (yellow ovals) are hydrophobic patches on the inside face of each apical domain.

29. PROTOINSULIN

T. Creighton Proteins Freeman & Co. 1993

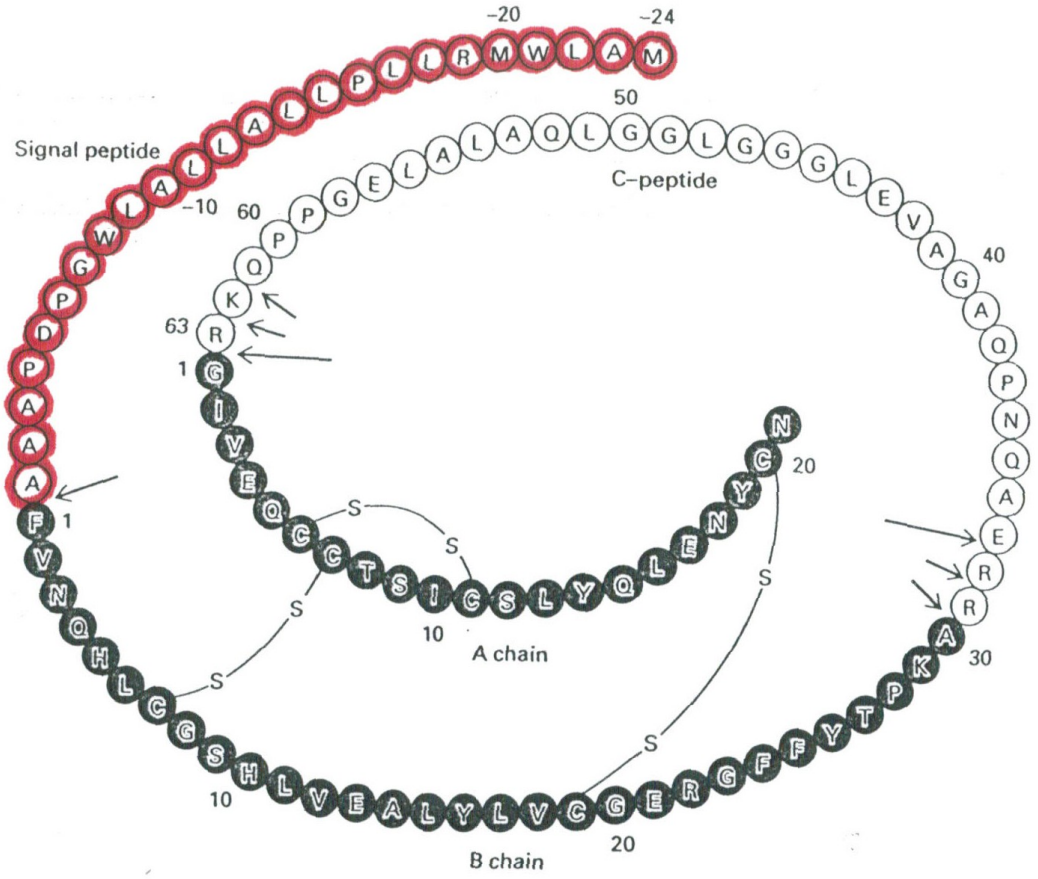

The primary structure of porcine proinsulin and the proteolytic cleavages that produce active insulin. The proteolytic cleavages are indicated by arrows. The initial cleavages (long arrows) occur after the pairs of basic residues Arg-Arg and Lys-Arg, which are then removed by a carboxypeptidase. The original proinsulin is folded and contains three disulfide bonds.

30. CONFORMATION OF POLYPEPTIDE CHAIN

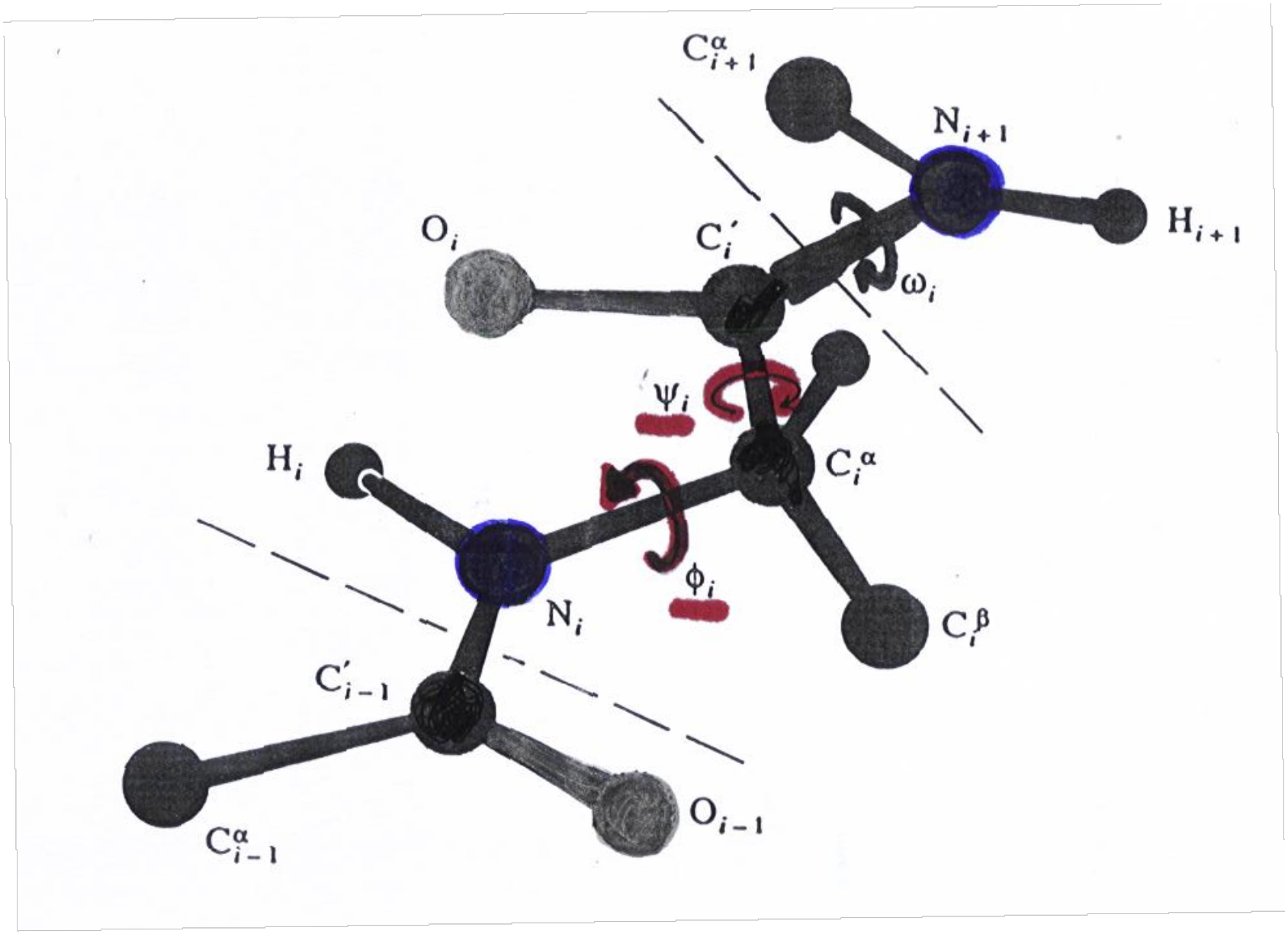

31. RAMACHANDRAN PLOT

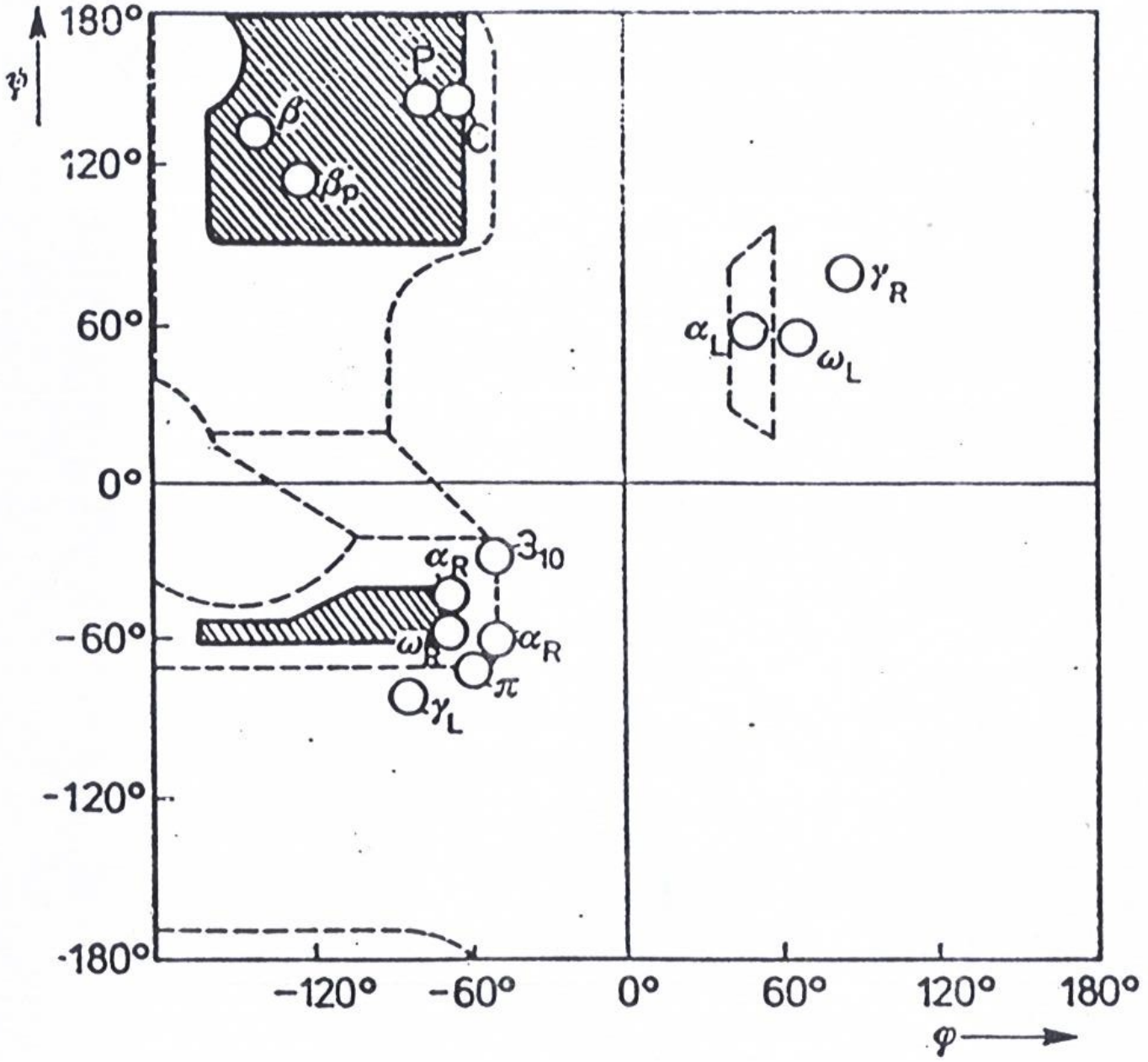

32. HYDROPHOBIC CORE OF INTRLEUKIN-4 SUPERPOSITION OF 21 NMR STRUCTURES

H. Oschinat et al. Angew. Chem. Int. Ed. Engl. 33, 277, 1993

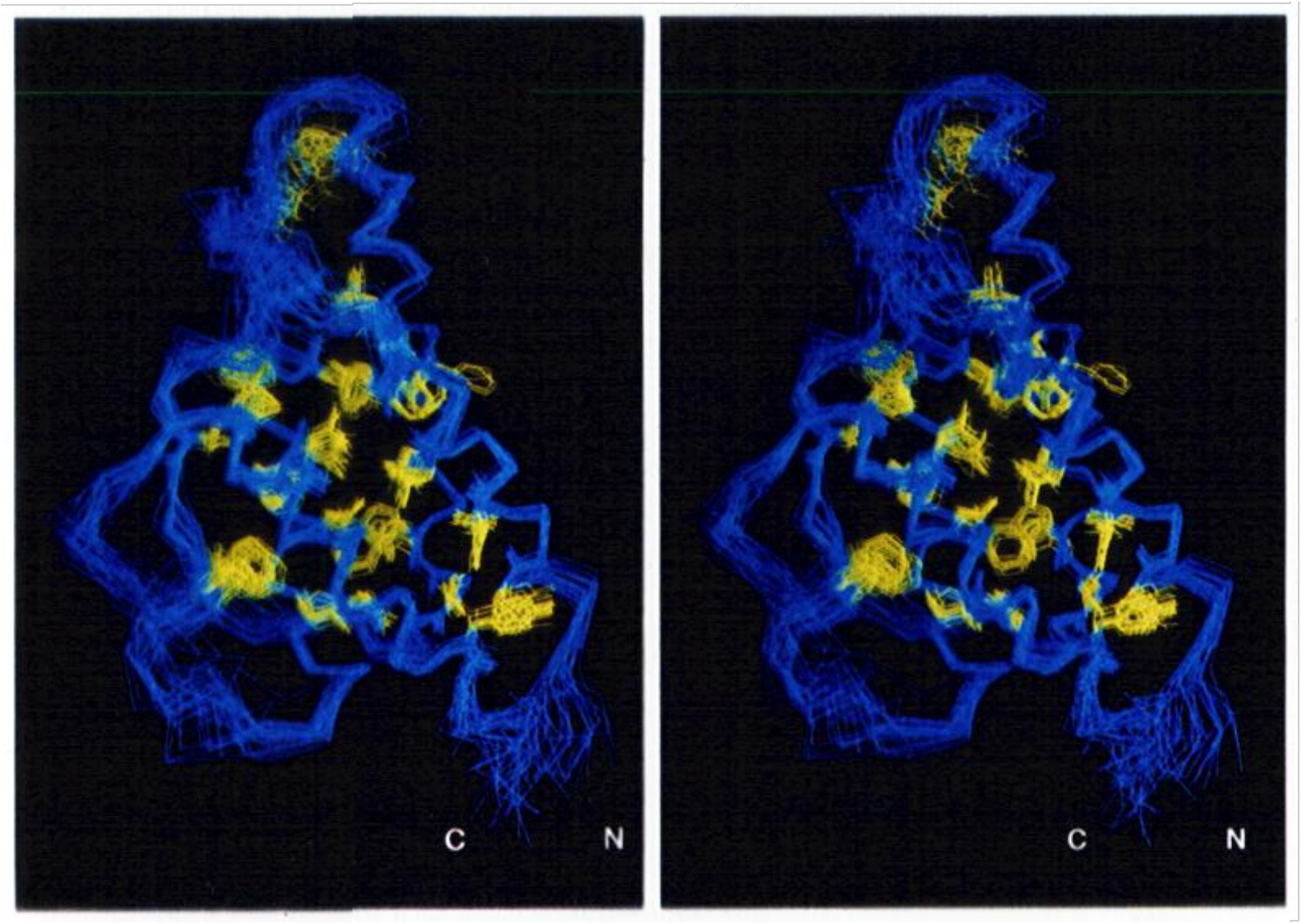

33. TWO-DOMAIN PROTEIN (344 AA)

T. Creighton Proteins Freeman & Co. 1993

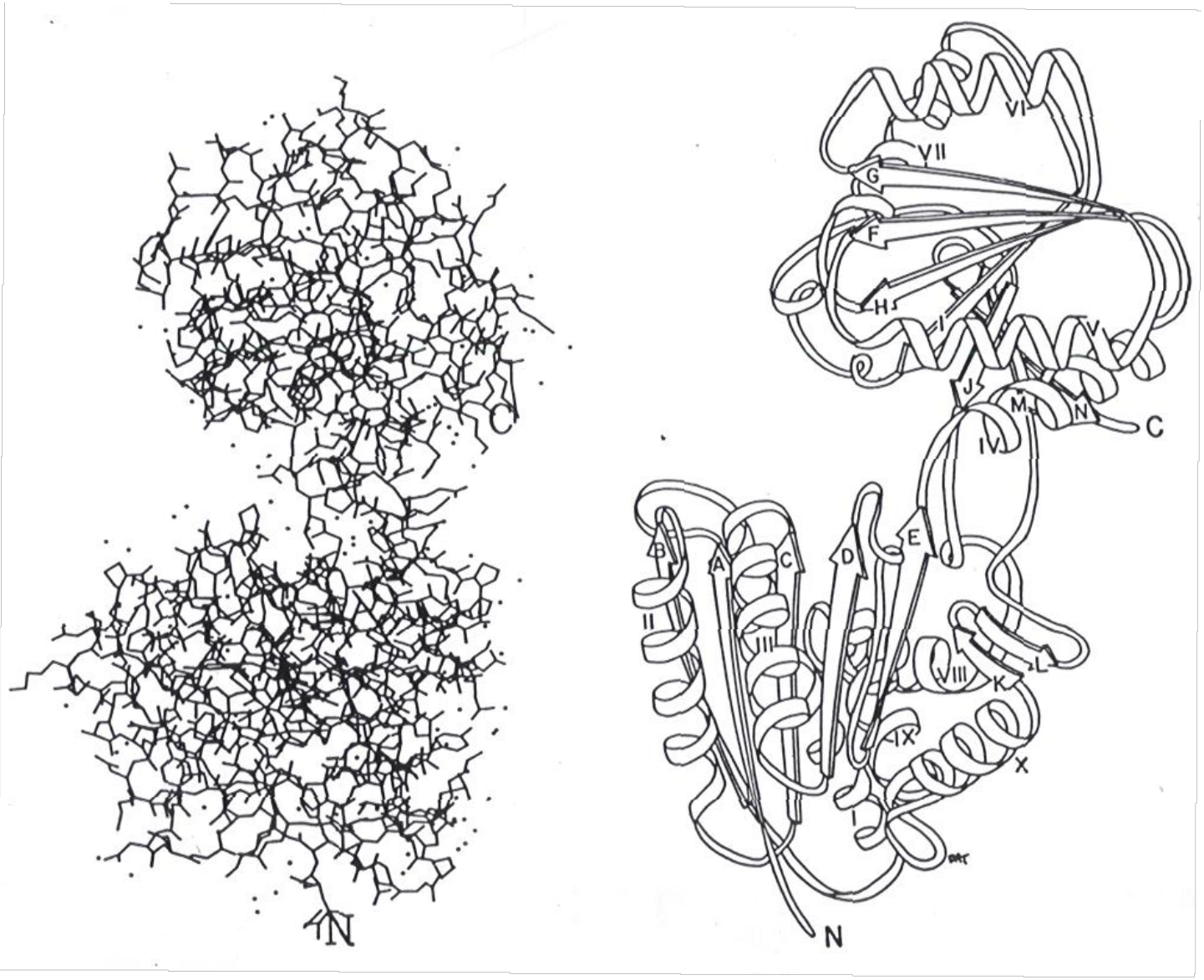

34. QUATERNARY STRUCTURE OF *trp* REPRESSOR

T. Creighton Proteins Freeman & Co. 1993

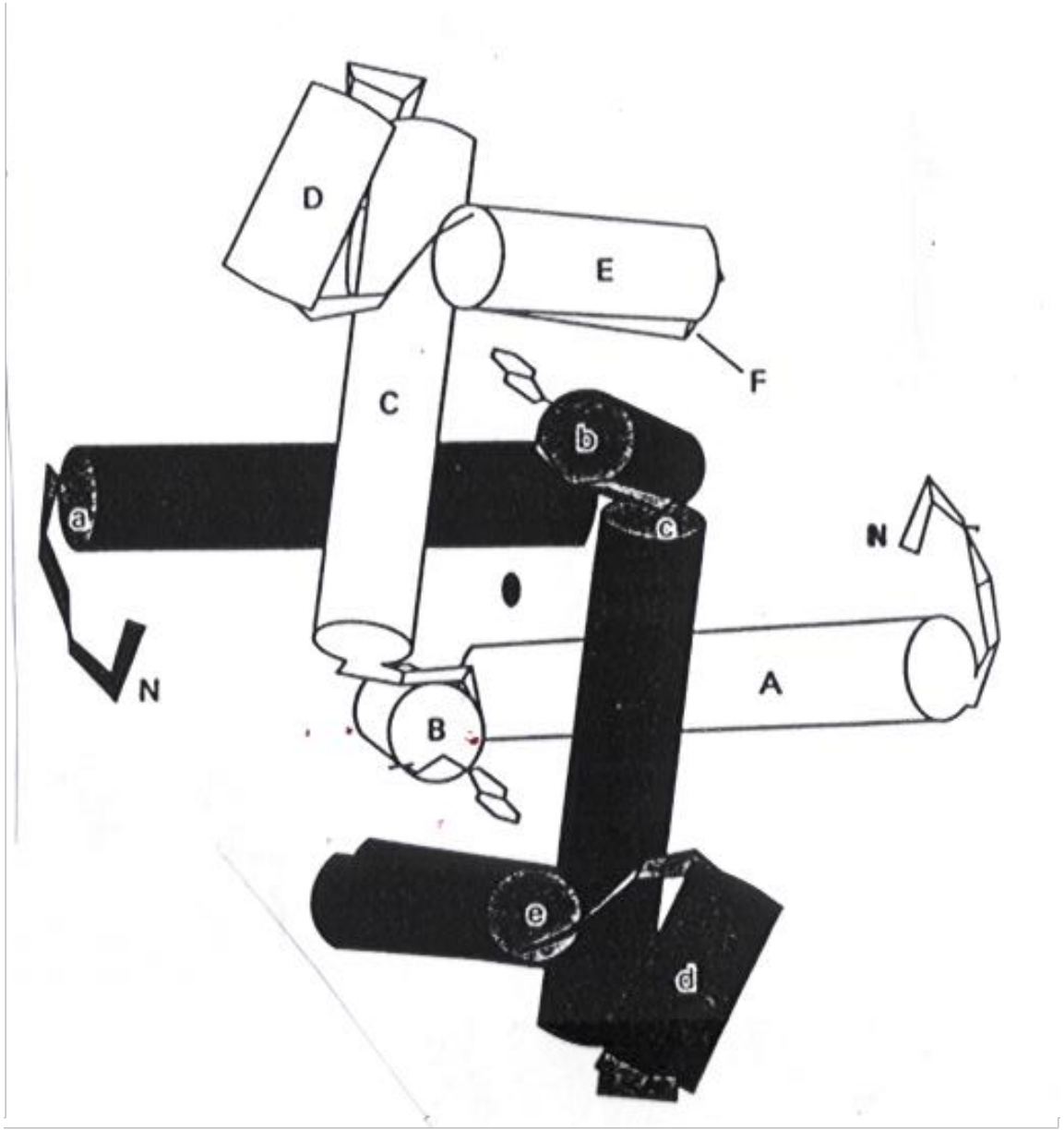

35. LIPID MEMBRANES

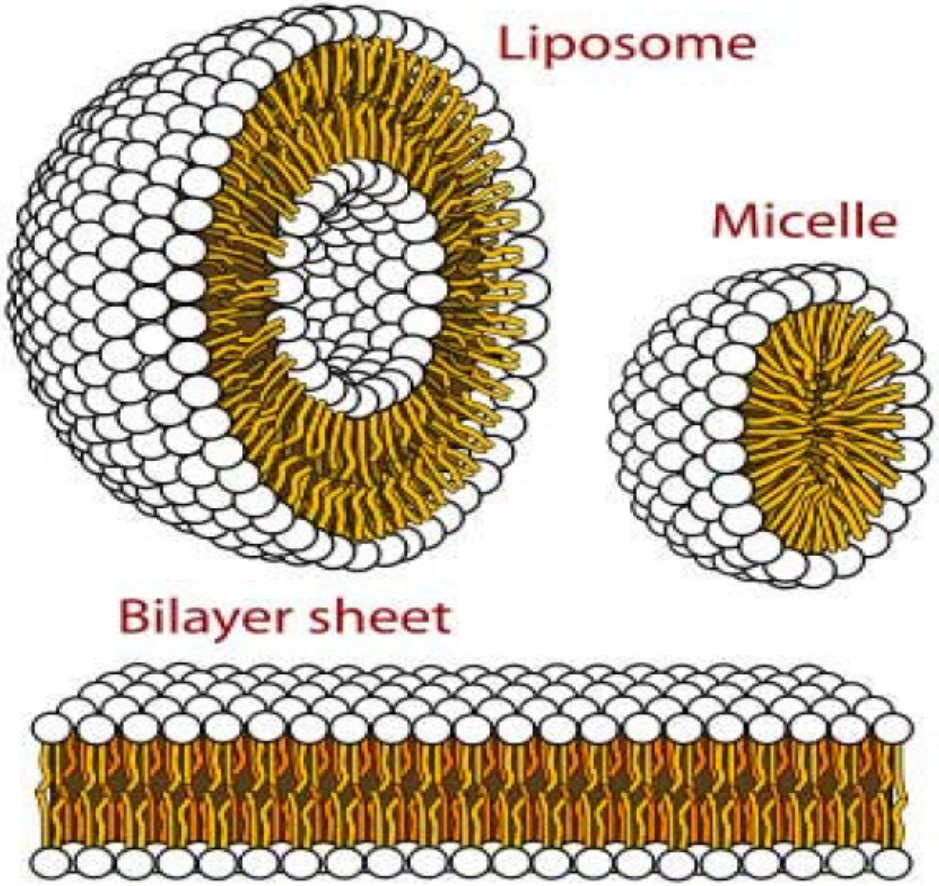

Hexagonal form

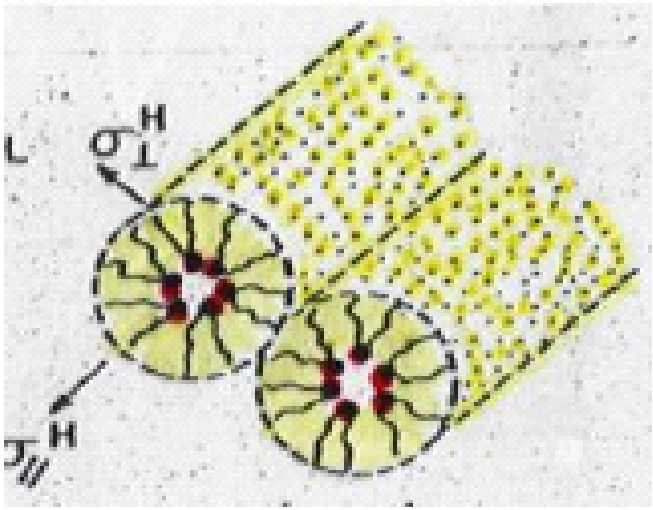

36. STRUCTURE OF CELLULOSE

B. Alberts et al. Molecular Biology of the Cell Garland Publish. 1989

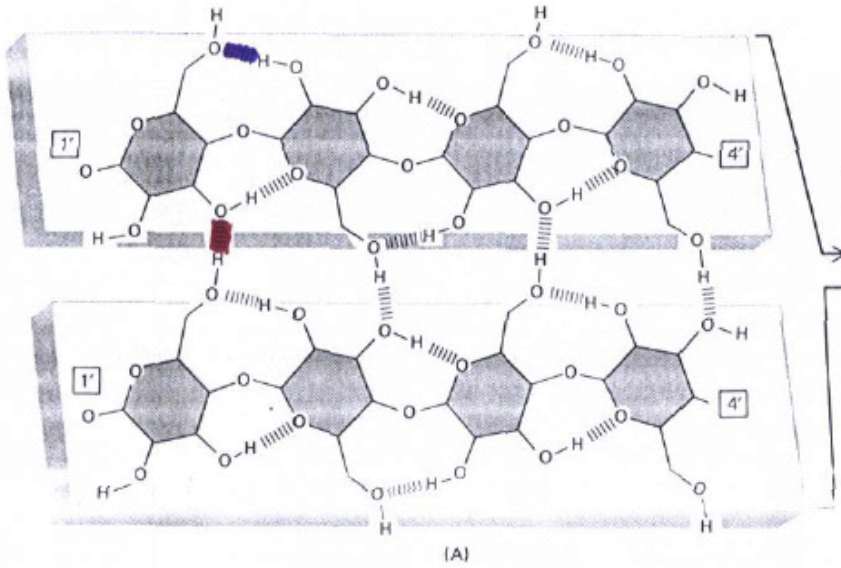

(A)

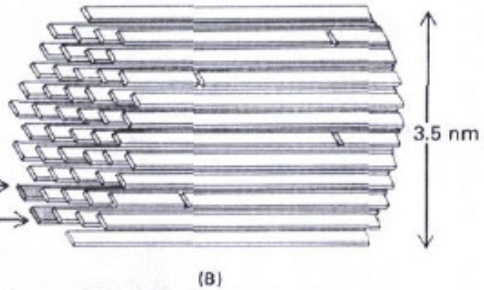

(B)

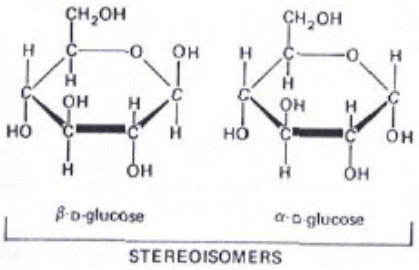

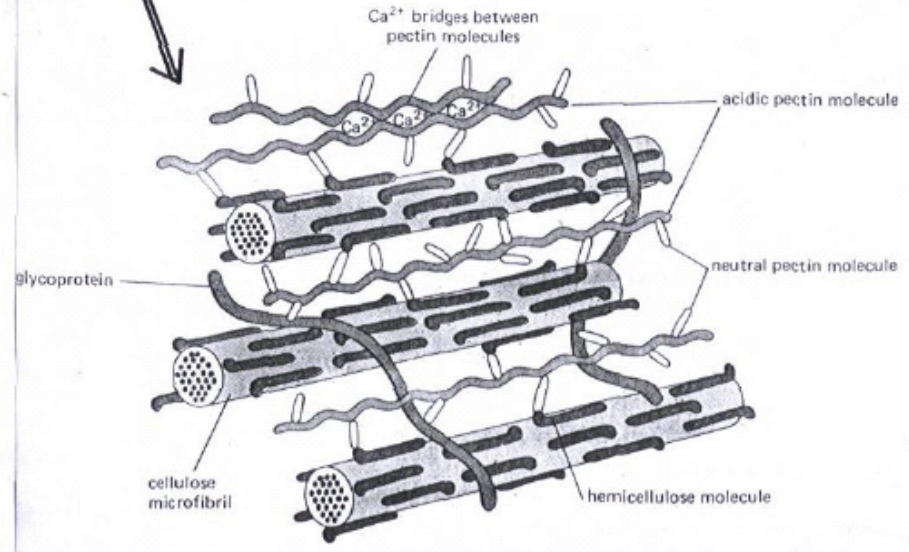

Figure 20–5 The structure of cellulose. (A) A small portion of two cellulose molecules, each consisting of a long planar chain of β1→4-linked glucose units, which may be many micrometers in length. Intramolecular hydrogen bonds stabilize each chain; intermolecular hydrogen bonds tightly cross-link adjacent chains. Other hydrogen bonds (not shown) cross-link each chain with other chains above and below it in the microfibril. (B) A cellulose microfibril in which many parallel cellulose molecules are hydrogen bonded together. In most higher plants a microfibril is about 3.5 nm in diameter, but in some algae it may be 10 times wider. Each cellulose molecule has a polarity (with a 1′ and a 4′ end), and all the molecules in each microfibril have the same polarity.

37. PROTEIN – DNA COMPLEX

Marmorstein et al. Nature 356, 408, 1992

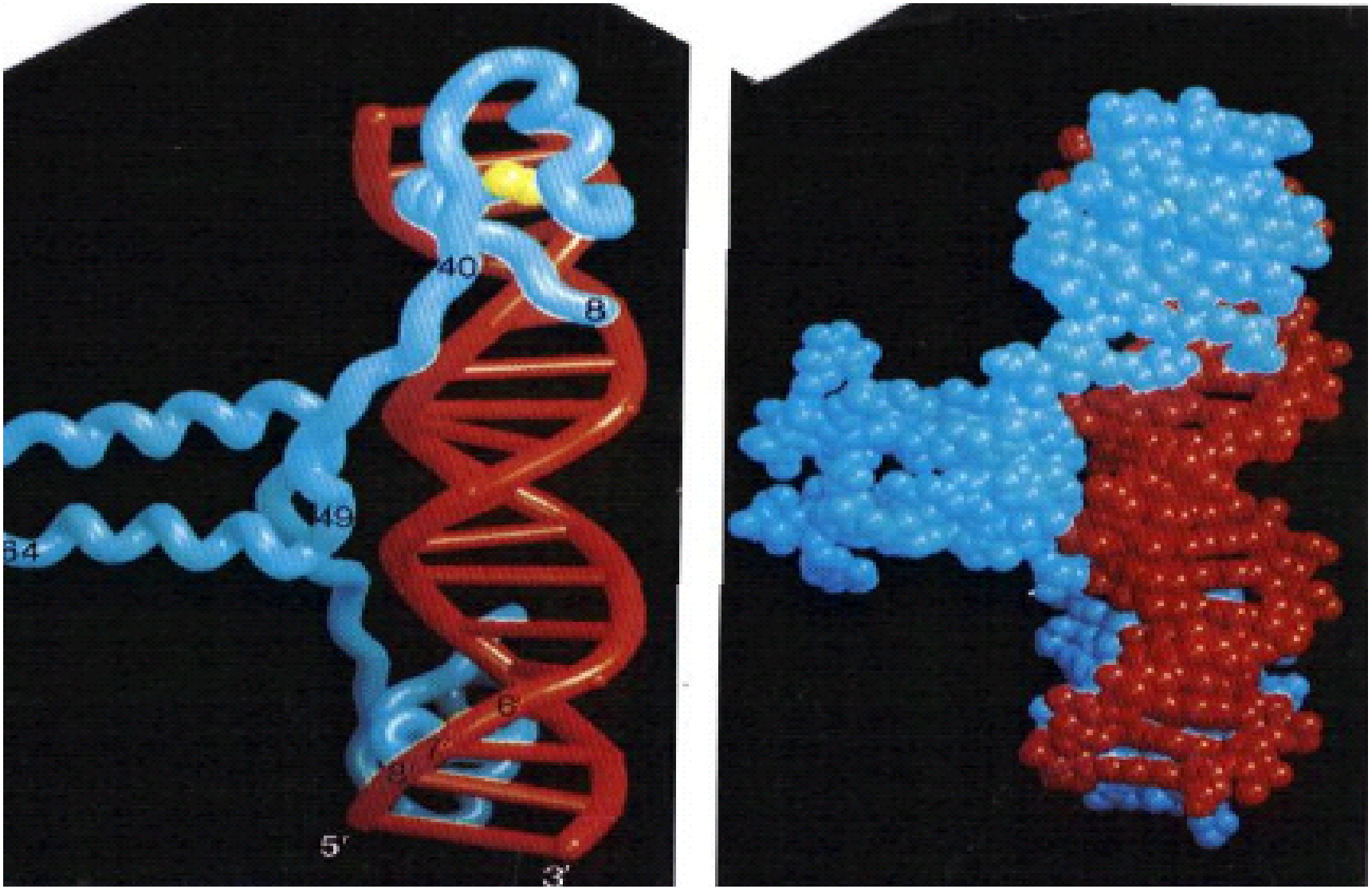

38. NONBONDED ELECTROSTATIC INTERACTIONS

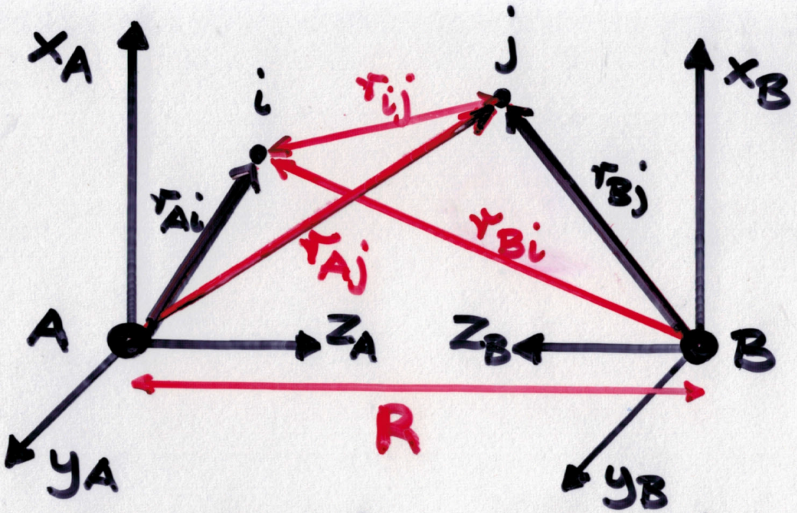

$$\hat{H} = \hat{H}_A + \hat{H}_B + \hat{H}_{AB} = \hat{H}^0 + \hat{H}'$$

$$\hat{H}' = \frac{Z_A Z_B e^2}{R} - \sum_{j=1}^{n_B} \frac{Z_A e^2}{r_{Aj}} - \sum_{i=1}^{n_A} \frac{Z_B e^2}{r_{Bi}} + \sum_{i=1}^{n_A}\sum_{j=1}^{n_B} \frac{e^2}{r_{ij}}$$

$$E_{AB} = \int \Psi^* \hat{H}' \Psi \, d\tau$$

POLARIZATION APPROXIMATION

$$\Psi^{(0)} = \Psi_A \Psi_B$$

EXPANSION OF $\hat{H}'$ IN MULTIPOLE SERIES

$$(1+x)^{-\frac{1}{2}} = 1 - \frac{1}{2}x + \frac{3}{8}x^2 - \ldots \quad x \ll 1$$

$r_{Ai}, r_{Bj} \ll R$

PERTURBATION THEORY

$$E_{AB} \approx E^{(1)} + E^{(2)} + \ldots$$

$$\langle E^{(1)} \rangle = \frac{\int E^{(1)} \exp\left(-\frac{E^{(1)}}{kT}\right) d\Omega}{\int \exp\left(-\frac{E^{(1)}}{kT}\right) d\Omega}$$

KEEPING THE TERMS $\frac{1}{kT}$

$$\langle E^{(1)} \rangle \approx E_{COU} = \frac{q_A q_B}{R}$$

$$q_k = e(Z_k - n_k) \quad k = A, B$$

$$E^{(2)} = E_{ind} + E_{dysp}$$

$$E_{ind} = -\frac{1}{R^6}\left(\alpha_A \mu_B^2 + \alpha_B \mu_A^2\right)$$

α - POLARYZOWALNOŚĆ

μ - MOMENT DIPOLOWY

$$E_{dysp} = -\frac{3}{2R^6} \cdot \frac{I_A I_B \alpha_A \alpha_B}{I_A + I_B}$$

$$E_{vdW} = E_{ind} + E_{dysp} + E_{rep} = -\frac{C}{R^6} + \frac{A}{R^{12}}$$

39. MOLECULAR ELECTROSTATICS

FORCE FIELD POTENTIAL

$$V = \frac{1}{2}\sum_{\text{bonds}} K_b(b-b_0)^2 + \frac{1}{2}\sum_{\substack{\text{bond}\\ \text{angles}}} K_\theta(\theta-\theta_0)^2 + \frac{1}{2}\sum_{\substack{\text{dihedral}\\ \text{angles}}} K_\phi[1+\cos(n\phi-\delta)] + \frac{1}{2}\sum_{\text{groups}} K_\chi \chi^2 +$$

$$+ \sum_{\substack{\text{nonbonded}\\ \text{pairs}}} \left(\frac{A}{R^{12}} - \frac{C}{R^6} + \frac{q_1 q_2}{\varepsilon R} \right)$$

K - force constants ε - dielectric constant

b_0, θ_0 - equilibrium bond lenghts and angles

FORCE IN POINT $\bar{R}_i$

$$\bar{F}_i = -\nabla_{\bar{R}_i} V \qquad i = 1, 2, \ldots, N \text{ atom}$$

POISSON-BOLTZMANN EQUATION (PB)

$$-\nabla\cdot(\varepsilon\nabla\bar{\Phi}) = \rho - 2n_\infty \sinh(e\bar{\Phi}/kT)$$

$\bar{\Phi}$ - electric potential ρ - charge density, T - temperature

n_∞ - ion density

$$-\nabla\cdot(\varepsilon\nabla\bar{\Phi}) + e\kappa^2\bar{\Phi} = \rho \qquad \text{(LPB)}$$

$$\kappa^2 = \frac{2Ie^2}{kT\varepsilon} \qquad I \text{ - ionic force}$$

ELECTRIC FIELD $\bar{E} = -\nabla\bar{\Phi}$

40. METHODS OF BIOMOLECULAR INVESTIGATIONS

(A) Molecular mass and separation: ultracentrifugation, gel (GE) and capillary (CE) electrophoresis, mass spectrometry (MS)

(B) Chemical structures (monomers), tautomerism of nucleic acids bases, **primary structures:** X-ray diffraction, molecular spectroscopy (NMR), sequencing of nucleic acids and proteins

(C) Energy, thermodynamical parameters, molecular stability and conformational equilibia: spectroscopy from Mössbauer to NMR, ITC and DSC calorimetry

(D) Structural methods at the atomic level of resolution: X-ray and neutron diffraction (molecular crystals), NMR in solution and in solids (magic angle spinning, MAS), electron diffraction (2D crystals)

(E) Determination of molecular shape: atomic force microscopy (AFM), electron cryo-microscopy of a single molecule (cryoEM), small angle X-ray scattering (SAXS)

(F) Molecular dynamics (kinetics), conformational changes, protein and RNA folding, molecular association: NMR relaxation, time-resolved fluorescence, fluorescence correlation spectroscopy (FCS), surface plasmon resonance (SPR), H/D-exchange NMR and MS, Laue X-ray diffraction, 2D IR vibrational echo

(G) Manipulation and observation of a single molecule: optical tweezers, magnetic tweezers, atomic force microscopy (AFM), single molecule spectroscopy (SMS)

(H) NMR in biochemistry (metabolism) and in medical diagnostics: *in vivo* NMR, in cell NMR, magnetic resonance imaging (MRI, fMRI), *topical* magnetic resonance

41. MOLECULAR SPECTROSCOPY METHODS

nuclear magnetic resonance NMR: and nuclear quadrupolar resonance NQR	ΔE ~10^{-6} eV; ν ~ MHz; λ ~m
electron paramagnetic resonance EPR:	ΔE ~10^{-4} eV; ν ~GHz; λ ~cm
microwave absorption and Raman:	ΔE ~10^{-4} eV; $1/\lambda$ ~$10^{-1} \div 10^{2}$ cm^{-1} (~$10^{9} \div 10^{12}$ Hz) λ ~ mm and cm
IR absorption and Raman:	ΔE ~10^{-1} eV; $1/\lambda$ ~$10^{4} \div 10^{2}$ cm^{-1} (ν ~$10^{12} \div 10^{14}$ Hz); λ ~ μm
vibrational circular dichroism VCD:	ΔE as for IR
resonance Raman (RR)	ΔE as for Raman
Ramana optical activity ROA:	ΔE as for Raman
UV-VIS absorption:	ΔE ~10^{4}eV; VIS: λ = 400÷800 nm; UV: λ = 100÷400 nm; $\nu \sim 10^{14} \div 10^{15}$ Hz
circular dichroism CD:	ΔE as for UV VIS
linear dichroism LD:	ΔE as for UV VIS
fluorescence and phosphorescence:	ΔE as for UV VIS
X-ray photoelectron spectroscopy: XPS (ESCA), XAS, BioXAS	ΔE ~$10^{2} \div 10^{4}$ eV; λ ~ Å (10^{-10} m)
Mössbauer spectroscopy:	gamma rays: λ ~10^{-13} m $\nu \sim 10^{21}$ Hz

42. CAPILLARY ELECTROPHORESIS CE

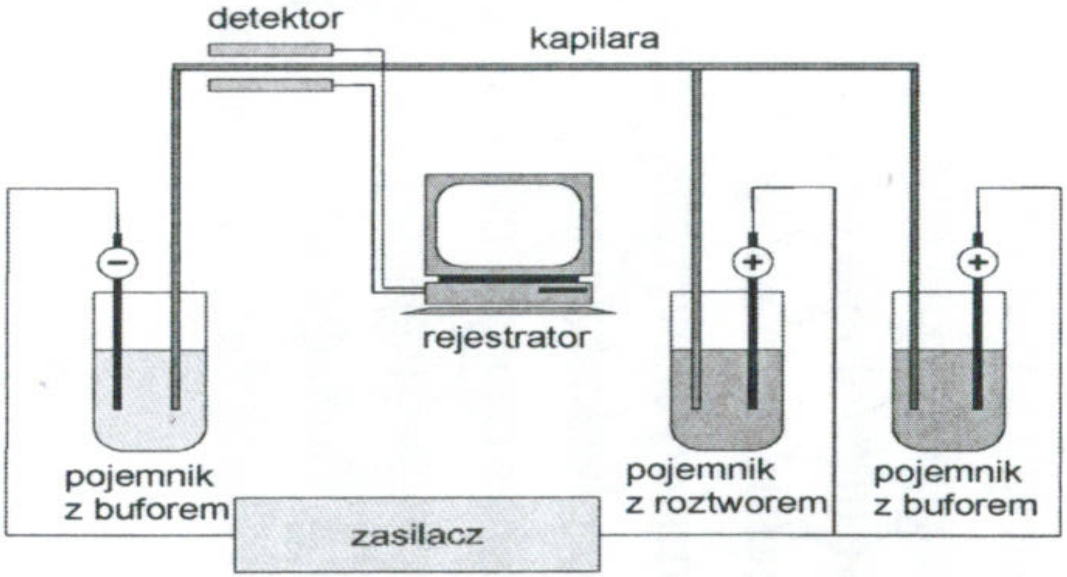

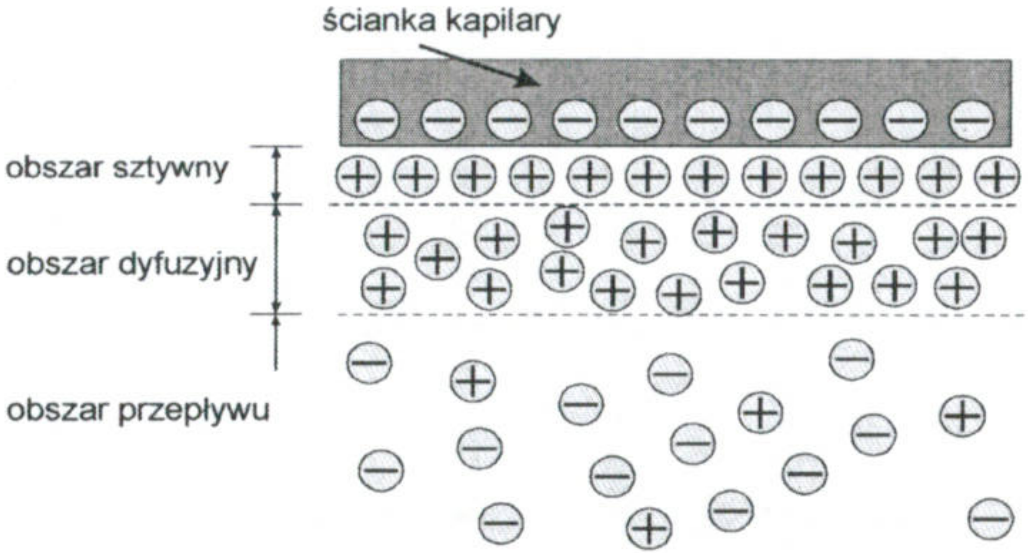

43. COMPARISON OF SEQUENCING PLATFORMS

Mardis Nature 470, 198, 2011

Table 1 | Sequencing platform comparison

	Roche/454	Life Technologies SOLiD	Illumina Hi-Seq 2000	Pacific Biosciences RS
Library amplification method	emPCR* on bead surface	emPCR* on bead surface	Enzymatic amplification on glass surface	NA (single molecule detection)
Sequencing method	Polymerase-mediated incorporation of unlabelled nucleotides	Ligase-mediated addition of 2-base encoded fluorescent oligonucleotides	Polymerase- mediated incorporation of end-blocked fluorescent nucleotides	Polymerase-mediated incorporation of terminal phosphate labelled fluorescent nucleotides
Detection method	Light emitted from secondary reactions initiated by release of PPi	Fluorescent emission from ligated dye-labelled oligonucleotides	Fluorescent emission from incorporated dye-labelled nucleotides	Real time detection of fluorescent dye in polymerase active site during incorporation
Post incorporation method	NA (unlabelled nucleotides are added in base-specific fashion, followed by detection)	Chemical cleavage removes fluorescent dye and 3′ end of oligonucleotide	Chemical cleavage of fluorescent dye and 3′ blocking group	NA (fluorescent dyes are removed as part of PPi release on nucleotide incorporation)
Error model	Substitution errors rare, insertion/deletion errors at homopolymers	End of read substitution errors	End of read substitution errors	Random insertion/deletion errors
Read length (fragment/paired end)	400 bp/variable length mate pairs	75 bp/50+25 bp	150 bp/100+100 bp	>1,000 bp

Comparison of commercially available next generation platforms (Roche/454, Life Technologies and Illumina) and a single molecule platform (Pacific Biosciences), illustrating the similarities and differences in these technologies, according to several metrics. NA, not applicable; PPi, pyrophosphate.

*emPCR (emulsion PCR) is a bulk amplification process whereby library fragments are combined with beads and PCR reactants in an oil emulsion that allows *en masse* amplification of millions of bead-DNA combinations in a single tube.

44. MASSIVELY PARALLEL SEQUENCING TECHNOLOGIES

Gundry & Vijg Mutation Res. 729, 1, 2012

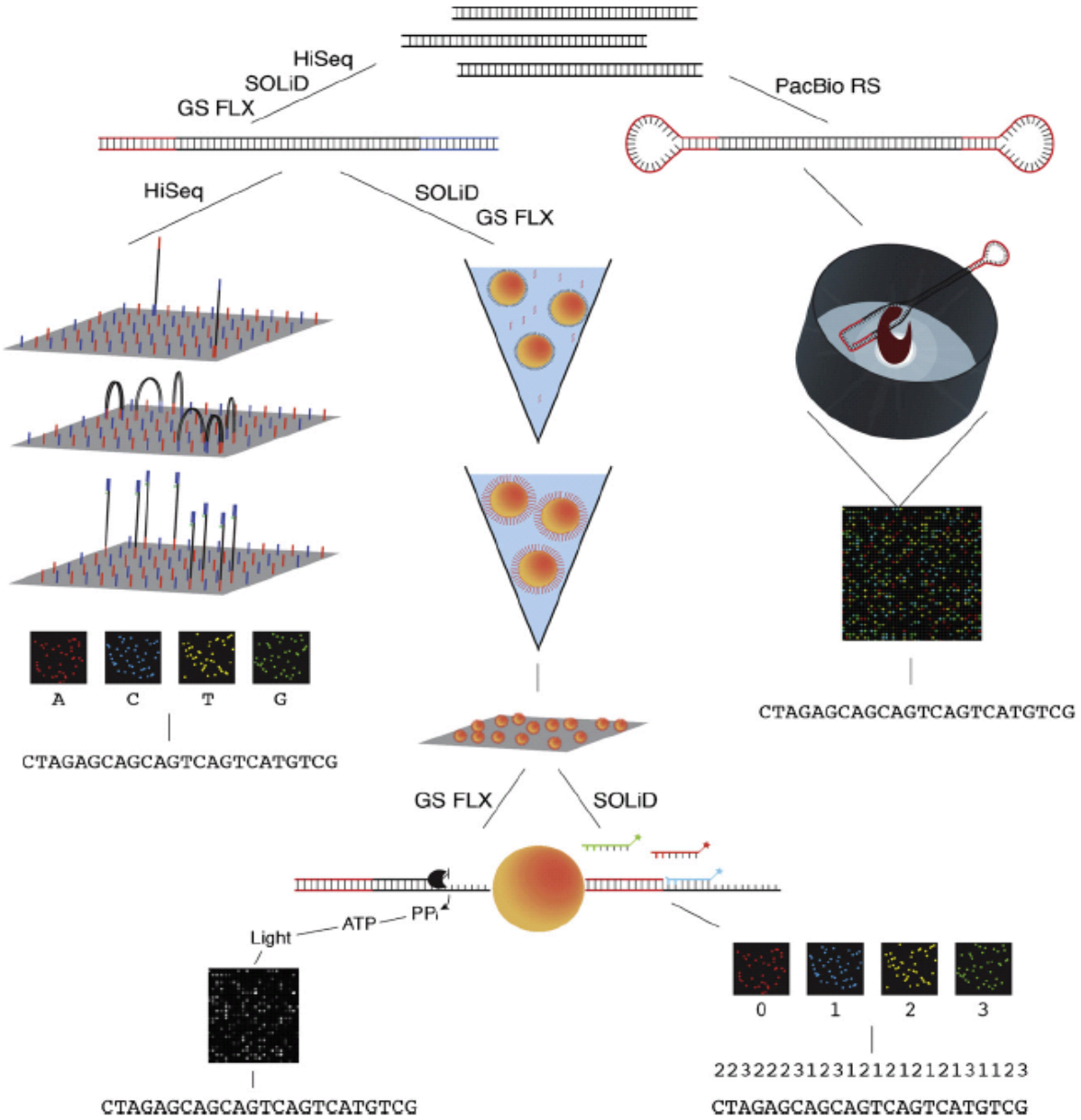

45. CLASSICAL DNA DOUBLE HELICES

W. Saenger Principles of Nucleic Acid Structure Springer 1984

B C D A Z

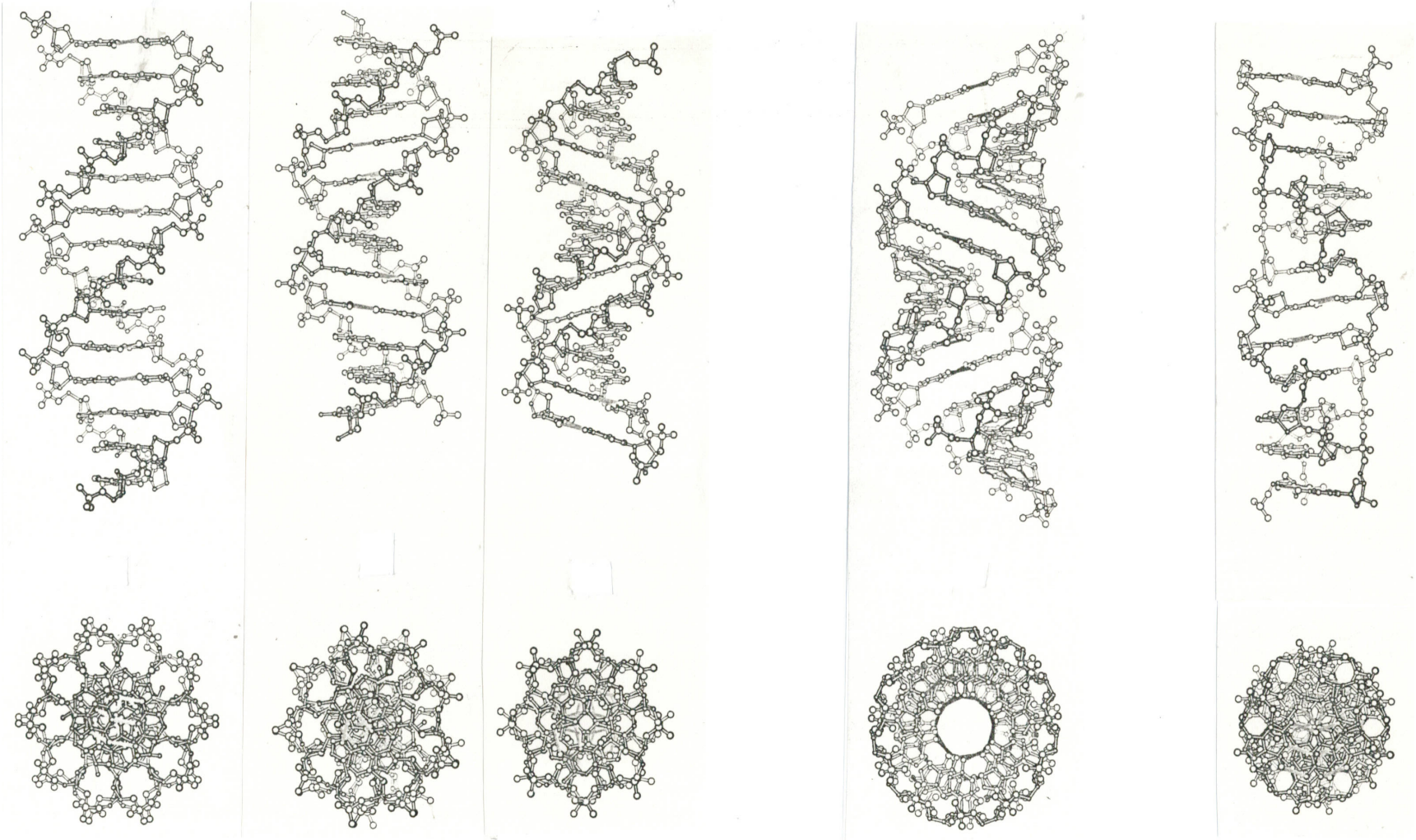

46. FIBER DIFFRACTION PATTERNS OF DNA HELICES

W. Saenger Principles of Nucleic Acid Structure Springer 1984

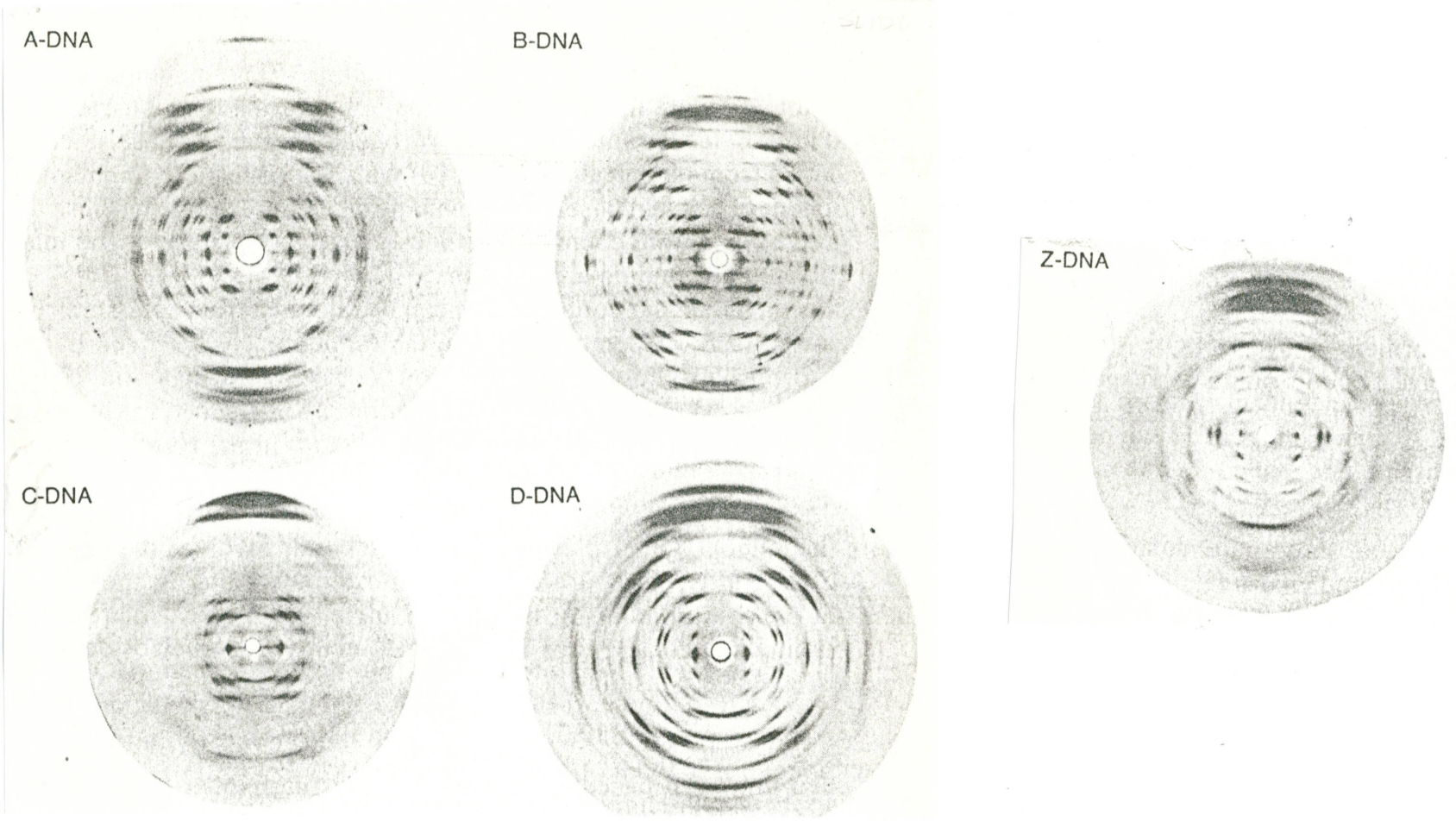

All patterns are on the same scale and fibers were tilted from vertical to the X-ray beam in order to produce the meridional reflection indicating the number of base-pairs per pitch: 11, 10, 9, 8 and 12 for A- to Z-DNA. In Z-DNA, a meridional reflection appears on the sixth layer line in the center of the "helical cross" because the repeat unit is a dinucleotide (pCpG) as outlined in Chapter 12, and not a mononucleotide as in all other DNA forms.

47. FIBER DIFFRACTION ANALYSIS

W. Saenger Principles of Nucleic Acid Structure Springer 1984

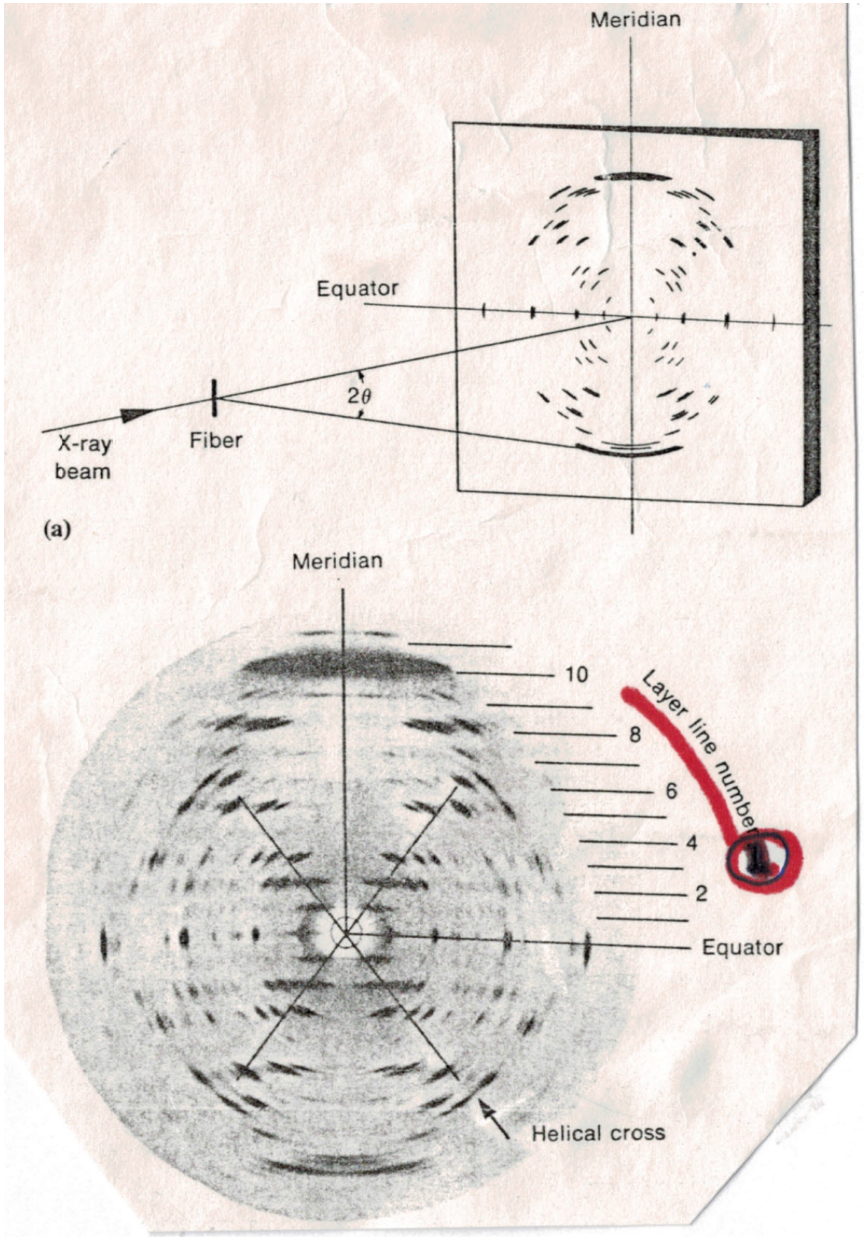

Figure 3-9.(a) Schematic representation of the X-ray fiber diffraction method [flat film technique (165)]. The monochromatic X-ray is collimated to 0.1 to 0.2 mm in diameter; fiber axis and film are perpendicular to the X-ray beam. Glancing angle θ and spacings are obtained via Bragg's law, Equation (3-1). (b) X-ray diffraction pattern of calf thymus DNA in the B form, courtesy Drs. S. Arnott and R. Chandrasekaran. Typical crosslike intensity distribution suggests helical structure. Separation of layer lines gives pitch height P; strong reflection on meridian (tenth layer line at 3.4 Å distance) indicates that one helix turn contains 10 nucleotides with bases stacked 3.4 Å apart nearly vertical to the helix axis. If the fiber had been exactly vertical to the X-ray beam during exposure, the diagram would be mirror-symmetrical about the equator. It is not because the fiber was tilted slightly to bring the base-pairs into reflecting position in order to produce the strong meridional reflection on the tenth layer line.

Structure factor $F(R, \zeta)$ for helical molecules. In fiber diffraction analysis, atomic coordinates are expressed in radial coordinates r, ϕ, z (Figure 2-15) rather than in Cartesian system and therefore, Bessel function terms are introduced (95 to 100). For the cylindrically averaged structure factor, we have:

$$F(R, \zeta) = \sum_n \sum_j f_j \cdot J_n(2\pi R r_j) \cdot e^{2\pi i(l z_j - n\Phi_j)} \qquad (3\text{-}6)$$

where R, ζ are radial and axial coordinates in reciprocal space. For each repeating subunit, r_j, Φ_j, z_j denote coordinates in real space of atom j with scattering factor f_j corrected for water of hydration (101). J_n is the n-th order Bessel function, the value of n being related to layer line number l, helix repeat c, pitch height P and axial rise per residue, h, by the selection rule

$$\zeta = l/c = n/P + m/h \qquad (3\text{-}7)$$

with m any positive or negative integer.

48. CONFORMATION OF DNA HELICES

W. Saenger Principles of Nucleic Acid Structure Springer 1984

DIHEDRAL ANGLES

	α	β	γ	δ	ε	ζ	χ
B-DNA	314	214	36 (+sc)	156 (S)	155	264	262 (anti)
C-DNA	321	200	37 (+sc)	157 (S)	161	254	263 (anti)
D-DNA	298	208	69 (+sc)	157 (S)	141	259	266 (anti)
A-DNA	310	172	41 (+sc)	79 (N)	214	282	206 (anti)
Z-DNA							
dG	52	207	187 (ap)	76 (N)	288	102	89 (syn)
dC	250	192	54 (+sc)	147 (S)	257	296	201(anti)

HELICAL PARAMETERS

	symmetry X_k	pitch P (Å)	axial rise h=P/X (Å)	twist Ω=360/X (°)	inclination η (°)	dislocation of bp D (Å)
B-DNA	10_1	33.8	3.38	36.0	−6	0.5
C-DNA	28_3	30.9	3.31	38.6	−8	1.0
D-DNA	8_1	24.2	3.03	45.0	−16	1.8
A-DNA	11_1	28.2	2.56	32.7	20	4.7
Z-DNA	6_5	43.5	7.25	−60.0 (−45; −15)	−5	

49. STRUCTURE OF IRREGULAR DUPLEX d[GGAAT^{F}UCC]$_2$

Stolarski et al. Biochemistry 31, 7027, 1992

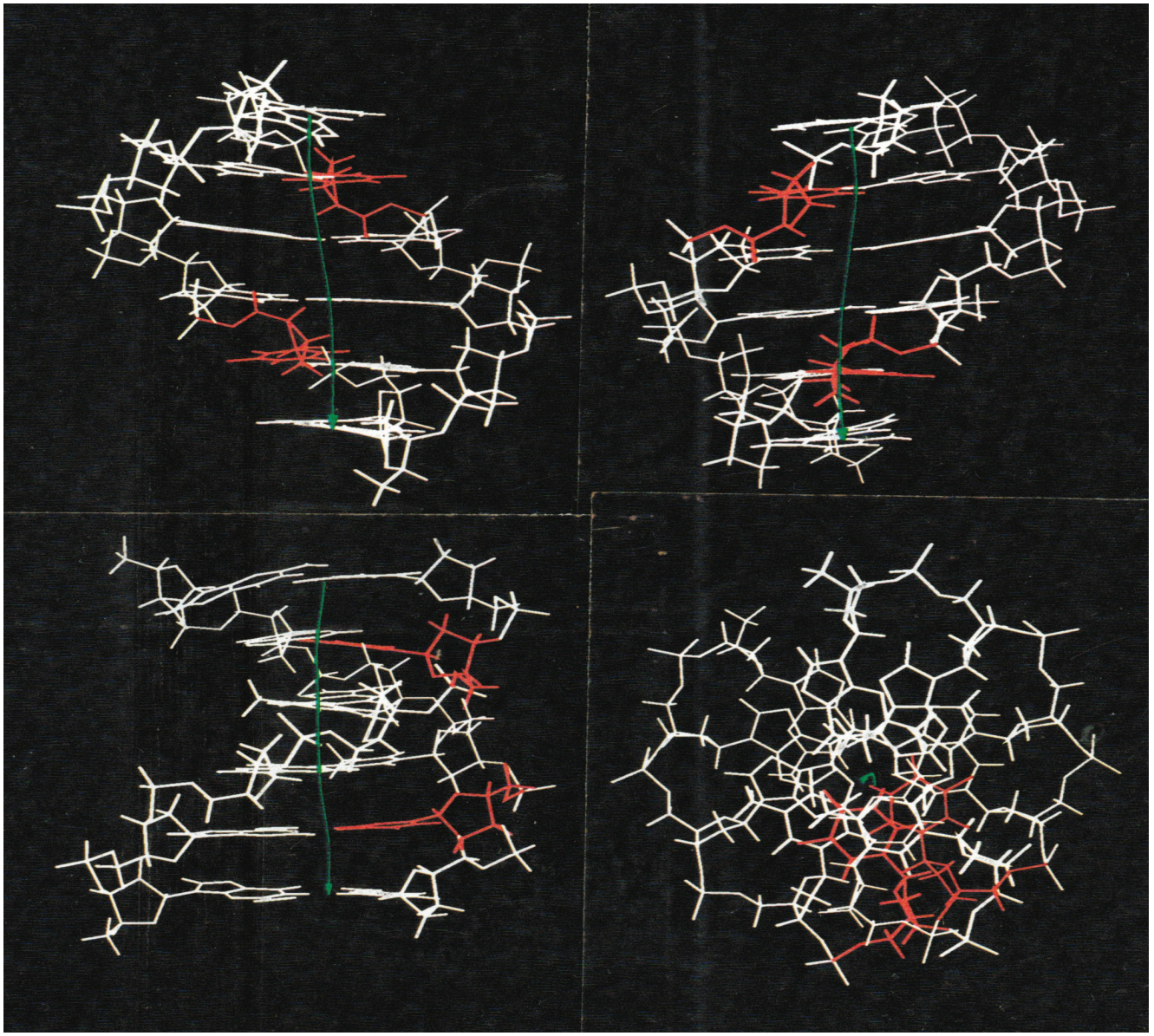

50. HELICAL PARAMETERS IN d[GGAAT^{F}UCC]$_2$

Stolarski et al. Biochemistry 31, 7027, 1992

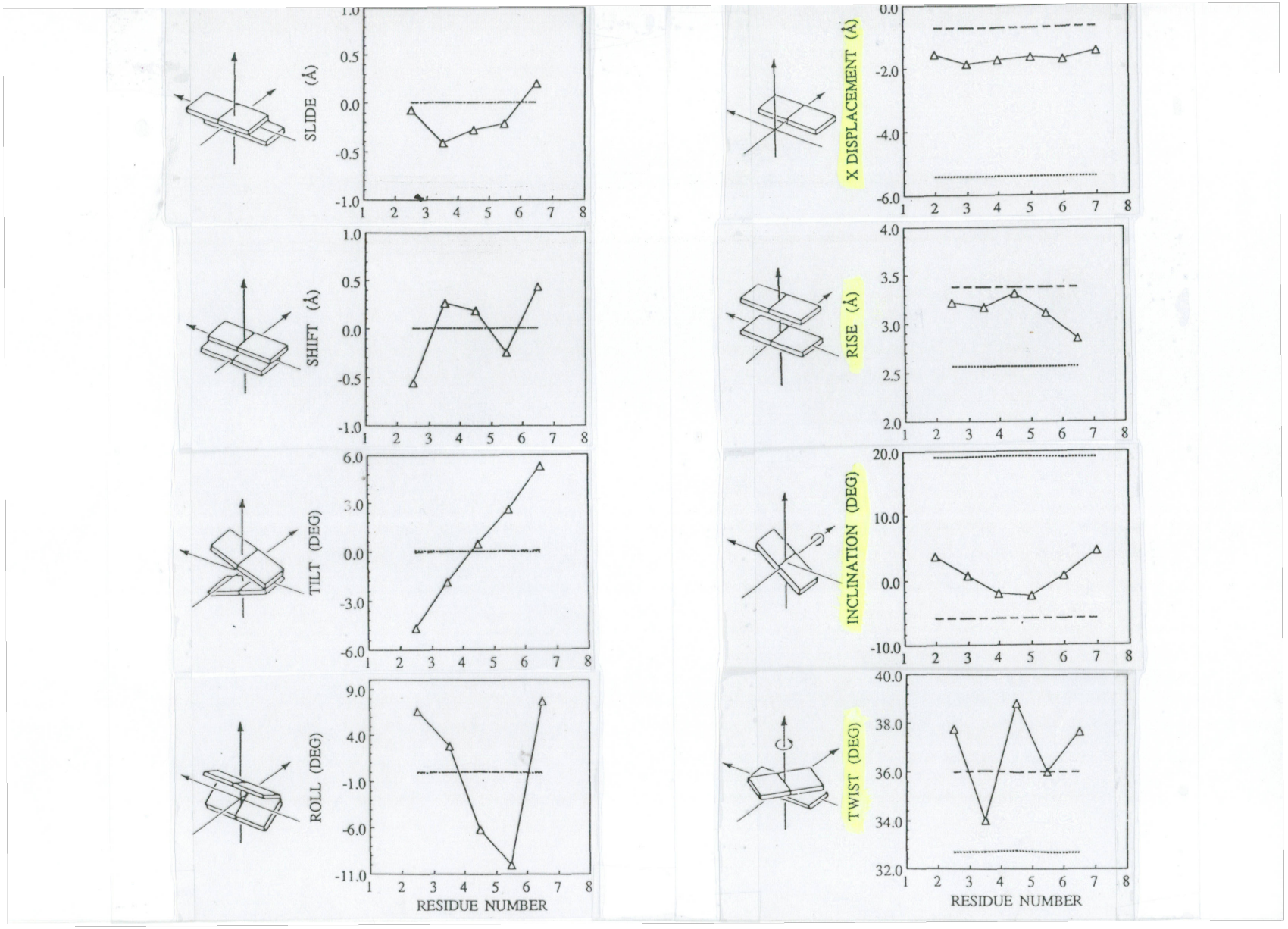

51. AFM AND CRYSTAL STRUCTURES OF NUCLEOSOME

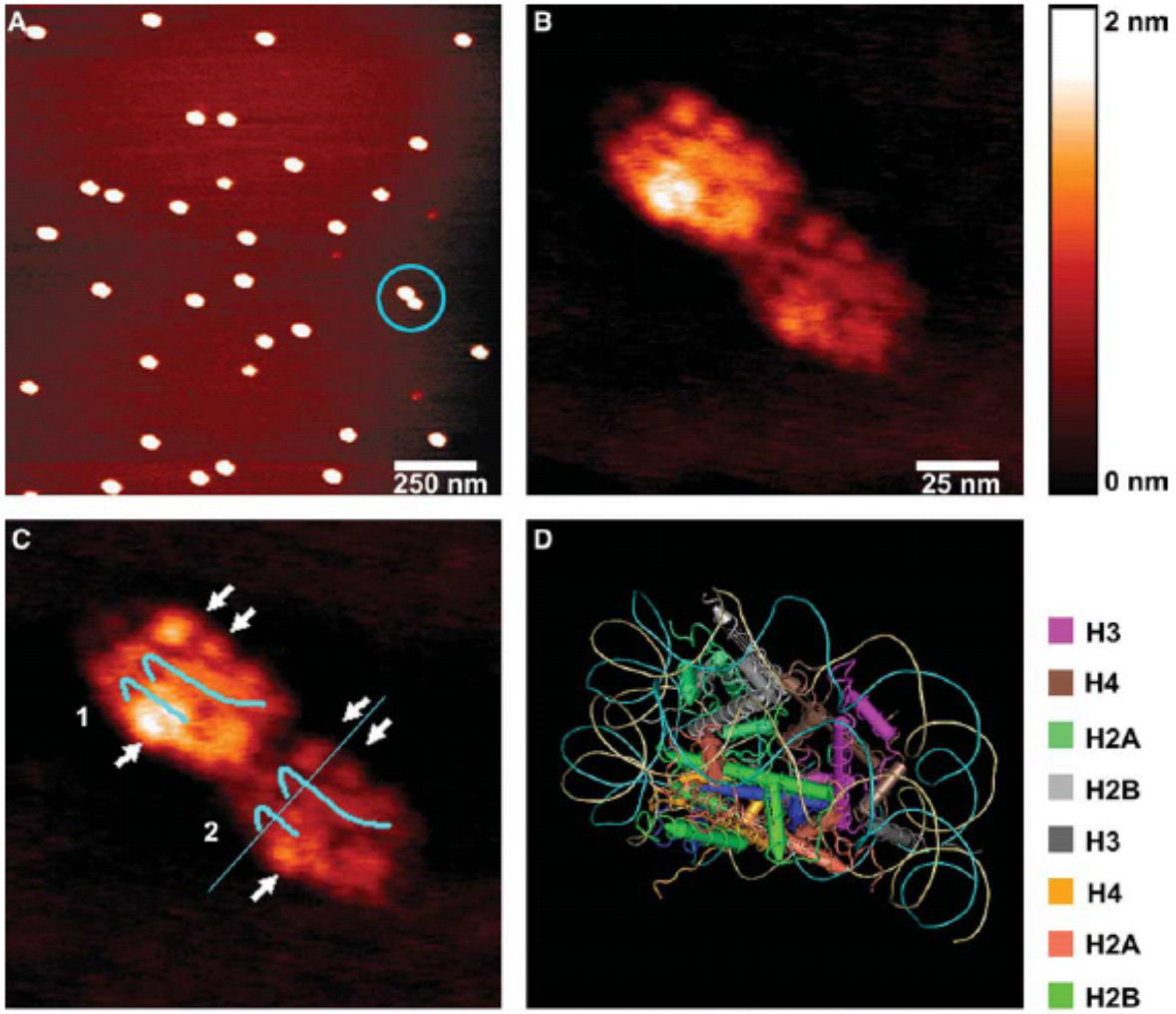

Davies et al. FEBS Lett. 579, 1702, 2005;
Richmond & Davey Nature 423, 145, 2003
Bovman Curr. Op. Struct Biol 20, 73, 2010.

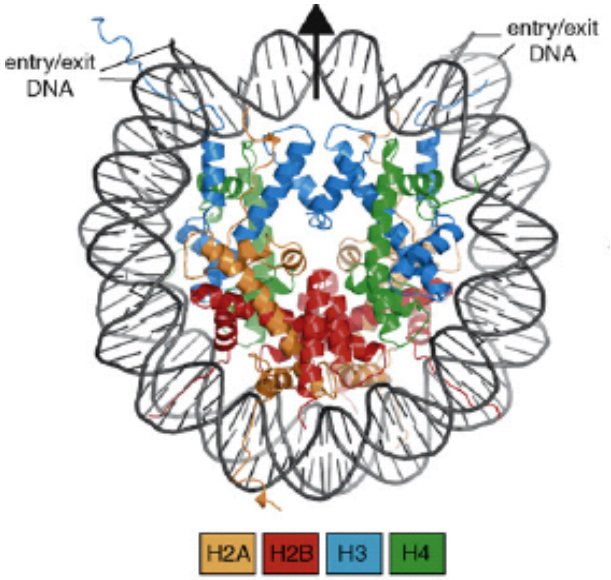

52. DNA AS FLEXIBLE ROD: PERSISTENCE LENGTH

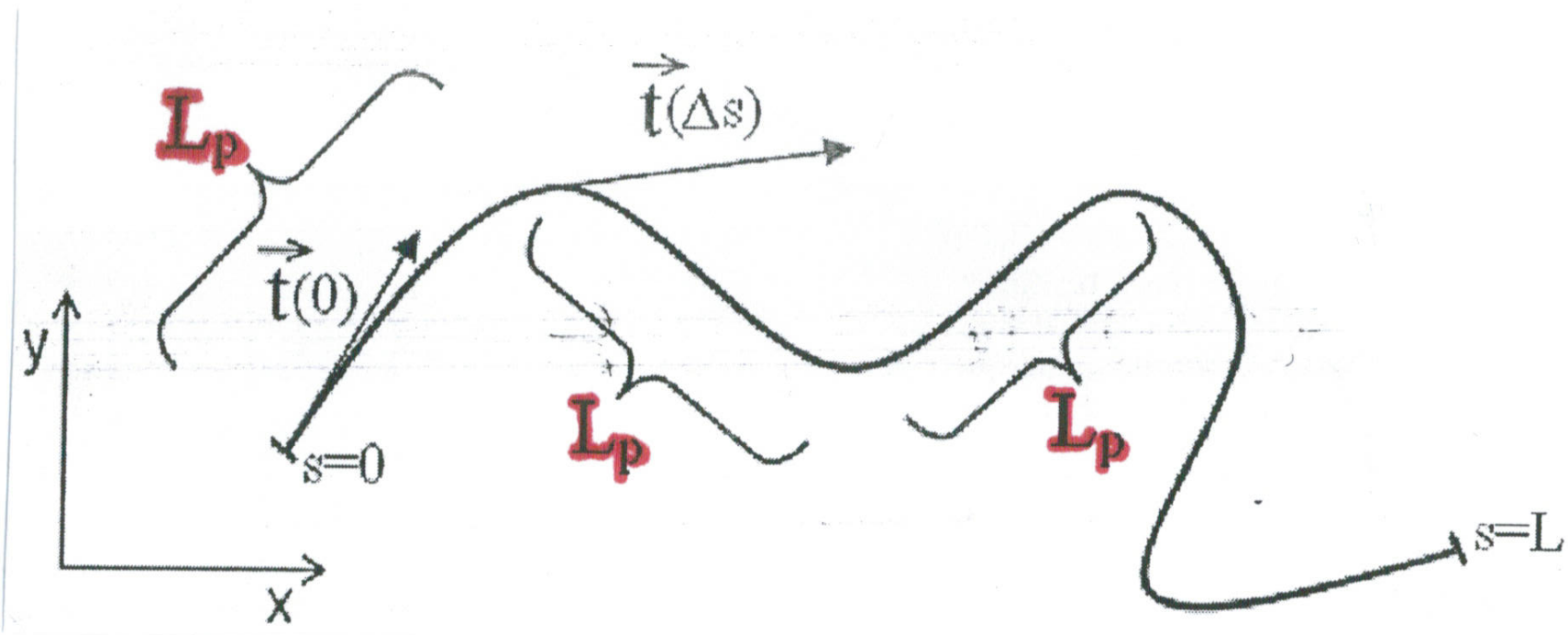

$$\left\langle \vec{t}(0)\vec{t}(s) \right\rangle = \exp\left(-\frac{s}{L_p} \right)$$

53. HELICAL TOPOLOGY

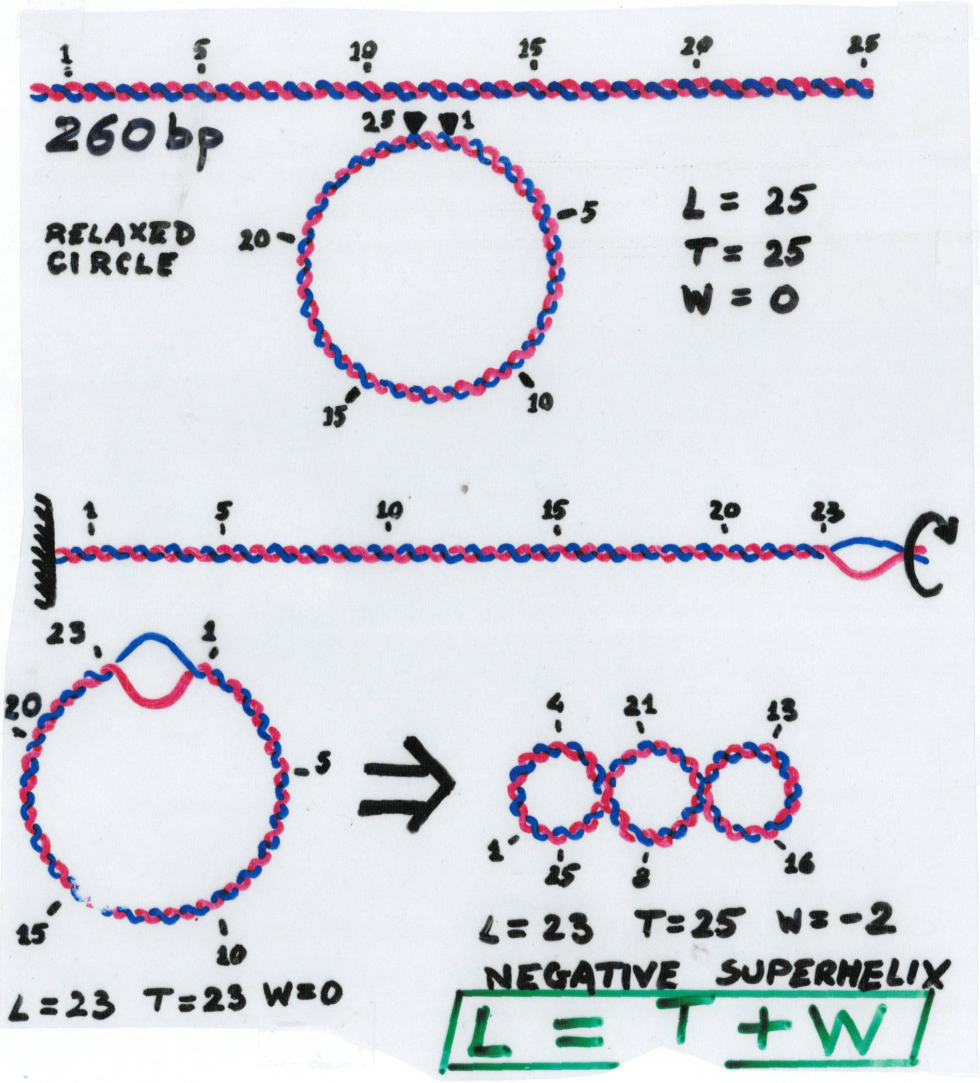

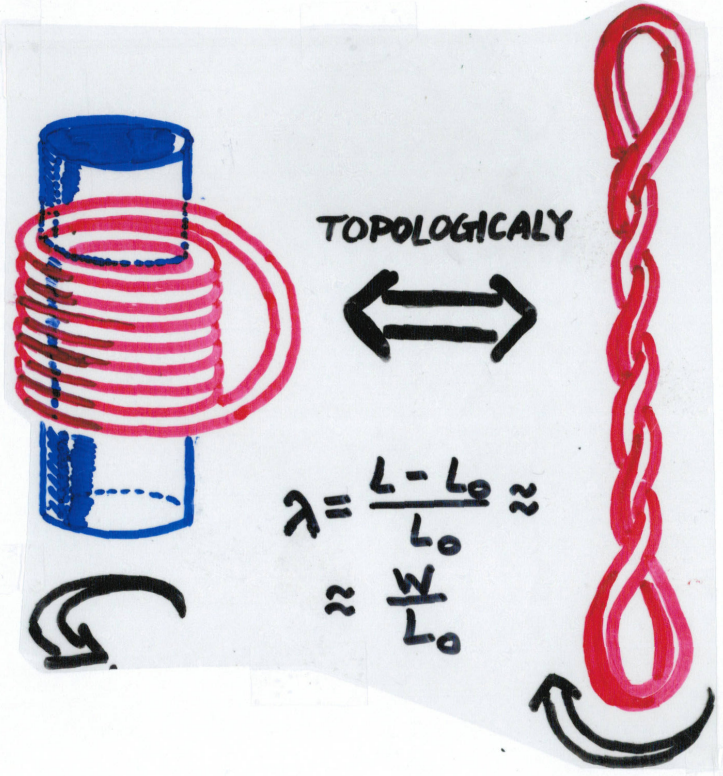

54. CHROMATIN FIBRE

Basset et al. Curr. Op. Gen. Develop 19, 159, 2009

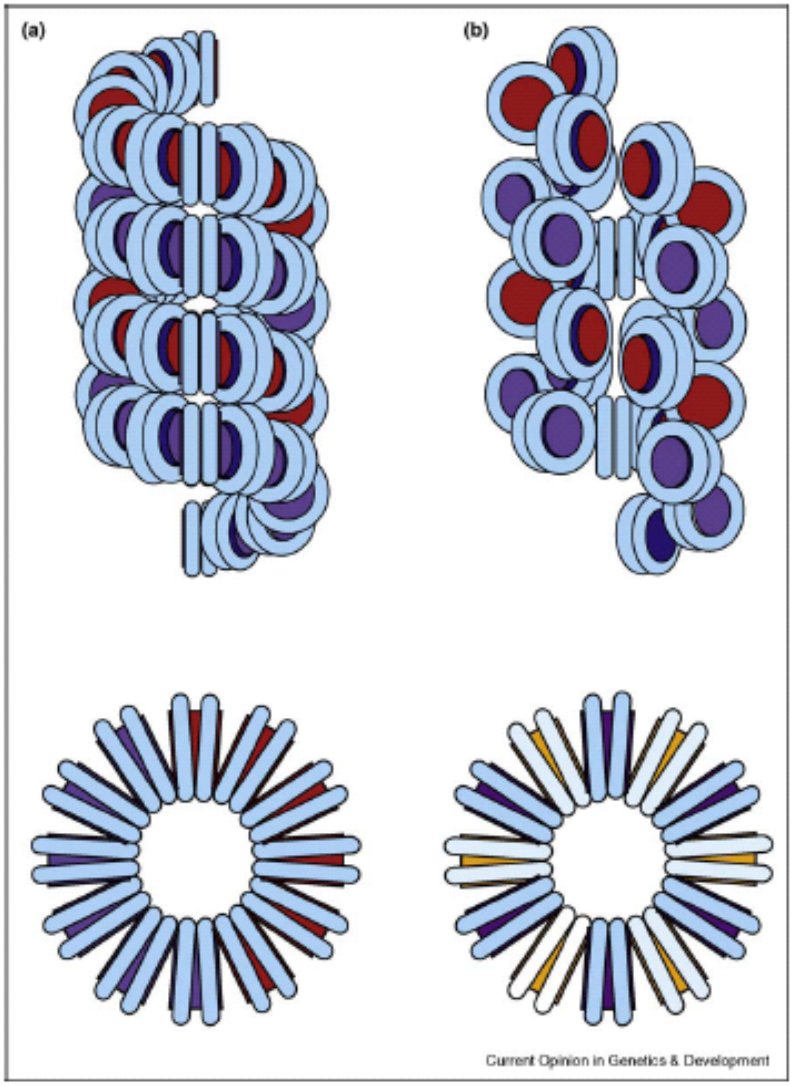

Schematic of nucleosome stacking organisation in 2-start fibres with a packing density of (a) 12 nucleosomes/11 nm and (b) 6 nucleosomes/11 nm. The figure shows the helical organisation in the top panels and the axial projection of the stack in the lower panels. The two helical stacks are distinguished by red and blue nucleosomes. The projection of (a) shows close packing of nucleosomes in each stack while that of (b) assumes the stacks are staggered relative to each other so that the blue stack is above the paler 'red' stack. For simplicity the nucleosomes are shown oriented parallel to the helical axis whereas in actuality they are tilted slightly.

55. ORGANISATION OF BACTERIAL CHROMOSOME

Wang et al. Nature Rev. 14, 191, 2013

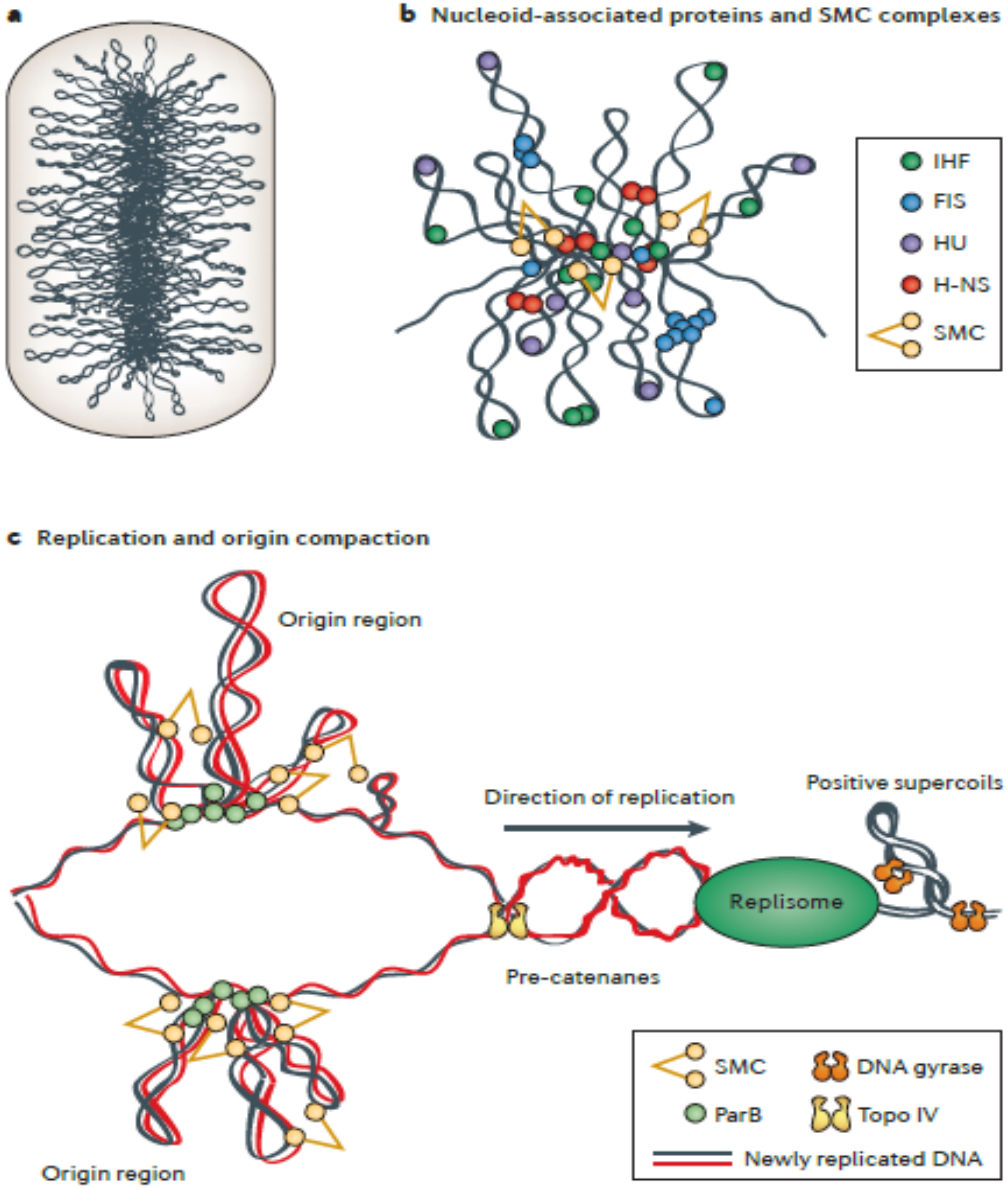

Figure 2 | **Topological organization of the bacterial chromosome.** **a** | Schematic representation of the bottlebrush model of the nucleoid. This diagram depicts the interwound supercoiled loops emanating from a dense core. The topologically isolated domains are on average 10 kb and therefore are likely to encompass several branched plectonemic loops. The macrodomains discussed in the main text are not depicted in this model. **b** | Schematic representation of the small nucleoid-associated proteins and the structural maintenance of chromosome (SMC) complexes. These proteins introduce DNA bends and also function in bridging chromosomal loci. **c** | The diagram depicts replication fork progression and compaction of the origin region. Replication generates positive supercoils ahead of the fork, which can diffuse behind the replisome, producing pre-catenanes. Positive supercoils are removed by DNA gyrase and topoisomerase IV (Topo IV), and pre-catenanes are unlinked by Topo IV. Newly replicated origin regions are thought to be compacted by the SMC complexes that are recruited to the origin by ParB and by the action of small nucleoid-associated proteins (not shown).

56. THE HIERARCHY OF THE EUKAYOTIC GENOME

Gibcus & Deccer Mol. Cell 49, 773, 2013

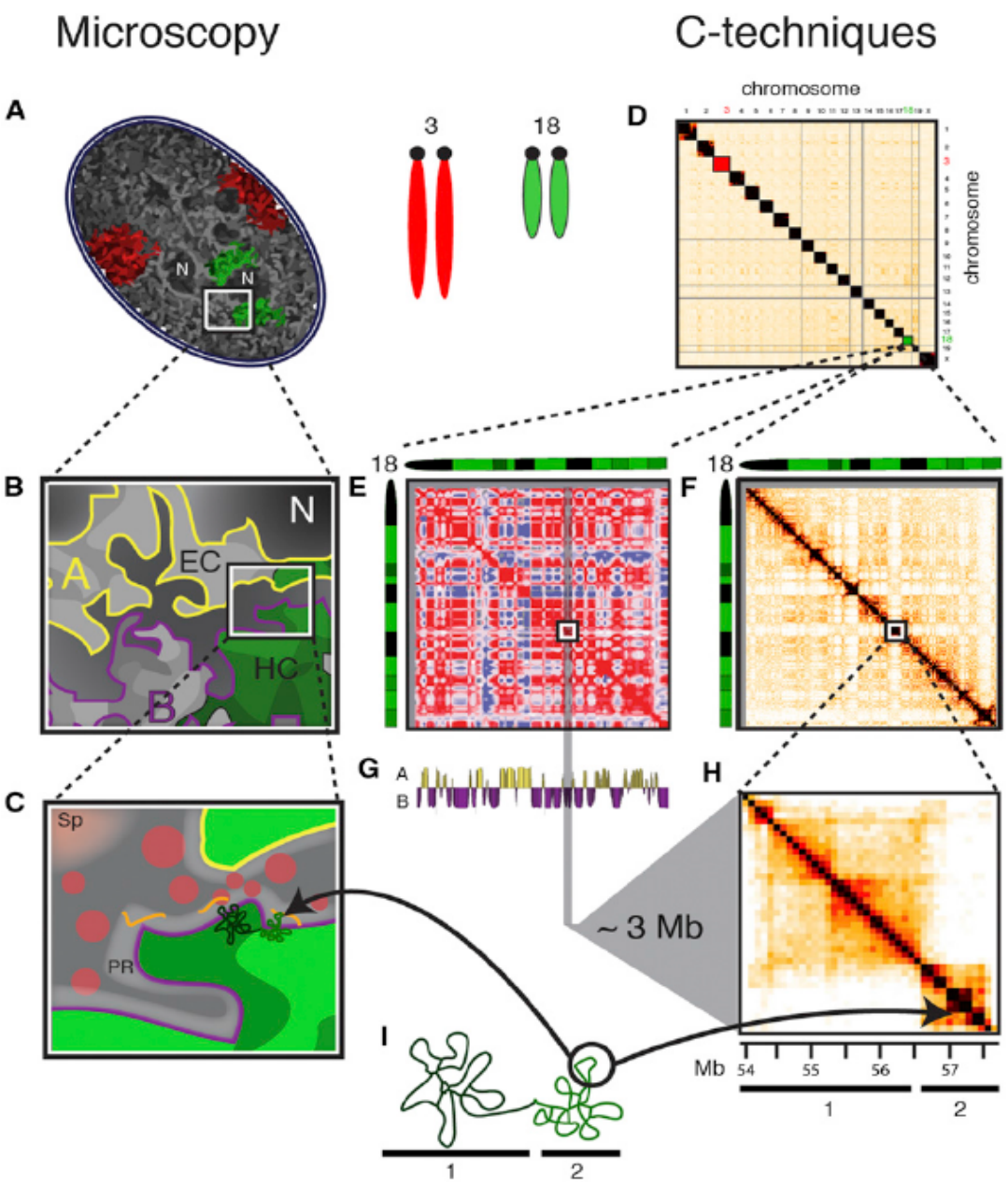

Figure 1. Large-Scale Nuclear Organization in Mammals

(A) The nucleus is composed of chromosome territories (for example, mouse chromosome 3 and 18 are depicted in red and green, respectively). DNA is organized in more or less condensed regions, as can be shown by DAPI staining (gray intensities). Nucleoli (N) are visible as dark spots (top inset).

(B) Inset shows a more detailed architecture of the nucleus with compartments (A and B), heterochromatin (HC), and euchromatin (EC) surrounding the interchromatin compartment.

(C) Zoomed-in view of chromosomal domains (hypothetical). Foci of factors interacting with looping chromatin in the perichromatin region (PR) are shown as pink circles, and RNA is shown as orange lines. The larger speckles (SP) are located in domains that are sparser in chromatin content and further away from the PR.

(D) All-by-all chromosome matrix showing the interactions within and between chromosomes.

(E) Red and blue "plaid" pattern of chromosome 18 emphasized through Pearson correlation shows the separation into two chromosomal domains (represented as red and blue).

(F) Detailed version of (D), sized equivalent to E, showing the *cis*-interaction matrix for chromosome 18. The inset indicates a ~3 Mb large B compartment.

(G) The clustering into compartments A and B after principal component analysis on the plaid pattern displayed in (E).

(H) Detailed version of the 3 Mb large B compartment from (F), revealing the organization of TADs (1 and 2).

(I) Representation of looping of chromatin as can be found at the PR (see C) or in deeper structures within TADs (see H). Nuclei were modeled to match Hi-C plots, which were adapted to scale from previously published data (Zhang et al., 2012).

57. 50Kbp DOMAIN OF HUMAN CHROMOSOME 16

Baker Nature 470, 289, 2011

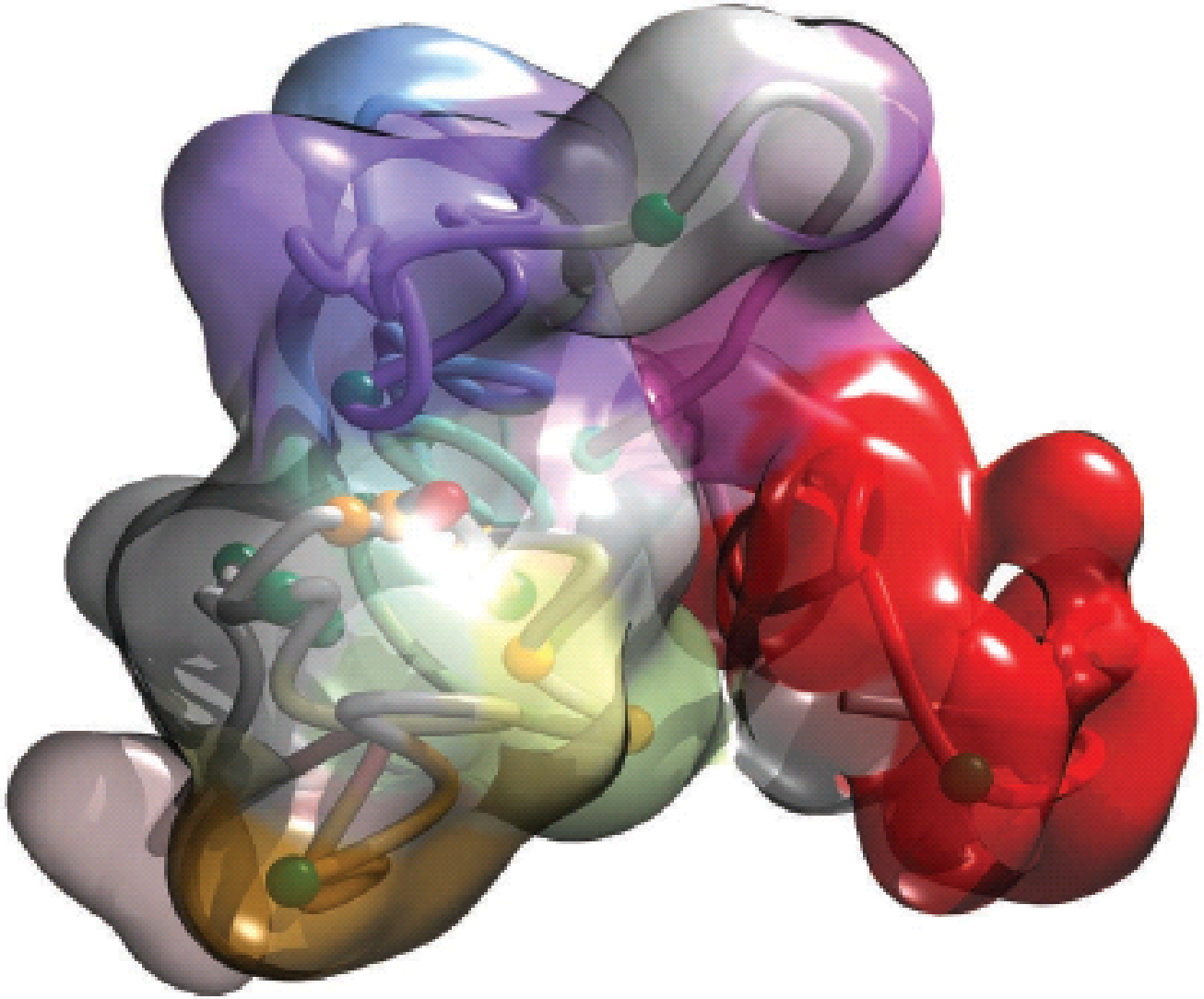

58. CHROMOSOME CONFORMATION CAPTURE METHODS

Davies et al. Nature Methods 14, 125, 2017

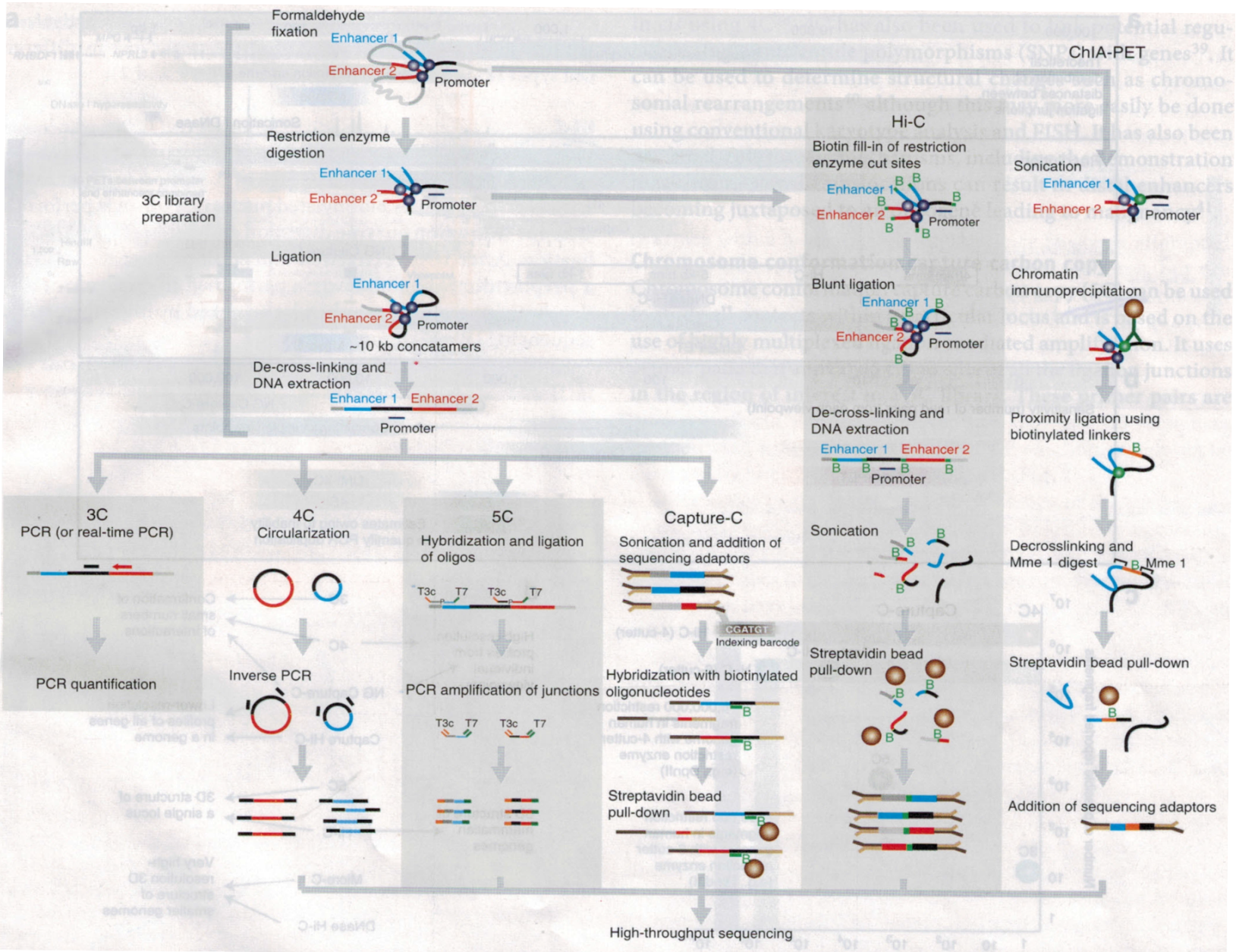

59. G - QUADRUPLEXES

Brooks et al. FEBS J. 277, 3459, 2011

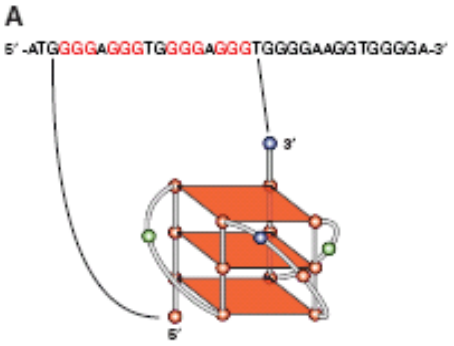

Single G-quadruplex structure
c-Myc
Class I

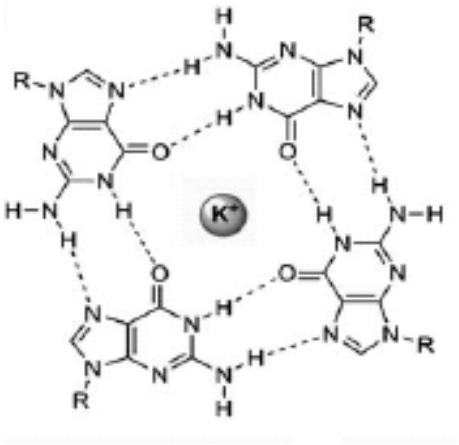

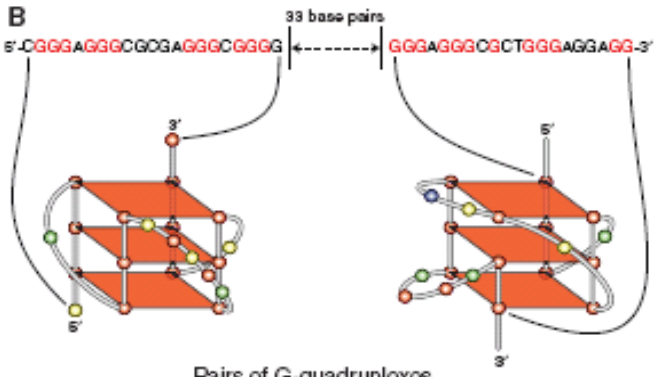

Pairs of G-quadruplexes
separated by about 30 bases
c-Kit
Class II

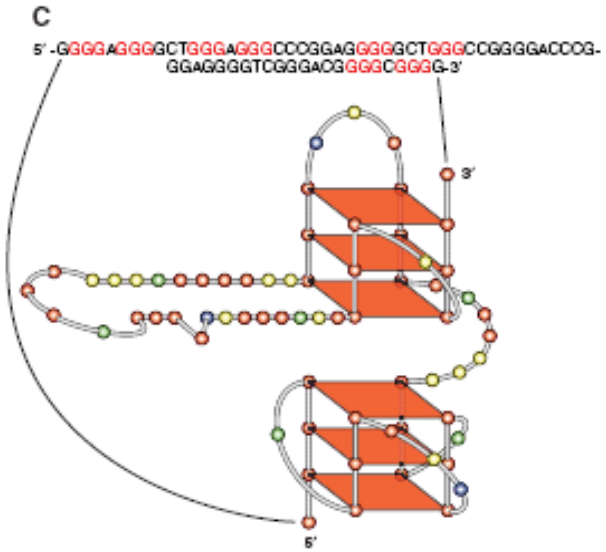

Pair of tandem G-quadruplexes having
intermolecular interactions
hTERT
Class III

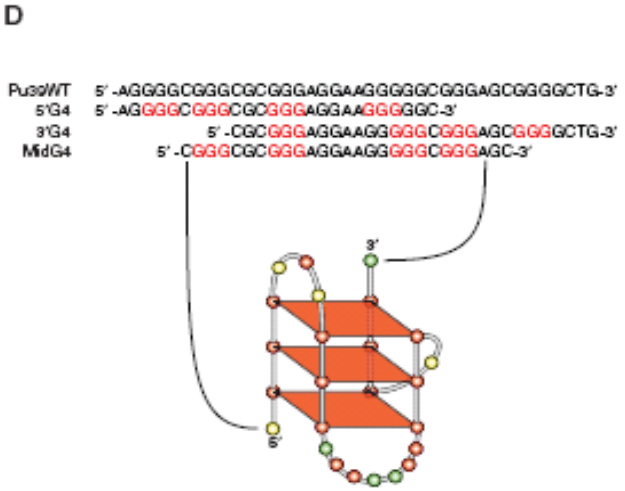

Multiple overlapping G-quadruplexes
(5′G4, MidG4, 3′G4)
Bcl-2
Class IV

60. C - QUADRUPLEXES

Class I

		N_2		$N_{3/4}$		N_2			Transitional pH
VEGF:	5′- CCC	GC	CCC	CGG	CCC	GC	CCC	-3′	5.8
RET:	5′- CCC	GC	CC	CGC	CCC	GC	CC	-3′	6.4
Rb:	5′- CC	GC	CC	AAAA	CC	CC	CC	-3′	5.9

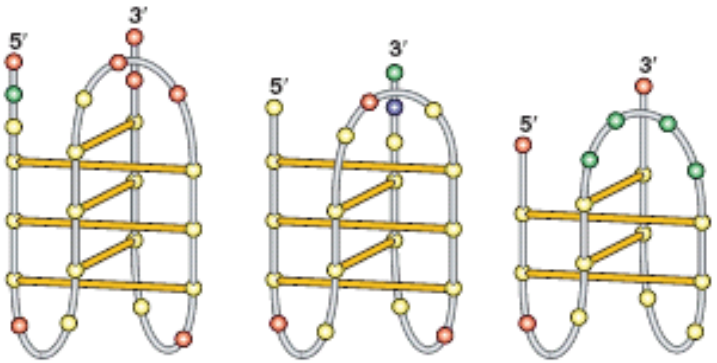

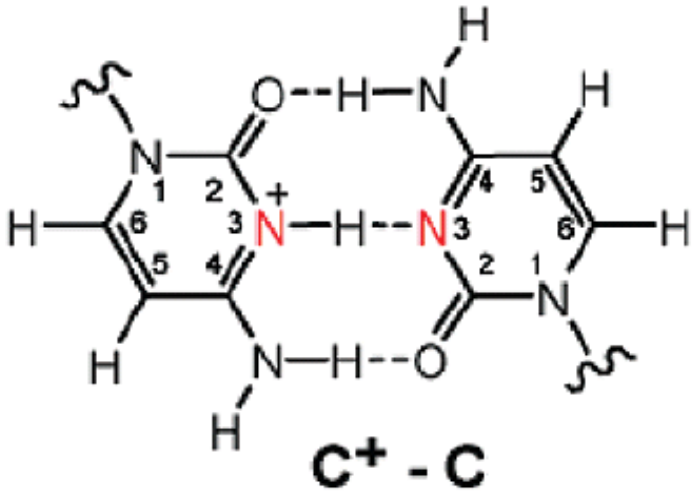

Class II

		$N_{6/8}$		$N_{2/5}$		$N_{6/7}$			Transitional pH
c-Myc:	5′- CCC	CACCTT	CCC	CA	CCC	TCCCCA	CCC	-3′	6.6
Bcl-2:	5′- CCC	GCTCCCGC	CCCC	TTCCT	CCC	GCGCCCG	CCCC	-3′	6.6

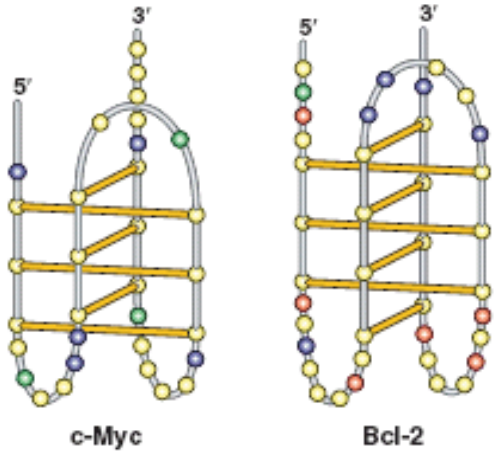

Brooks et al. FEBS J. 277, 3459, 2011

61. TAUTOMERISM AND MUTAGENESIS

Topal & Fresco Nature 263, 285, 1976

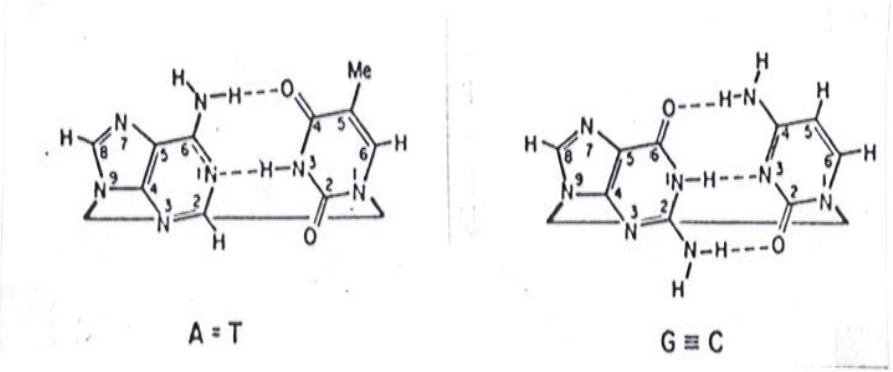

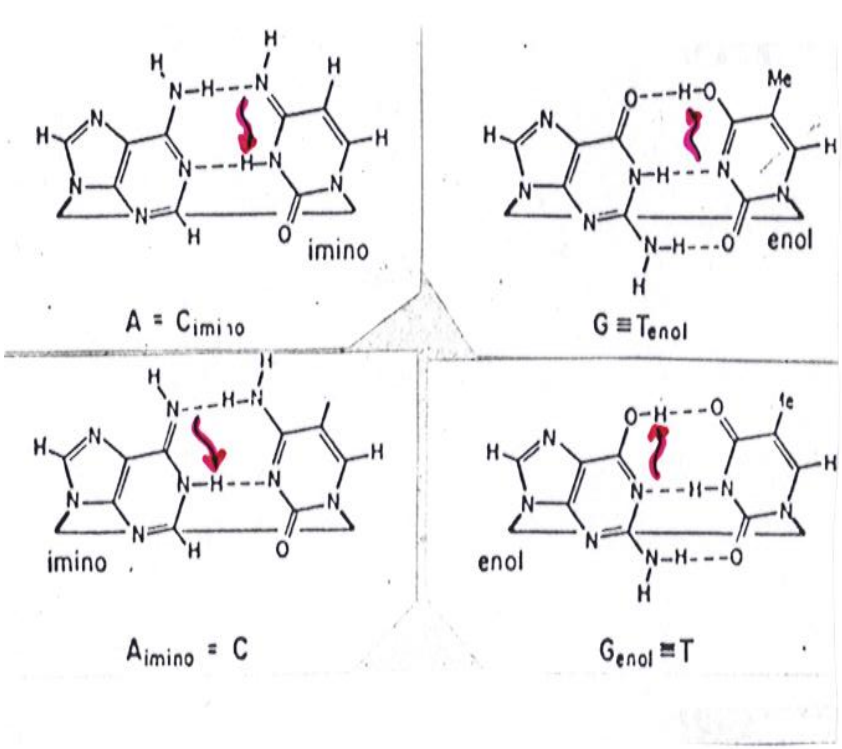

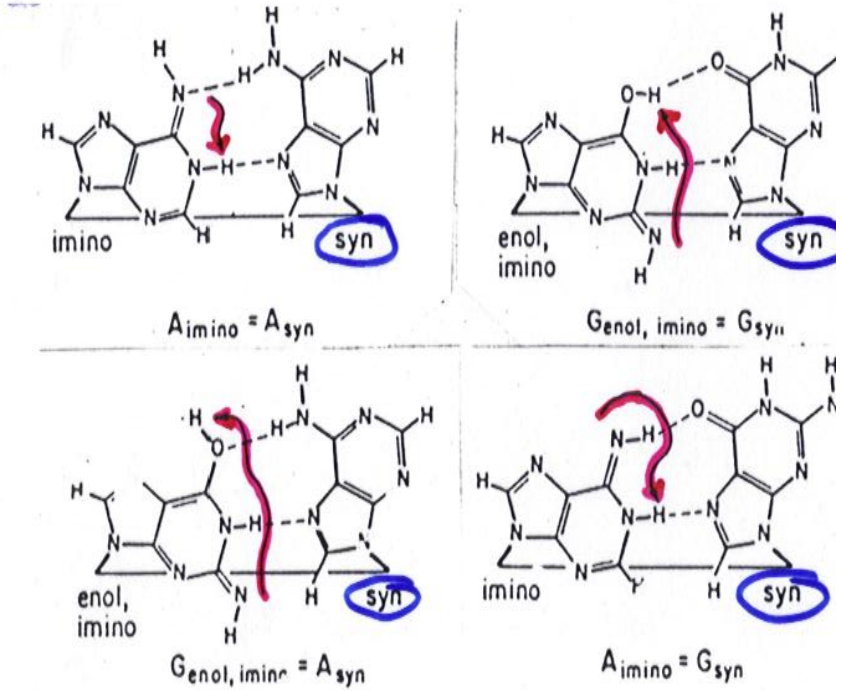

62. BASICITY METHOD

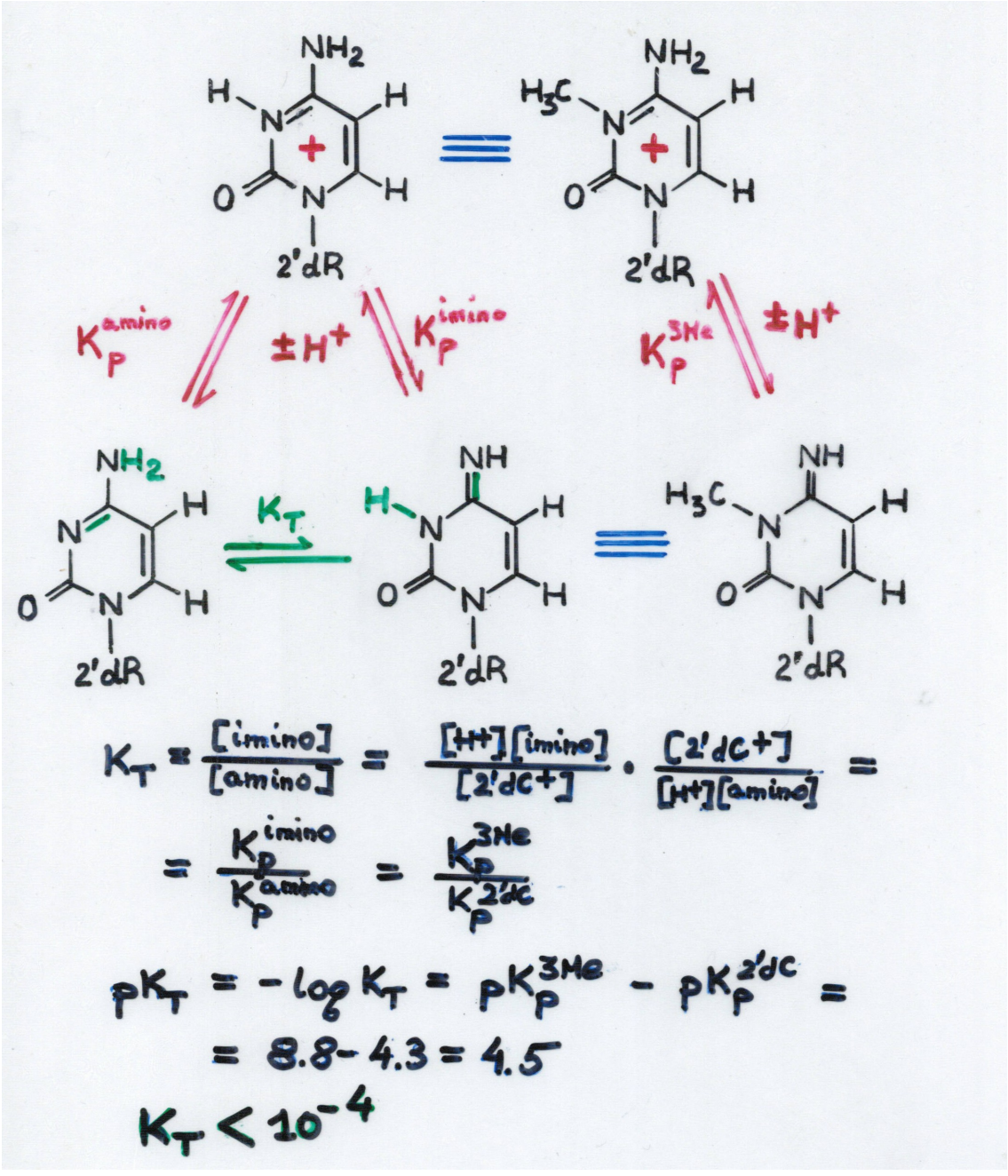

$$K_T = \frac{[\text{imino}]}{[\text{amino}]} = \frac{[H^+][\text{imino}]}{[2'dC^+]} \cdot \frac{[2'dC^+]}{[H^+][\text{amino}]} =$$

$$= \frac{K_P^{\text{imino}}}{K_P^{\text{amino}}} = \frac{K_P^{3Me}}{K_P^{2'dC}}$$

$$pK_T = -\log K_T = pK_P^{3Me} - pK_P^{2'dC} =$$

$$= 8.8 - 4.3 = 4.5$$

$$K_T < 10^{-4}$$

63. IR SPECTRUM OF 9-CH_3-GUANINE IN ARGON MATRIX

Szczepaniak et al. Chem. Phys. Lett. 153, 39, 1088

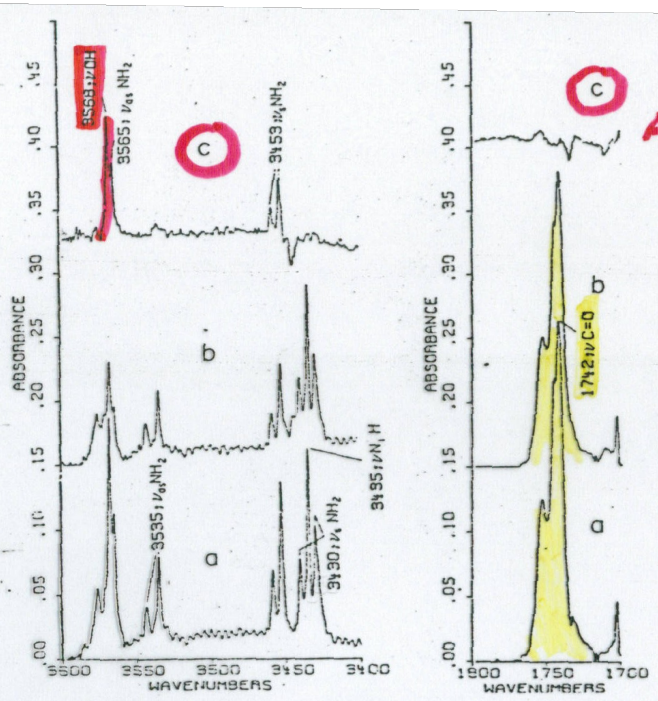

Fig. 1. IR spectrum of 9MG in Ar matrix (15 K). 3600–3400 and 1800–1700 cm^{-1} region. (a) Spectrum after deposition (with marked frequencies and assignment of the main bands of (a-o) tautomer (ν, stretching; δ, bending; r, ring; Ro, rocking; γ, out-of-plane modes). (b) Spectrum of the same sample after UV irradiation (16 h). (c) Spectrum for the (a-h) tautomer (with marked frequencies and assignment of the main bends) obtained by subtraction of spectrum (b) (absorbances scaled by 1.16) from spectrum (a). Scaling factor 1.16 accounts for 16% decrease of the absorbance of the (a-o) form accompanying 50% decrease of the absorbance of the bands of the (a-h) form after UV irradiation. The band with negative absorption appear after UV irradiation.

$$K_T = \frac{[oxo]}{[hydroxy]} = 1.2$$

64. C:A$^+$ BASE PAIRING IN 12-bp DNA DOUBLE HELIX d[CGCAAATTCGCG]$_2$

Hunter et al. Nature 320, 552, 1986

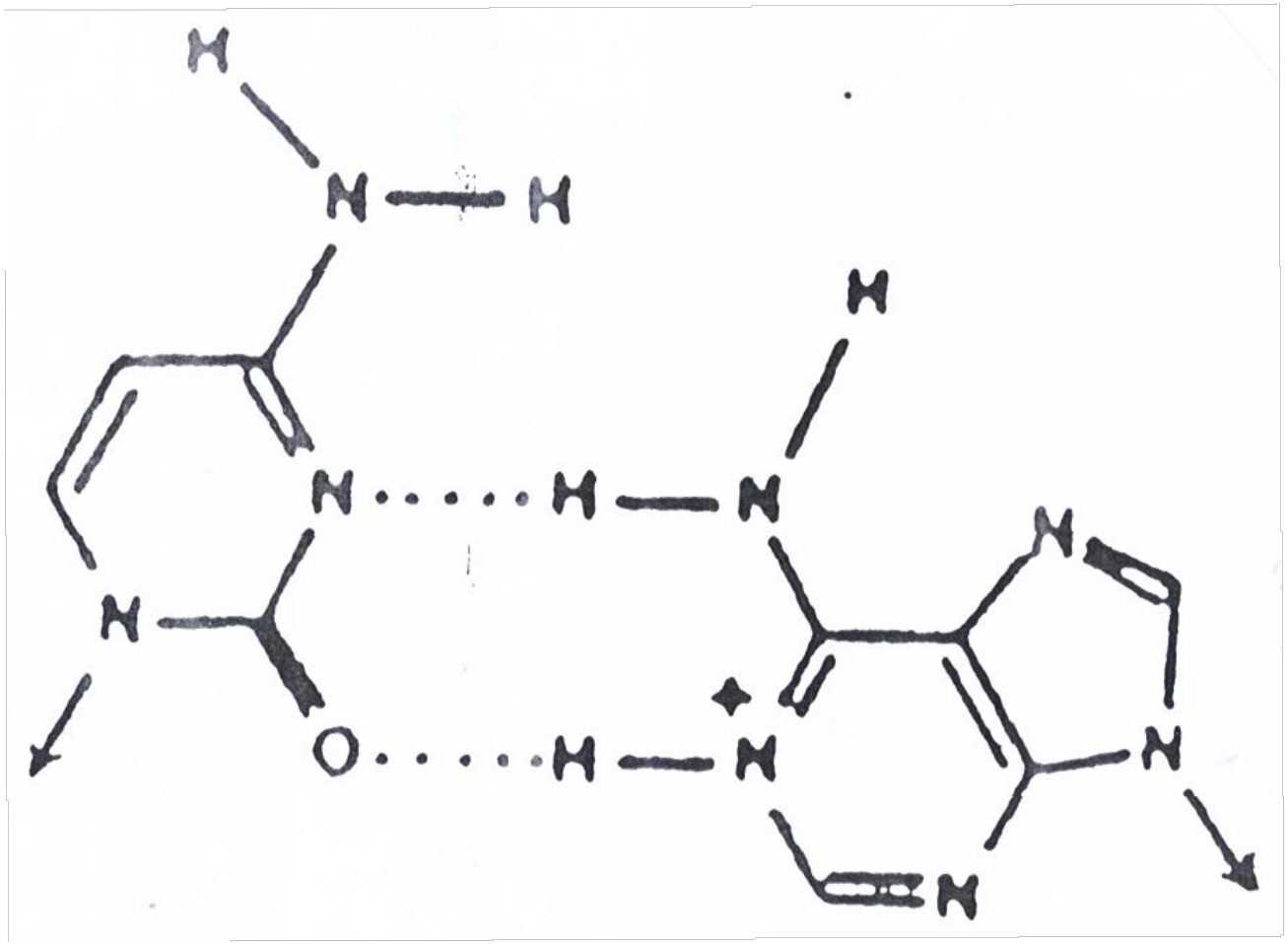

65. ADENINE : DIFLUOROTOLUEN PAIRING

Kool et al. Biopolymers 48, 3, 1998

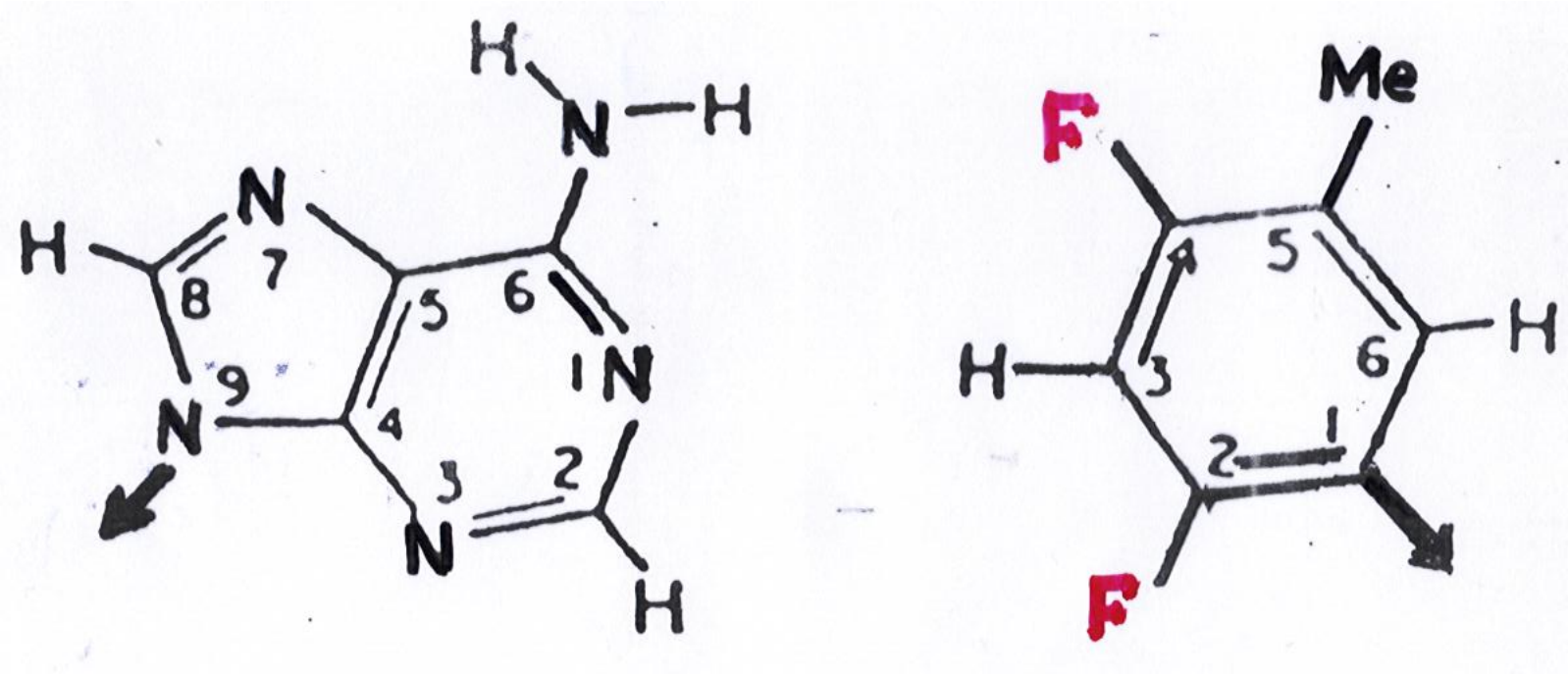

Nucleoside triphosphate	Template base	V_{max}/K_m *E. coli* DNA pol I (Kf)
TTP	A	1
dFTP	A	2.5×10^{-2}
dFTP	G	1.7×10^{-6}

66. WOBBLE G:T PAIRING; SUPERPOSITION OF $d[GGGTGCCC]_2$ AND $d\{GGGCGCCC]_2$

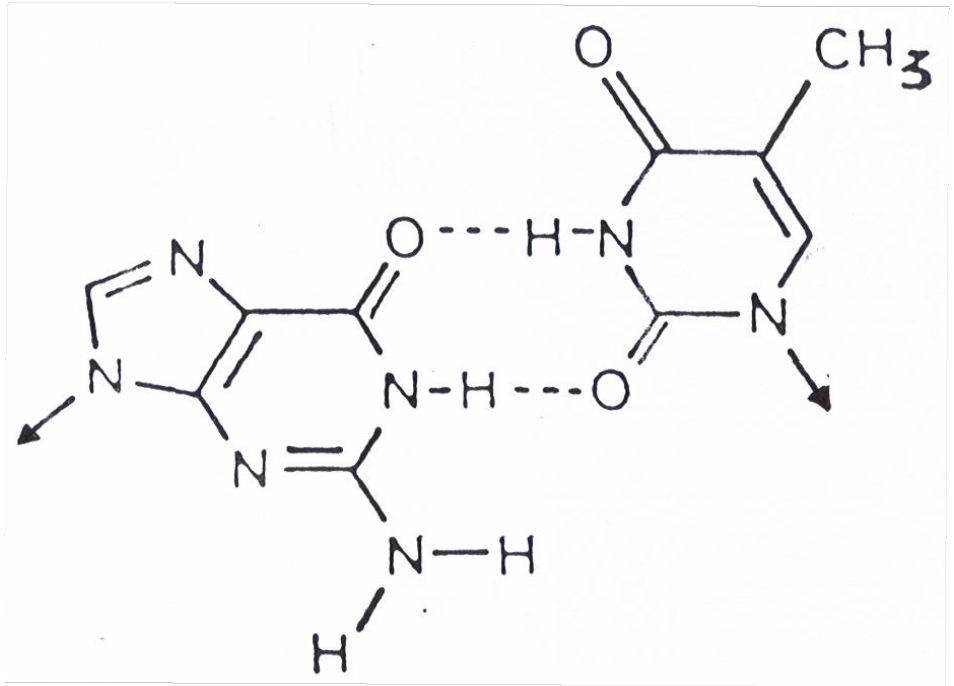

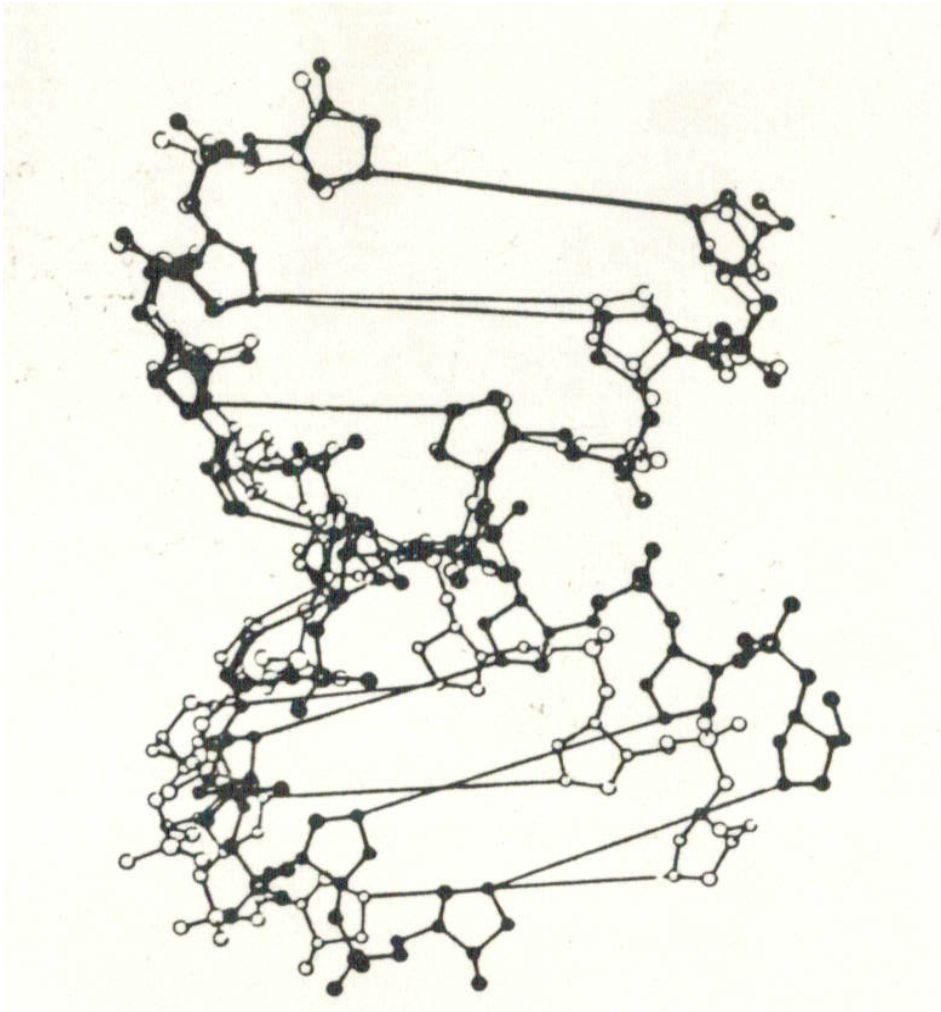

Kneale et al. J. Mol. Biol. 186, 805, 1985

67. THE HALLMARKS OF CANCER

Hanahan & Weinberg Cell 144, 646, 2011

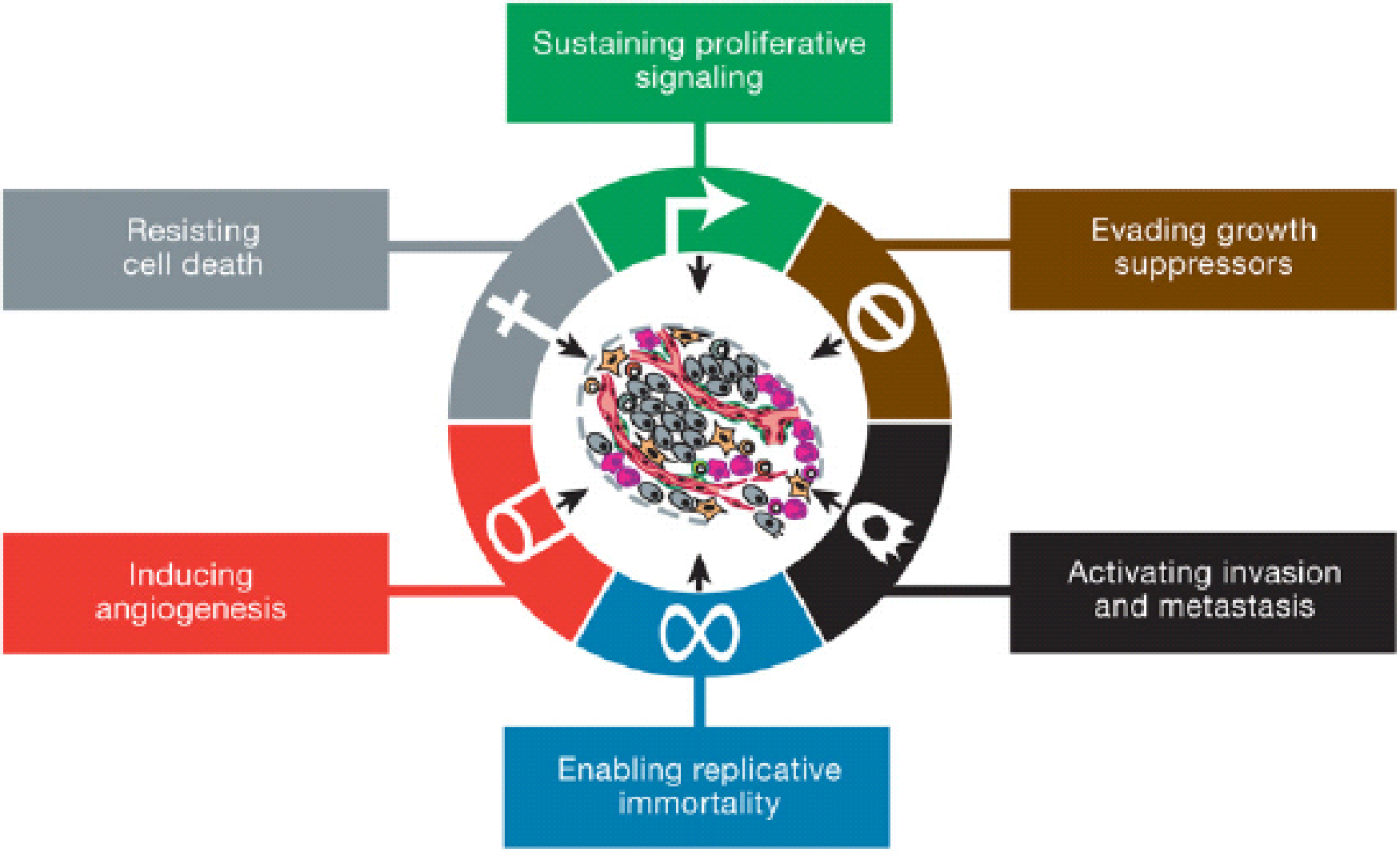

68. INTERCALATION OF HELICAL DNA

Jagiełło et al. Postępy Biochemii 56, 341, 2010

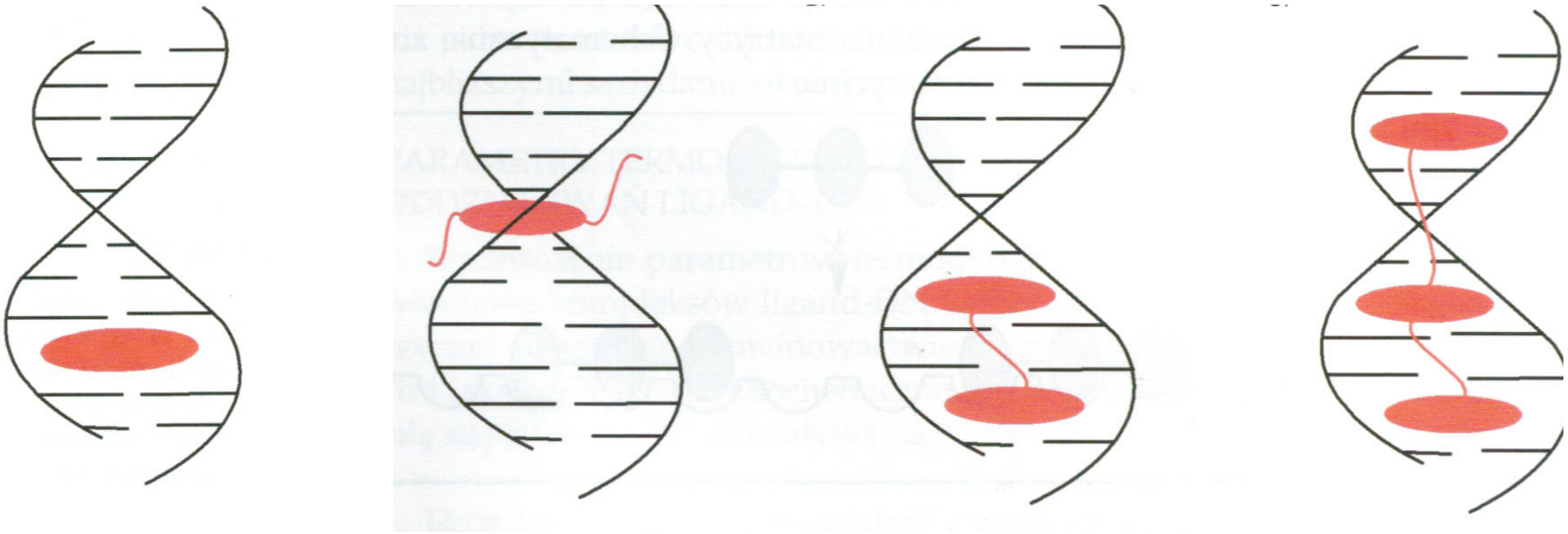

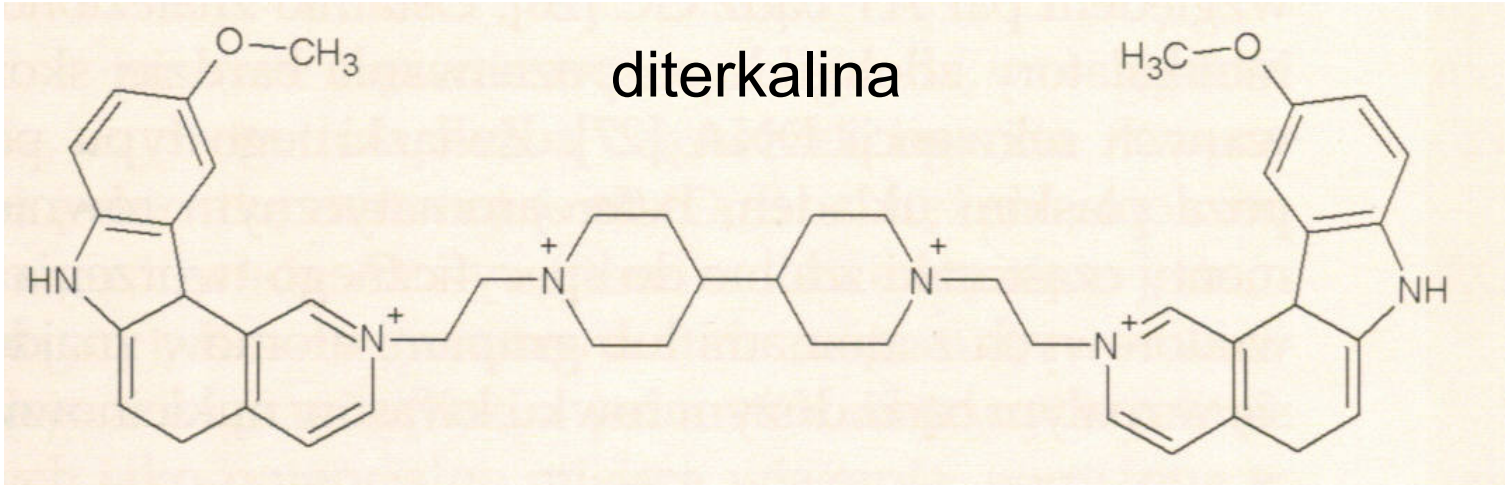

69. DNA DAMAGE REPAIR PATHWAYS

Hakem et al. EMBO J. 27, 589, 2008

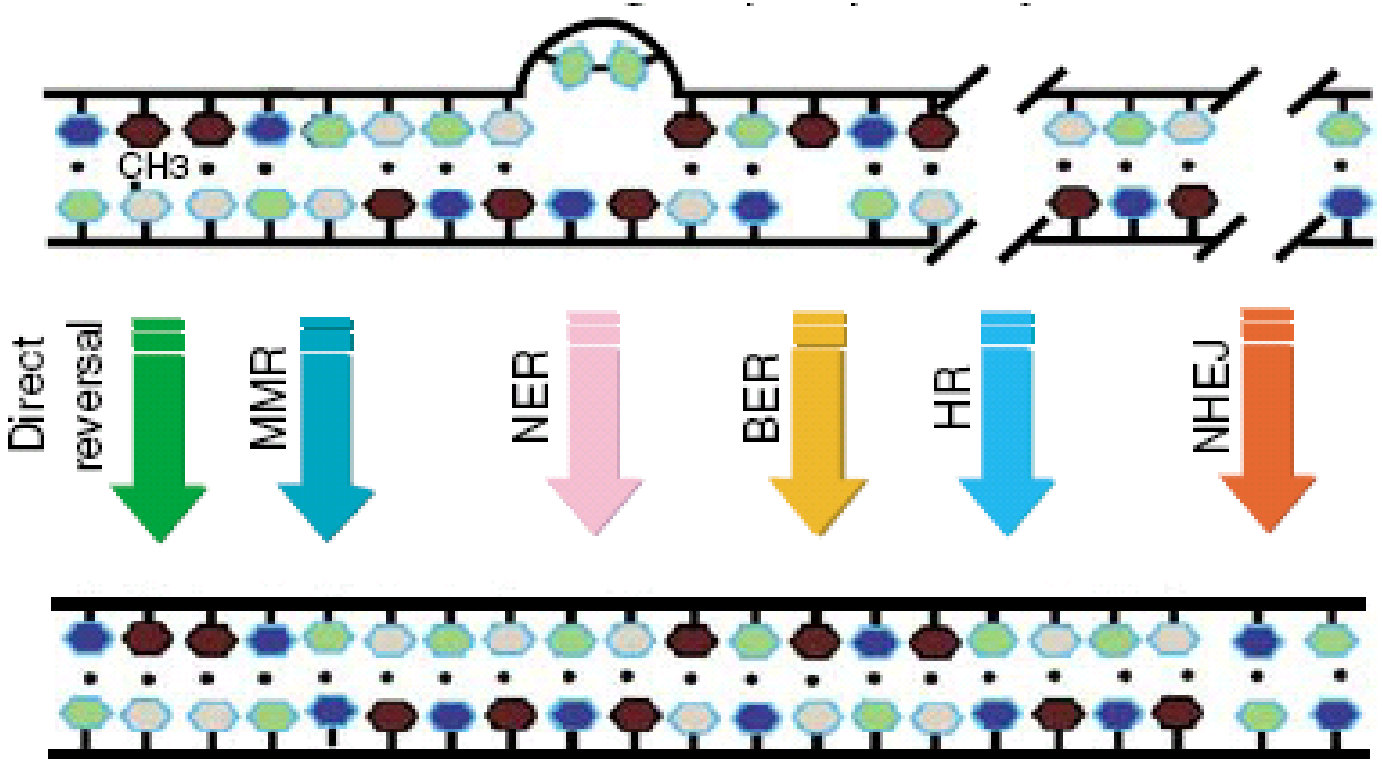

Figure 1 DNA-repair pathways. Several DNA-repair pathways exist and deal with various types of DNA insults. These pathways include (1) the direct reversal pathway, (2) the MMR pathway, (3) the NER pathway, (4) the BER pathway, (5) the HR pathway, and (6) the NHEJ pathway.

70. URACIL - DNA GLYCOSYLASE BOUND TO DNA

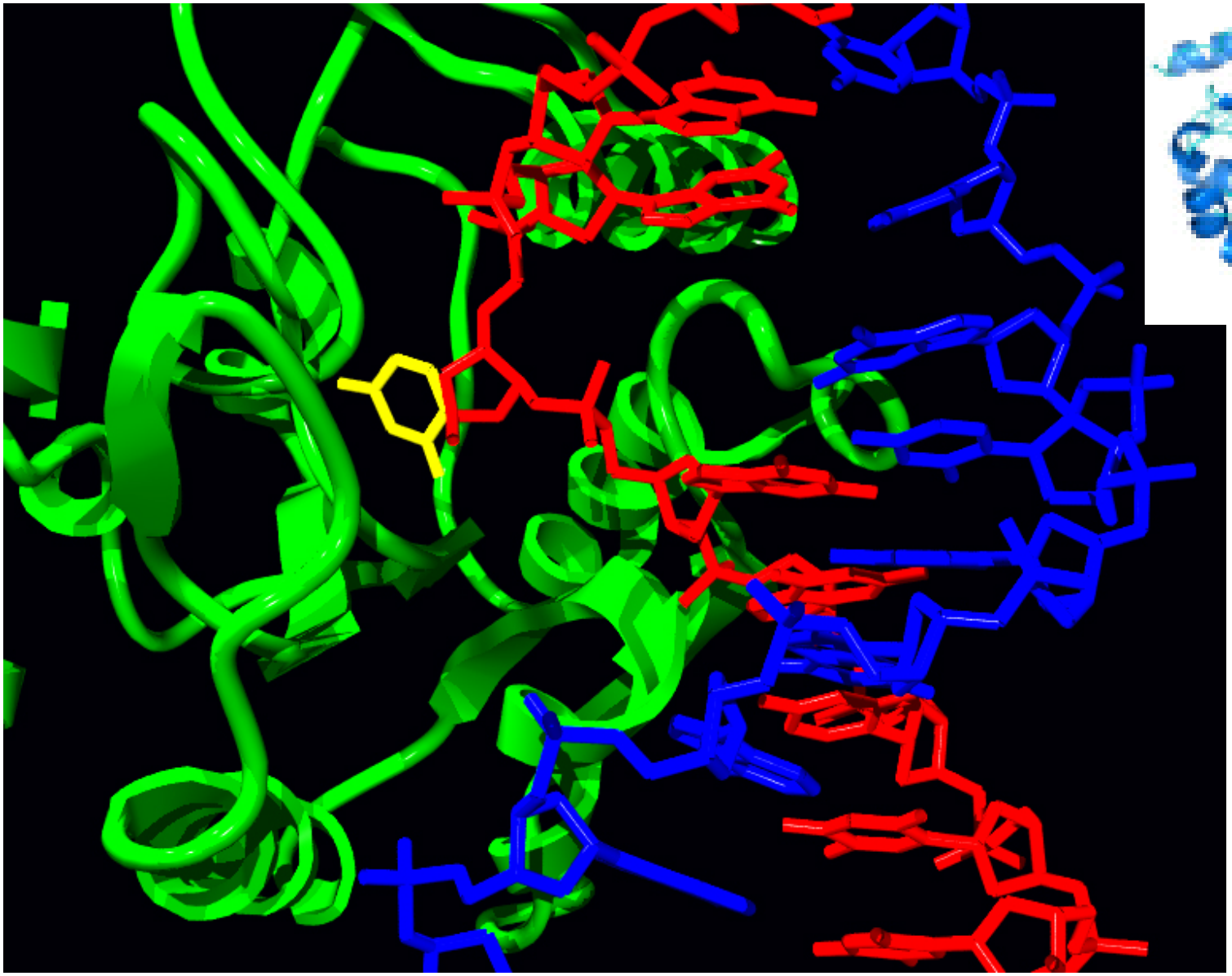

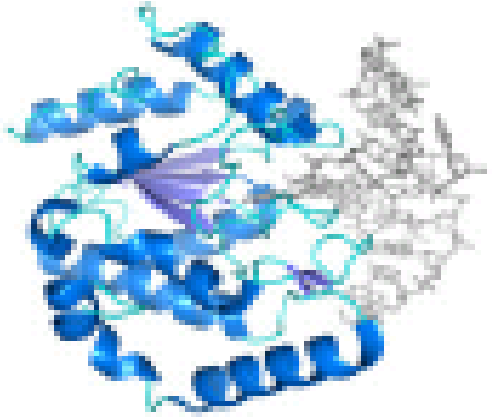

Slupphaug et al. Nature 384, 87, 1996

71. NANO-DNA BUILDING BLOCKS DX

Shih & Lin Curr. Op. Struct. Biol. 20, 276, 2010

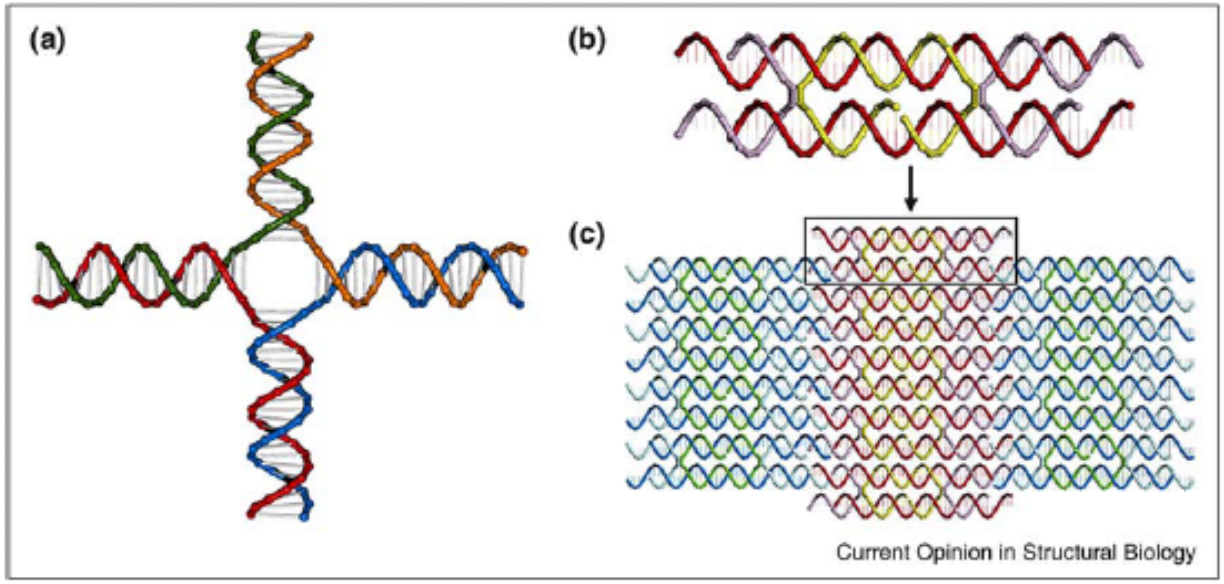

Branched DNA molecules as basic building blocks for nanoconstruction. **(a)** A Holliday junction is formed by four DNA oligonucleotides each pairing with its neighboring two partners. **(b)** An antiparallel double-crossover molecule with single-stranded overhangs is formed by five DNA oligonucleotides. It can be conceptualized as two parallel DNA double helices brought together through strand exchange at junction points. **(c)** A two-dimensional array assembled from the molecule shown in (b) through base paring between the single-stranded overhangs. Note the green-tinted molecules are identical to the red-tinted ones but rotated 180° in the plane of the page.

72. NANO-DNA STRUCTURES

Endo & Sugiyama ChemBiochem 10, 2420, 2009

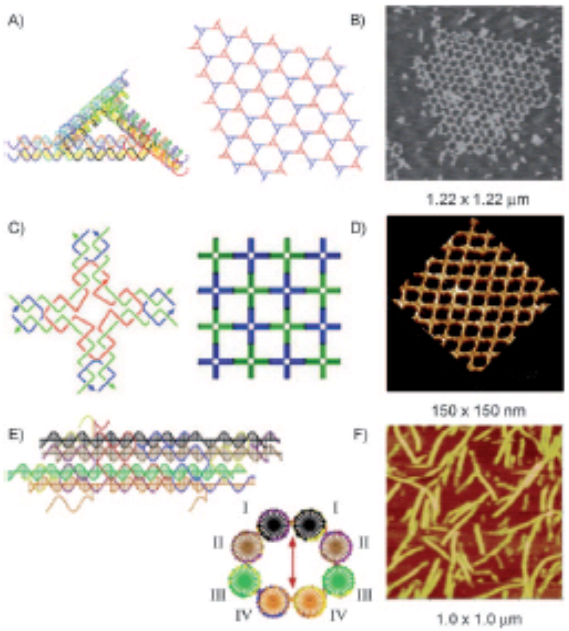

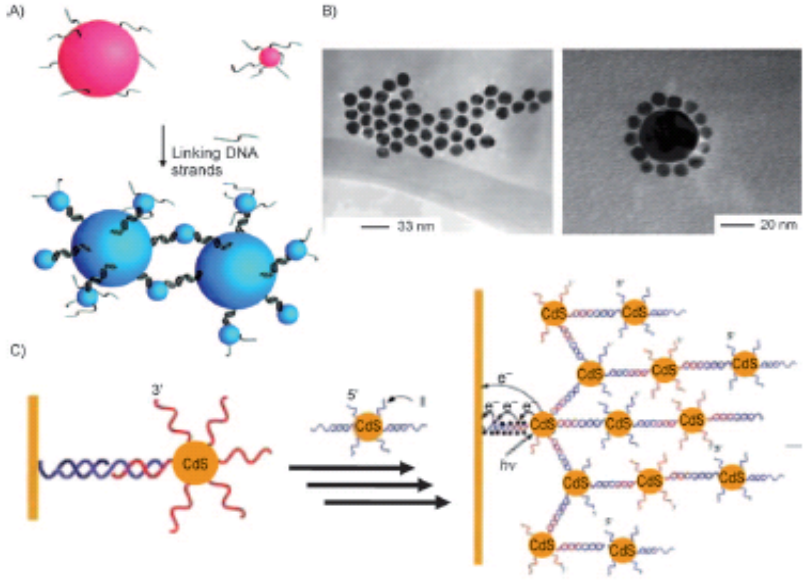

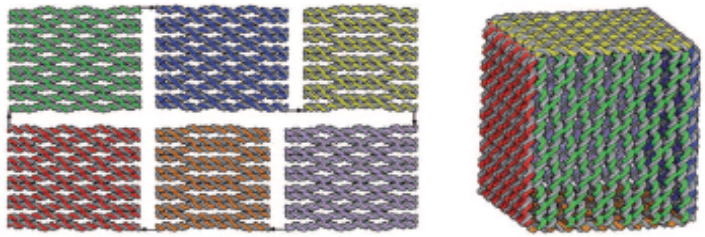

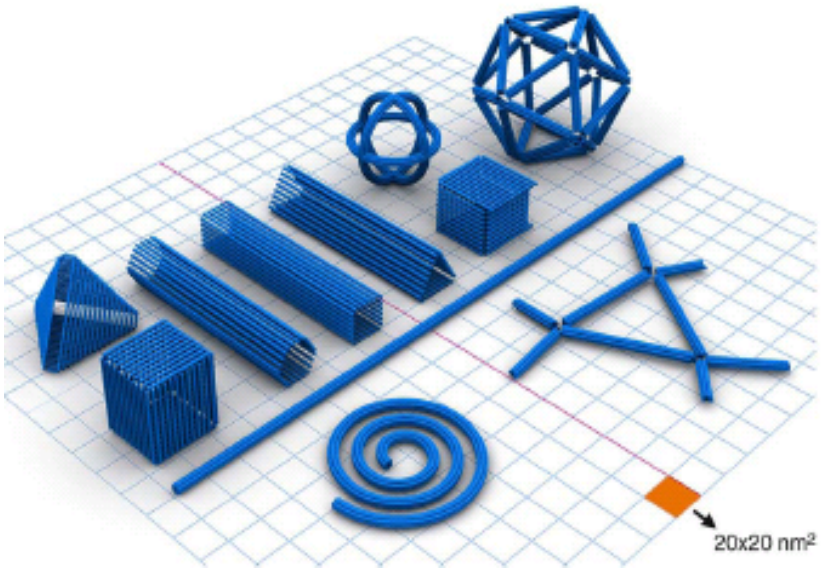

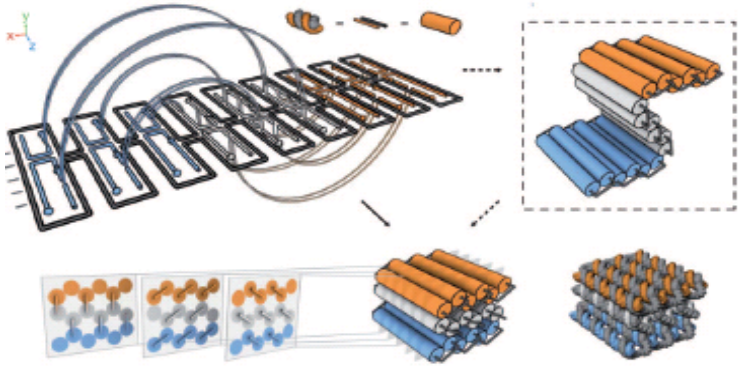

73. PROTEOMICS

(I) Identification of the proteins expressed in the cell, tissue, and/or the whole organism by means of (mainly) mass spectrometry (MS)

- **determination of the primary structure (sequencing)**
- **quantitative characteristics of the proteins expressed in the cell, *e. g.* heavy isotope labelling (SILAC, iTRAQ)**
- **characteristics of post-translational modifications.**

(II) Determination of the 3D protein structures (structural proteomics):

- **obtaining suitable amounts of the protein by overexpression in various cells (bacteria) or in cell-free systems:**
  - **(a) containing selenometionine: X-ray diffraction in the synchrotron beam and solution of the phase problem by anomalous scattering (MAD, SAD)**

    OR

  - **(b) double labelled $^{15}N/^{13}C$ and/or tripple labelled $^{2}H/^{15}N/^{13}C$ (larger proteins): multidimensional nuclear magnetic resonance, 2D, 3D and 4D NMR**
  - **(c) data base search for the proteins of known structures and high sequence homology for computer homology modelling; *de novo* folding**
- **preparation of the protein specimen: crystallization (X-ray diffraction) or attaining suitable solubility in water buffers and diluted micellar solutions (NMR)**
- **resolving the structure: molecular model building of the protein and its verification.**

(III) Determination and visualization of the protein interactom (PPI) by means of specific methods: AP-MS in yeast, TAP for membrane proteins, Tango, F/BRET, LUMIER

74. MS – BASED PROTEOMICS WORKFLOW

Altelaar et al. Nature Rev. Gen. 14, 35, 2013

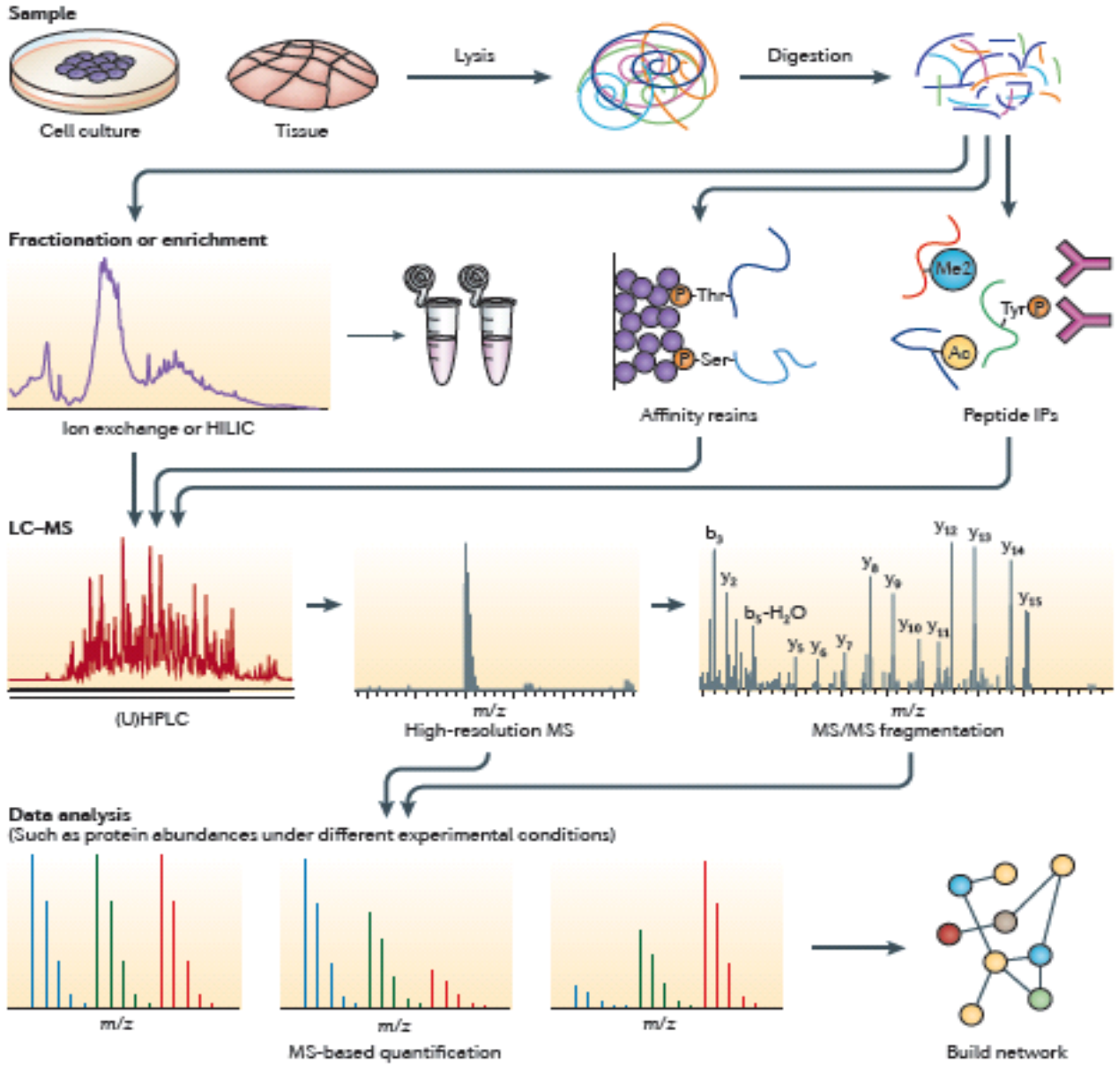

75. PROTEIN CRYSTAL AND ITS DIFFRACTION PATTERN

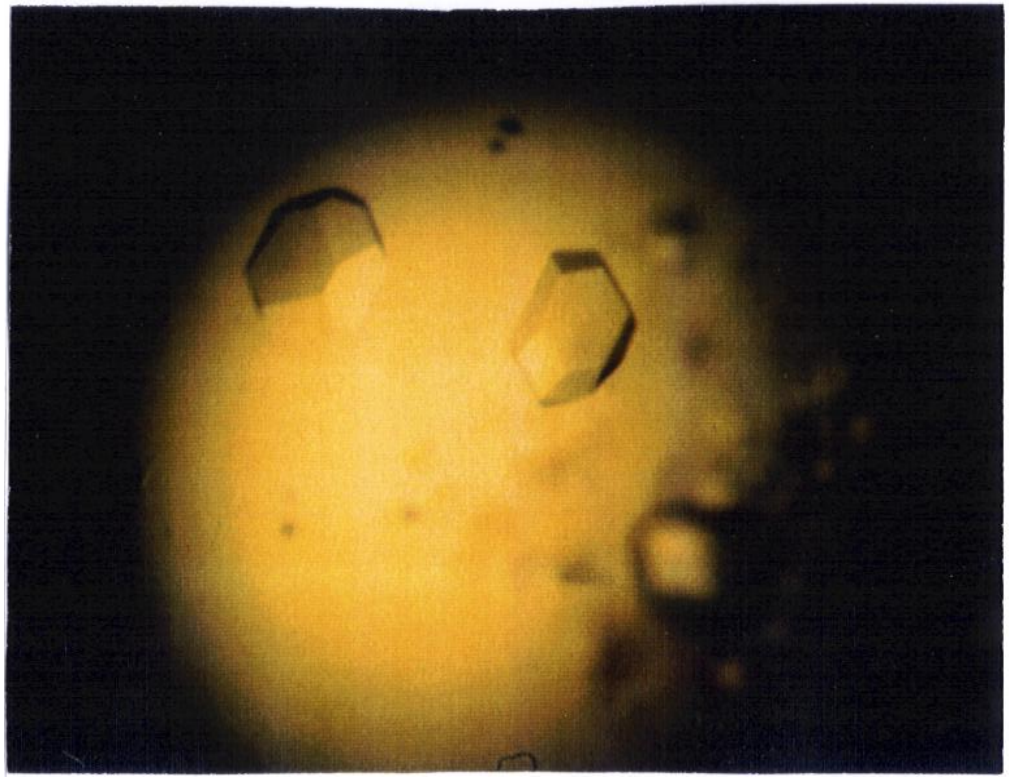

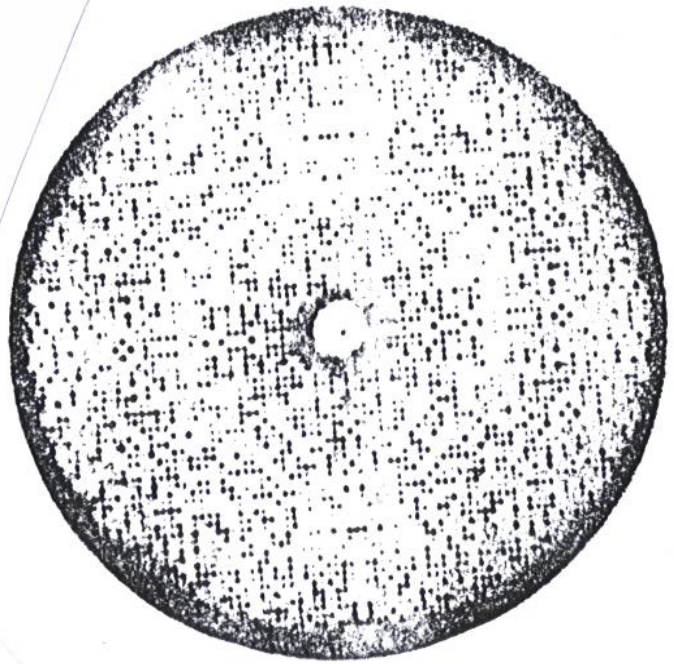

76. MICROSCOPIC STRUCTURES OF CRYSTALS

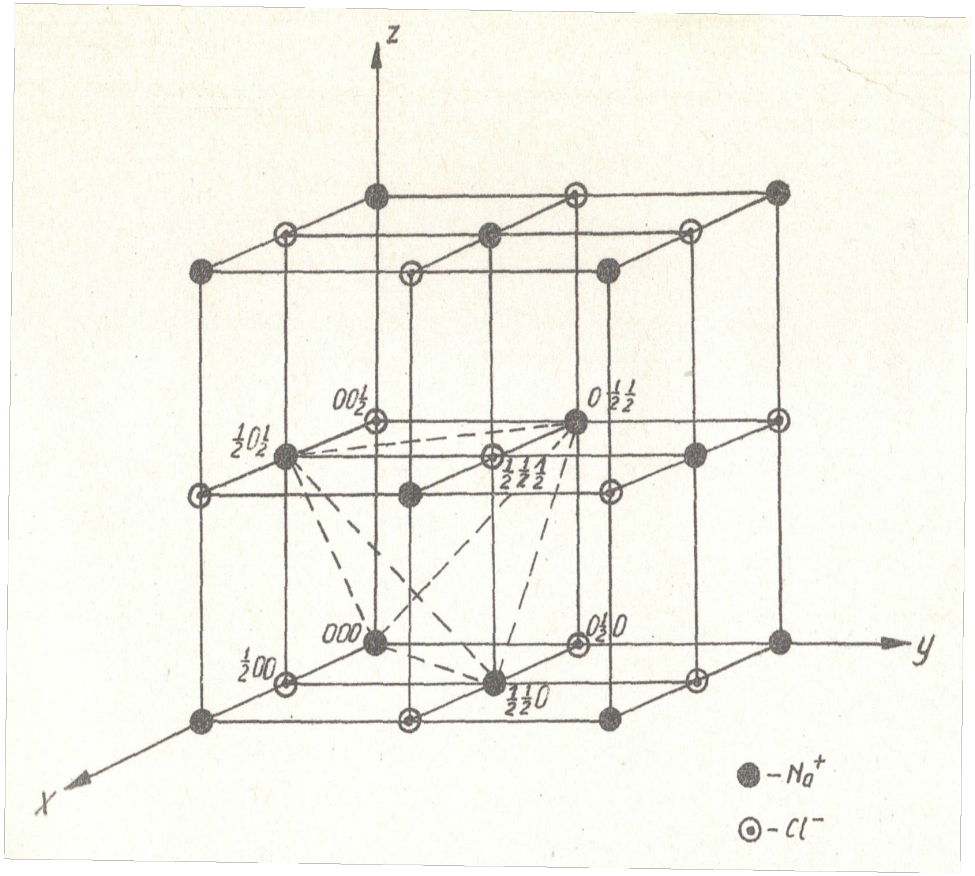

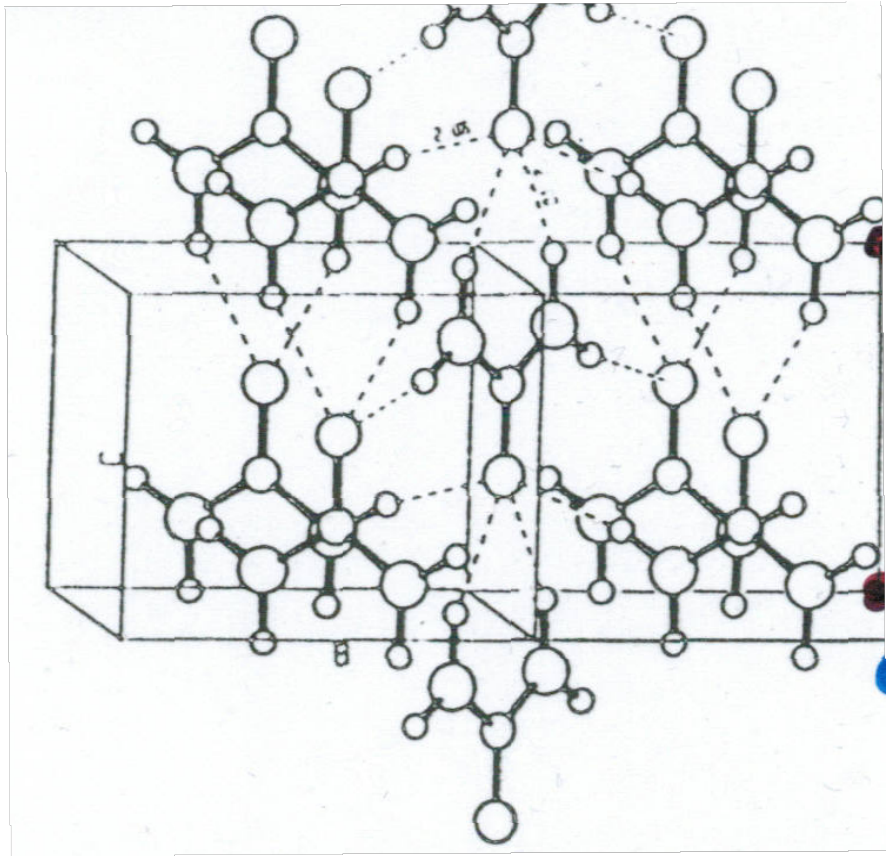

CRYSTAL GEOMETRY

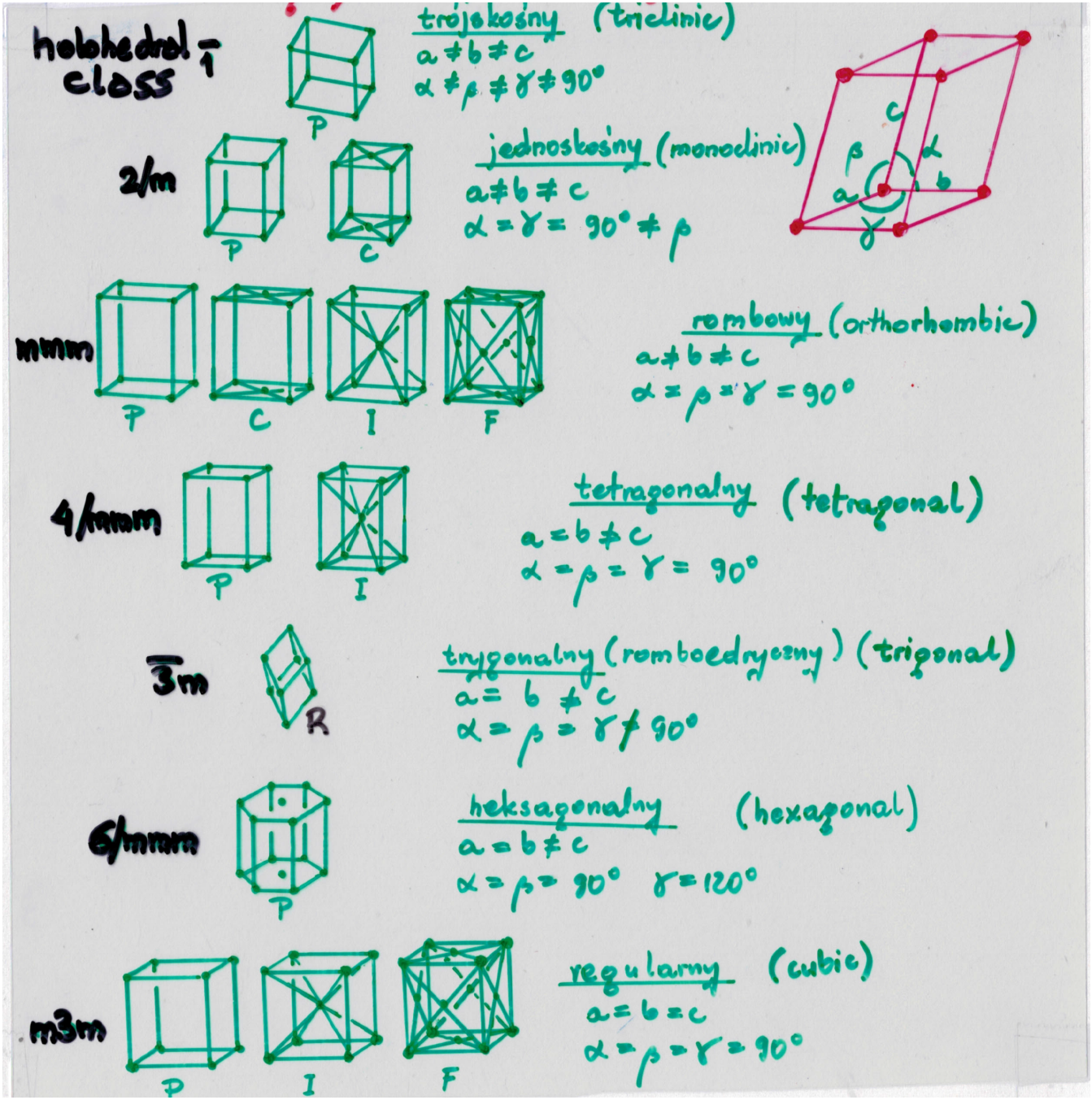

78. X-RAY DIFFRACTION BACKGROUND

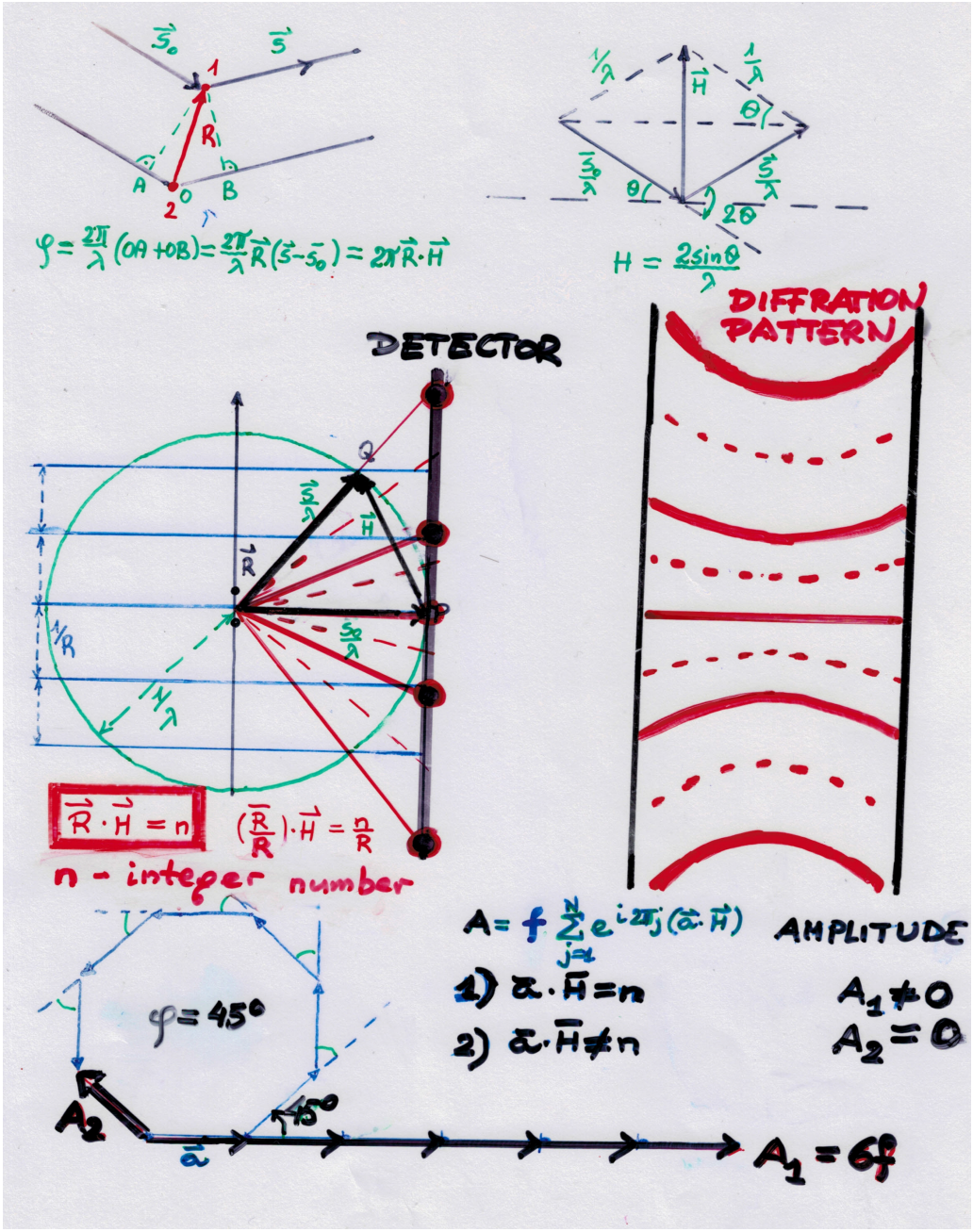

79. EWALD CONSTRUCTION

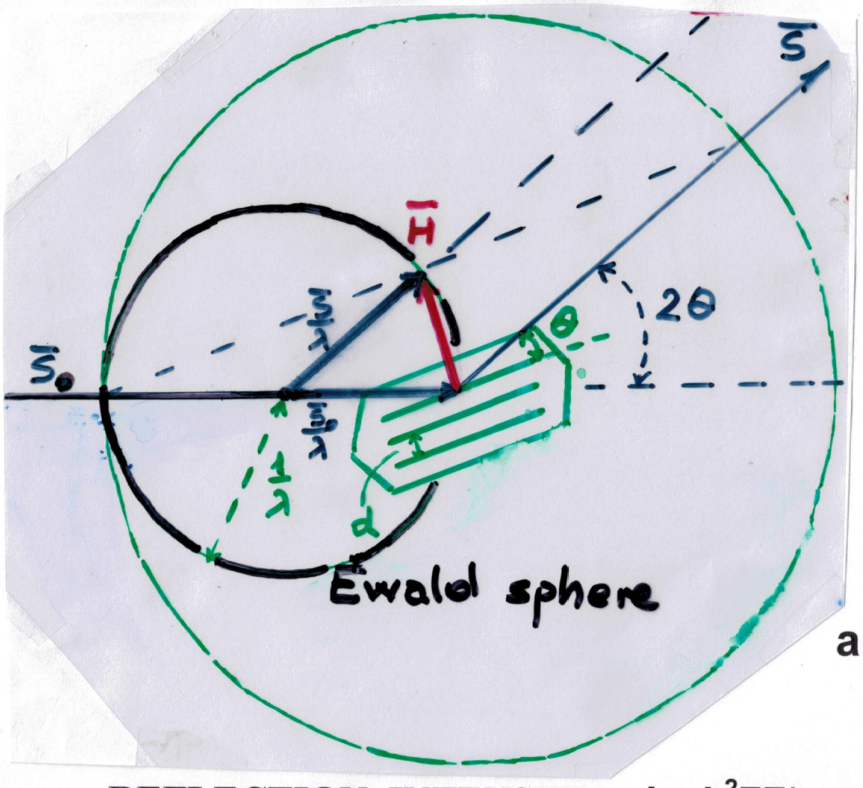

DIRECTION OF THE ENHANCED SCATTERED BEAM (reflected from hkl planes) determined by the reciprocal lattice vector

$$\mathbf{H} = h'\mathbf{a}^* + k'\mathbf{b}^* + l'\mathbf{c}^*$$

$$||\mathbf{H}|| = (2/\lambda)\sin\Theta$$

LAUE'S CONDITIONS:

$$\mathbf{a}\cdot\mathbf{H} = h' = nh; \quad \mathbf{b}\cdot\mathbf{H} = k' = nk; \quad \mathbf{c}\cdot\mathbf{H} = l' = nl$$

BRAGG'S LOW: $2d\sin\Theta = n\lambda$

REFLECTION INTENSITY: $I = k^2FF^*$ (k - normalization factor)

STRUCTURE FACTOR:

$$F(\mathbf{H}) = F(hkl) = C\sum_j f_j \exp\{2\pi i(hx_j + ky_j + lz_j)\} =$$

$$= CV\iiint \rho(x\ y\ z)\exp\{2\pi i(hx + ky + lz)\}dxdydz$$

ELECTRON DENSITY:

$$\rho(x\ y\ z) = 2V^{-1}\sum\sum\sum_{hkl=0}^{+\infty} ||F(hkl)||\cos\{2\pi(hx+ky+lz) - \Phi(hkl)\}$$

$f_j \sim Z$ atomic scattering factor; $(x_j\ y_j\ z_j)$ coordinates of atom j in an unit cell of volume V; $C = \exp(B_{11}h^2 + B_{12}hk + \ldots + B_{33}l^2)$

temperature factor expressed by Debye-Waller coefficients: B_{ij}

80. ELECTRON DENSITY MAP

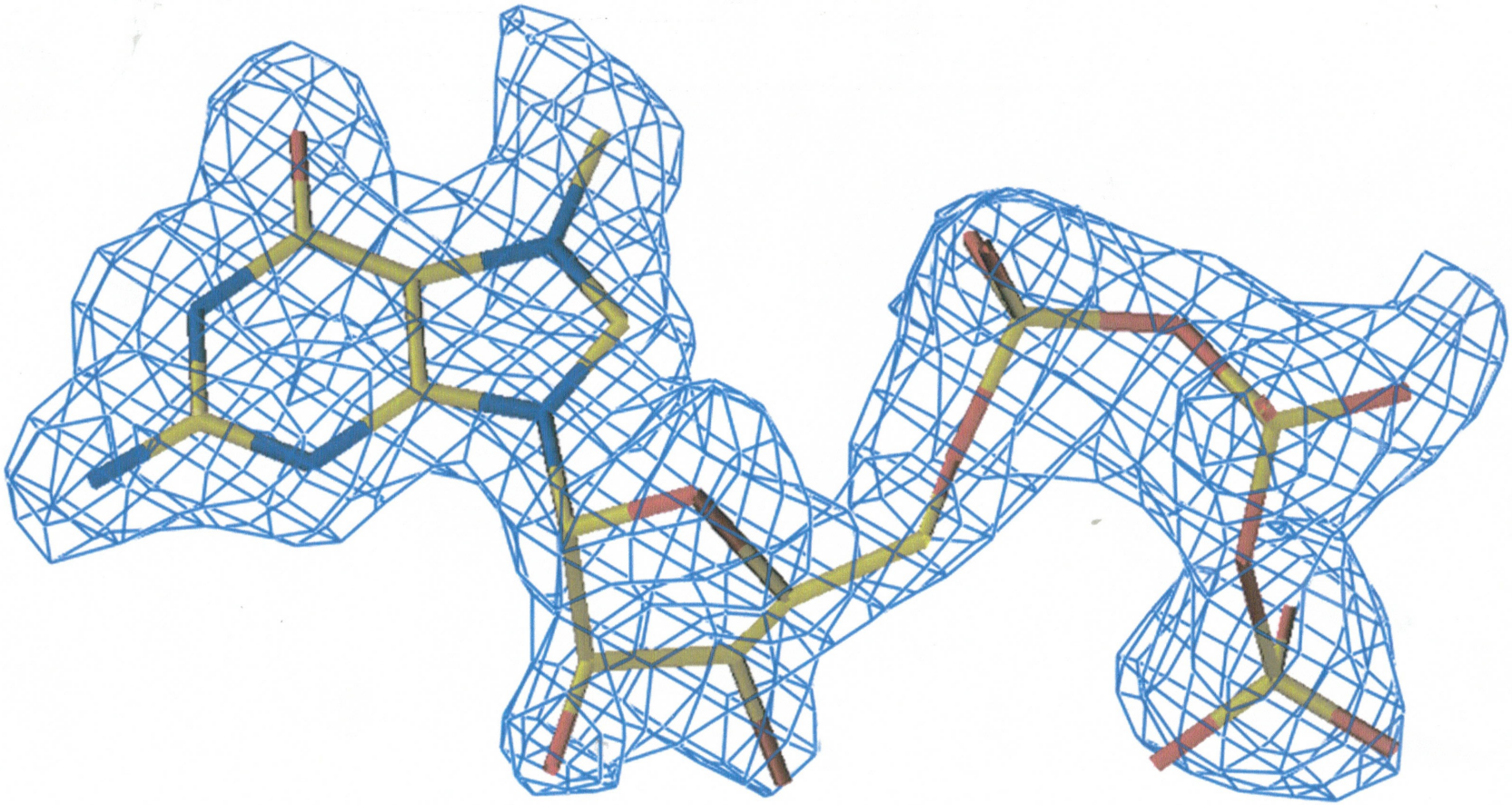

81. PATTERSON FUNCTION AND MAPS

J. Drenth Principles of Protein Crystallography, Springer 1995

$$P(uvw) = \cdot\iiint \rho(xyz)\rho(x+u, y+v, z+w)dxdydz =$$

$$= (1/V)\Sigma\Sigma\Sigma_{hkl}||F(hkl)||^2\cos\{2\pi(hu + kv + lw)\}$$

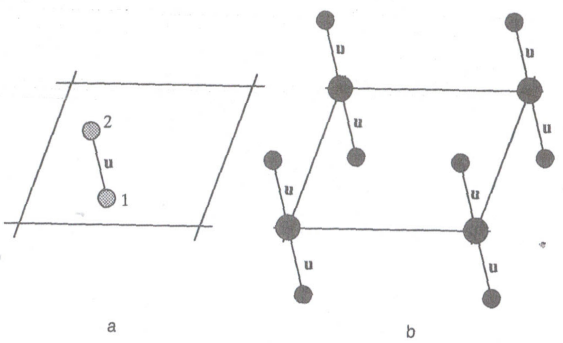

Figure 7.1. (a) A two-dimensional unit cell with only two atoms. (b) The corresponding Patterson cell.

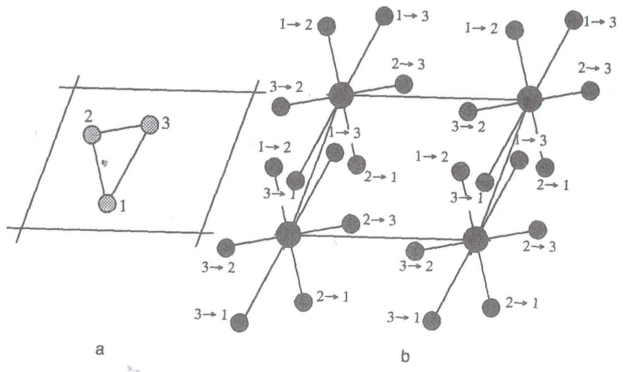

Figure 7.2. (a) A two-dimensional unit cell with three atoms. (b) The corresponding Patterson map. Note the large increase in the number of Patterson peaks compared with Figure 7.1. The total number of peaks is N^2, but the N self-peaks overlap at the origin and, therefore, $N(N-1)$ nonorigin peaks are found in a Patterson map. Because of the centrosymmetry in the map the number of unique peaks is $[N(N-1)]/2$; in this figure $1 \rightarrow 2$, $1 \rightarrow 3$, and $2 \rightarrow 3$ are unique peaks.

82. HARKER CONSTRUCTION

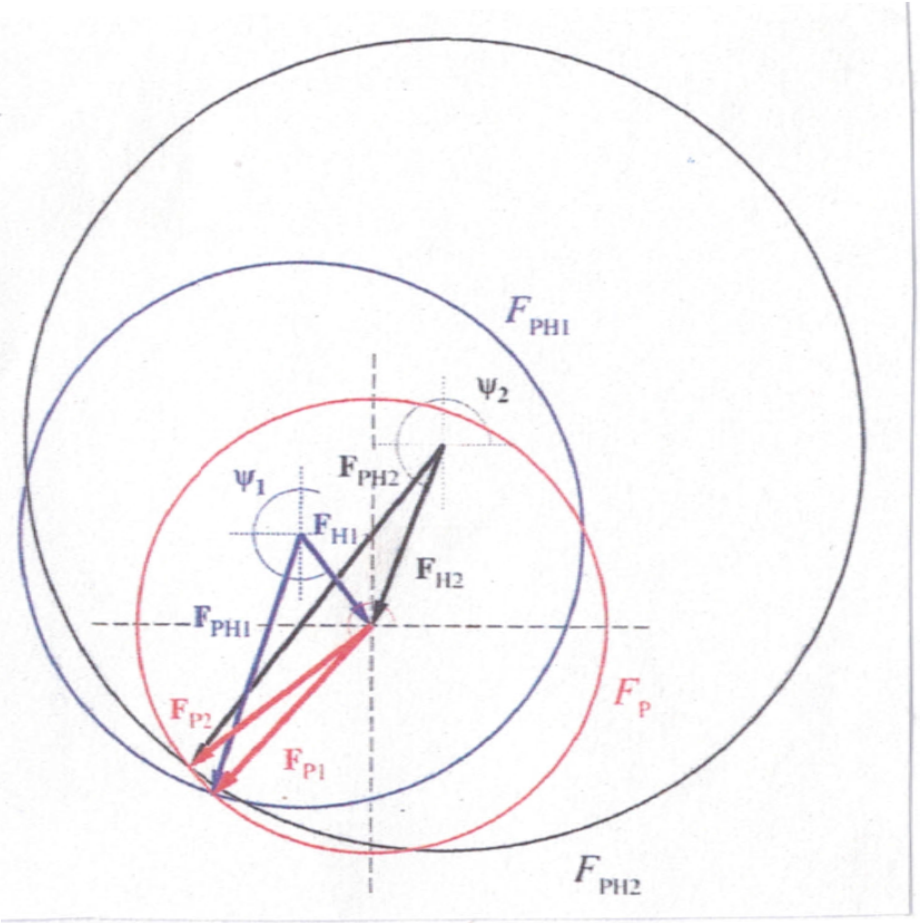

Argand diagram of the determination of unknown phases from a protein crystal structure using multiple isomorphous derivatives (Harker, 1956). Throughout this paper we will adopt a different convention from what is normally used. In this convention, protein structure factors $\mathbf{F}_P$ (red) are vectors that radiate from the origin of coordinates, with amplitude F_P and phase α; heavy-atom structure factors $\mathbf{F}_{Hi}$ (blue for $i = 1$, black for $i = 2$) are represented by vectors of amplitudes F_{Hi} and phases ψ_i, that start at $(-F_{Hi}\cos\psi_i, -F_{Hi}\sin\psi_i)$ and end at the origin of coordinates; derivative structure factors are represented by vectors beginning at the origin of their respective heavy-atom vectors and finishing at the end of the protein structure factor vectors, such that $\mathbf{F}_{PHi} = \mathbf{F}_{Hi} + \mathbf{F}_P$. Possible solutions for the protein complex structure factor $\mathbf{F}_{Pi}$ are given by the intersections between the circle of radius F_P centered at the origin and the derivative circles of radii F_{PHi} centered at their respective $\mathbf{F}_{Hi}$ origins. In absence of any error, all circles should intersect at only one point, which would give the correct solution for $\mathbf{F}_p$. In practice, every derivative circle may intersect with the native circle in a different position or may not even intersect at all.

83. ANOMALOUS DIFFRACTION

Hendrickson et al. EMBO J. 9, 1665, 1990

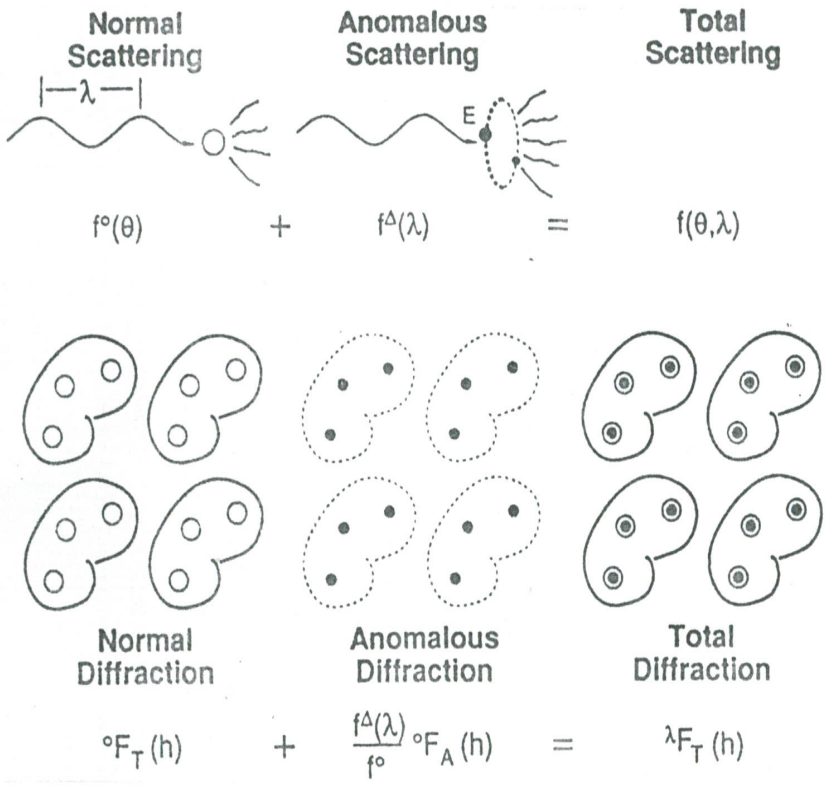

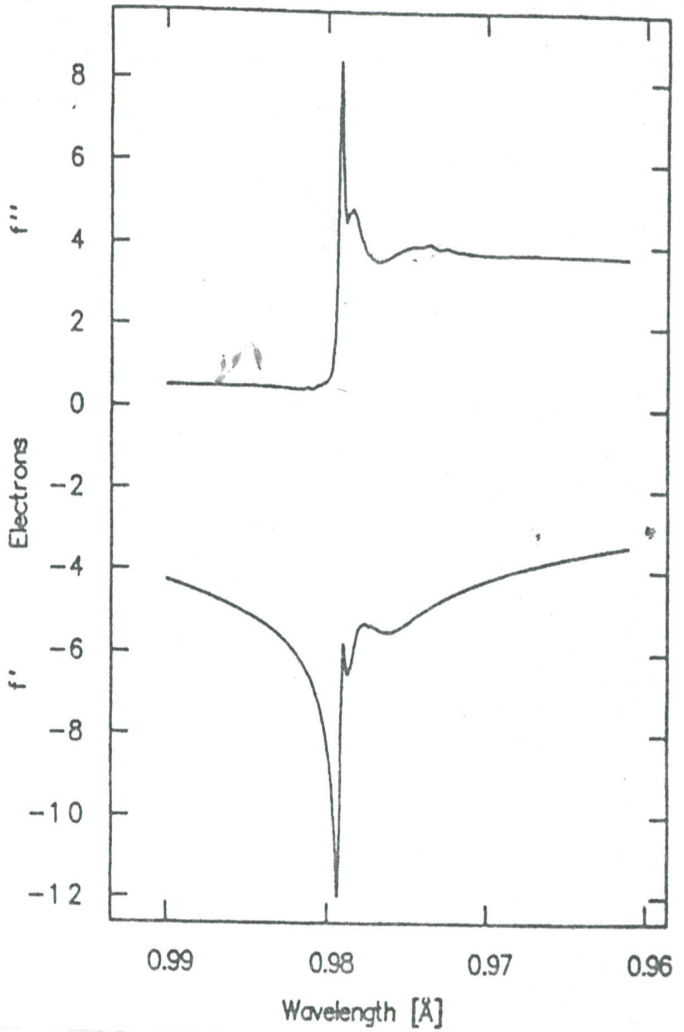

Fig. 4. Anomalous scattering factors near the absorption edge of selenium measured from a crystal of selenomethionyl *E.coli* thioredoxin. Here the electric vector E of the synchrotron X-ray beam was parallel with the b axis of the crystal.

84. DIFFRACTOMETER AND CRYSTALIZATION SYSTEM

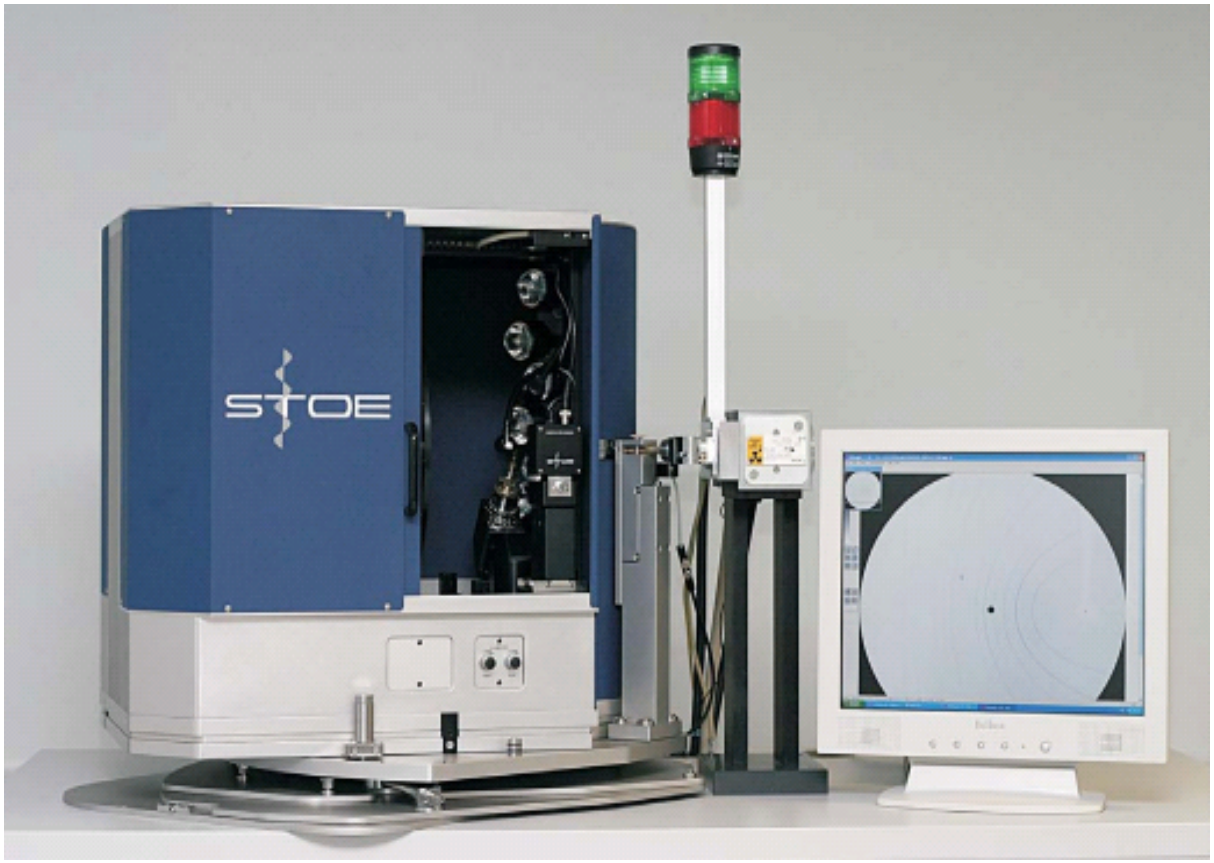

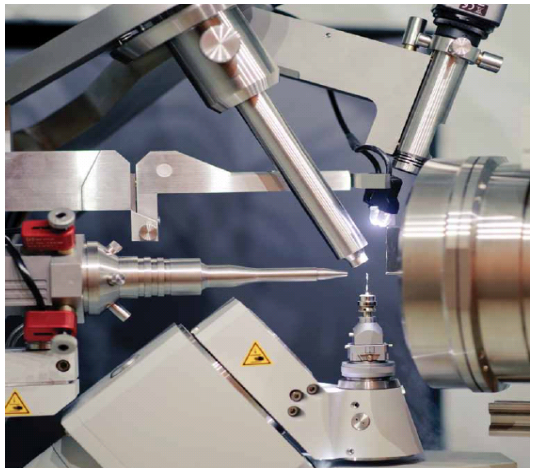

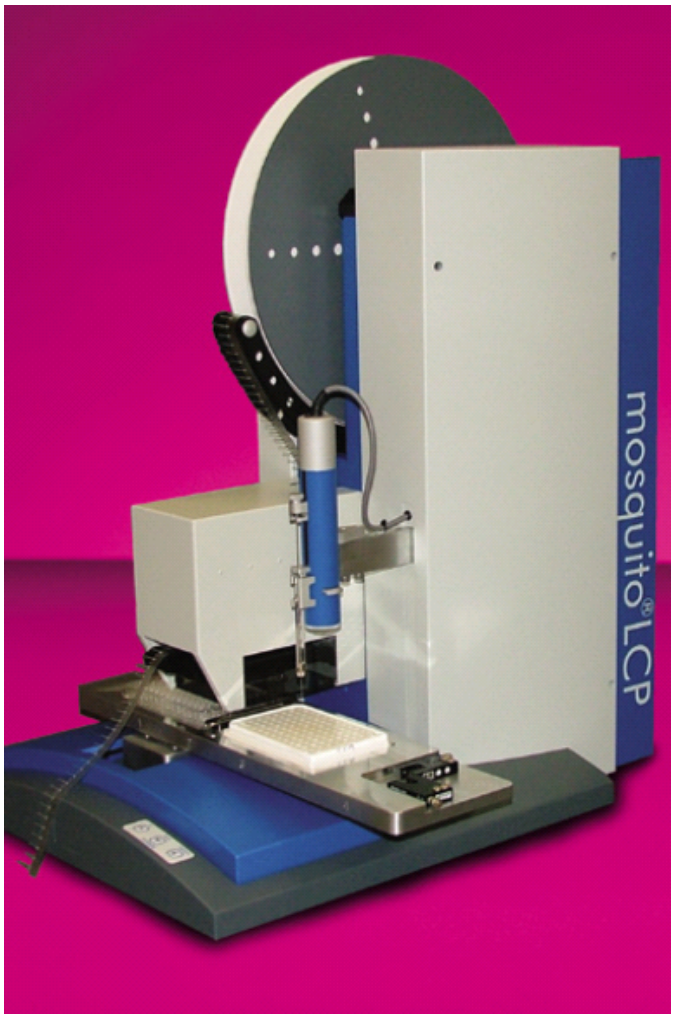

85. X-RAY FREE ELECTRON LASERS DIFFRACTION

Shlichting & Miao Curr. Op. Struct. Biol. 22, 613, 2012

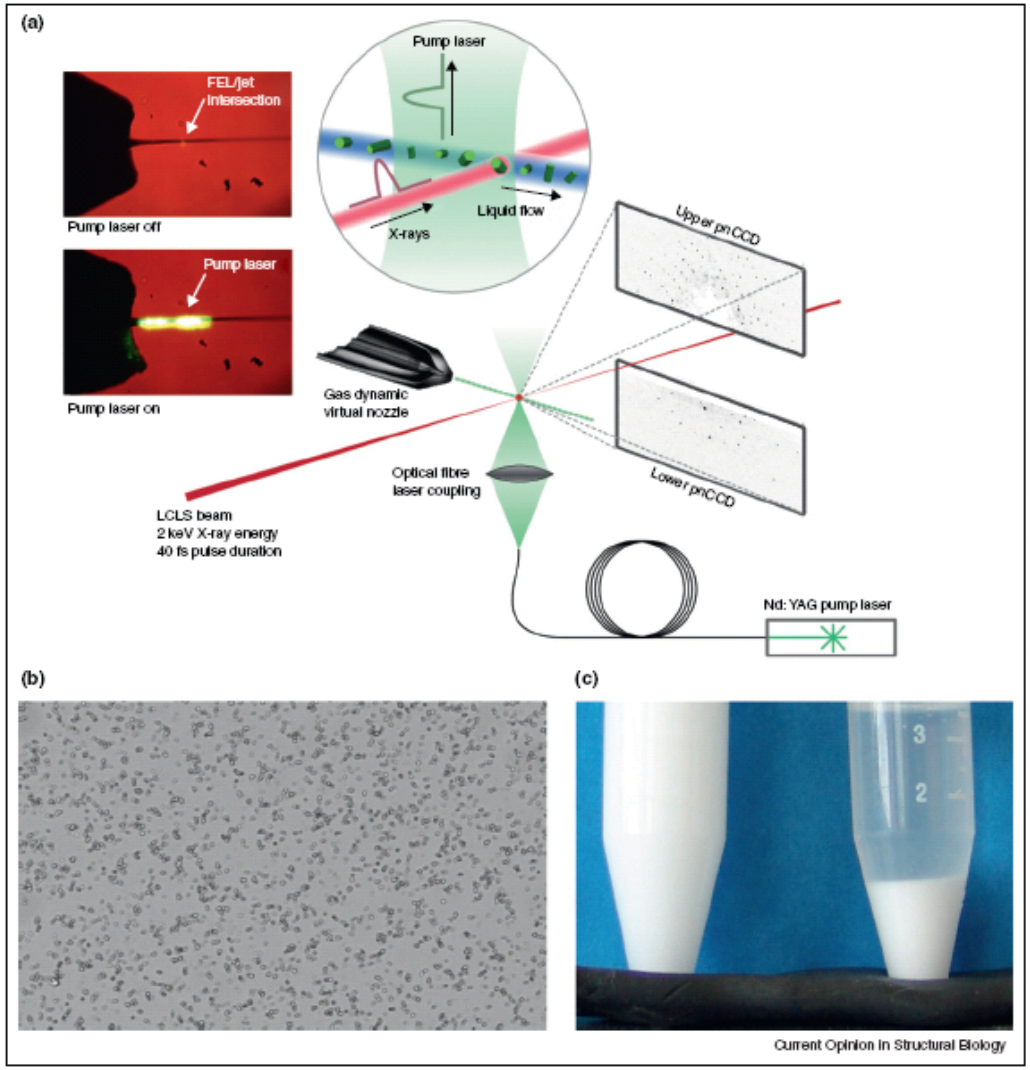

(a) Experimental setup for serial femtosecond crystallography. Tiny crystals are injected into an X-FEL beam using a liquid microjet. This setup is very convenient for pump-probe experiments using laser excitation. Shown is an experiment on the light-induced dissociation of photosystem I–ferredoxin cocrystals, taking place on a microsecond time-scale (from Ref. [43]). **(b)** Microcrystalline sample for serial femtosecond crystallography data collection. Lysozyme crystals ($\leq 1\ \mu m \times 1\ \mu m \times 3\ \mu m$) as seen through a conventional light microscope. **(c)** Microcrystalline lysozyme suspended in solution (left) and after settling (right) (from Ref. [42], reproduced with permission from the IUCr (http://dx.doi.org/10.1107/S0021889812024557)). It is important to note that the quantities depicted here are by no means excessive; several milliliters of very dense crystalline slurry are currently required for SFX experiments.

86. CATH PROTEIN CLASSIFICATION

Orengo et al. Structure 5, 1093, 1997

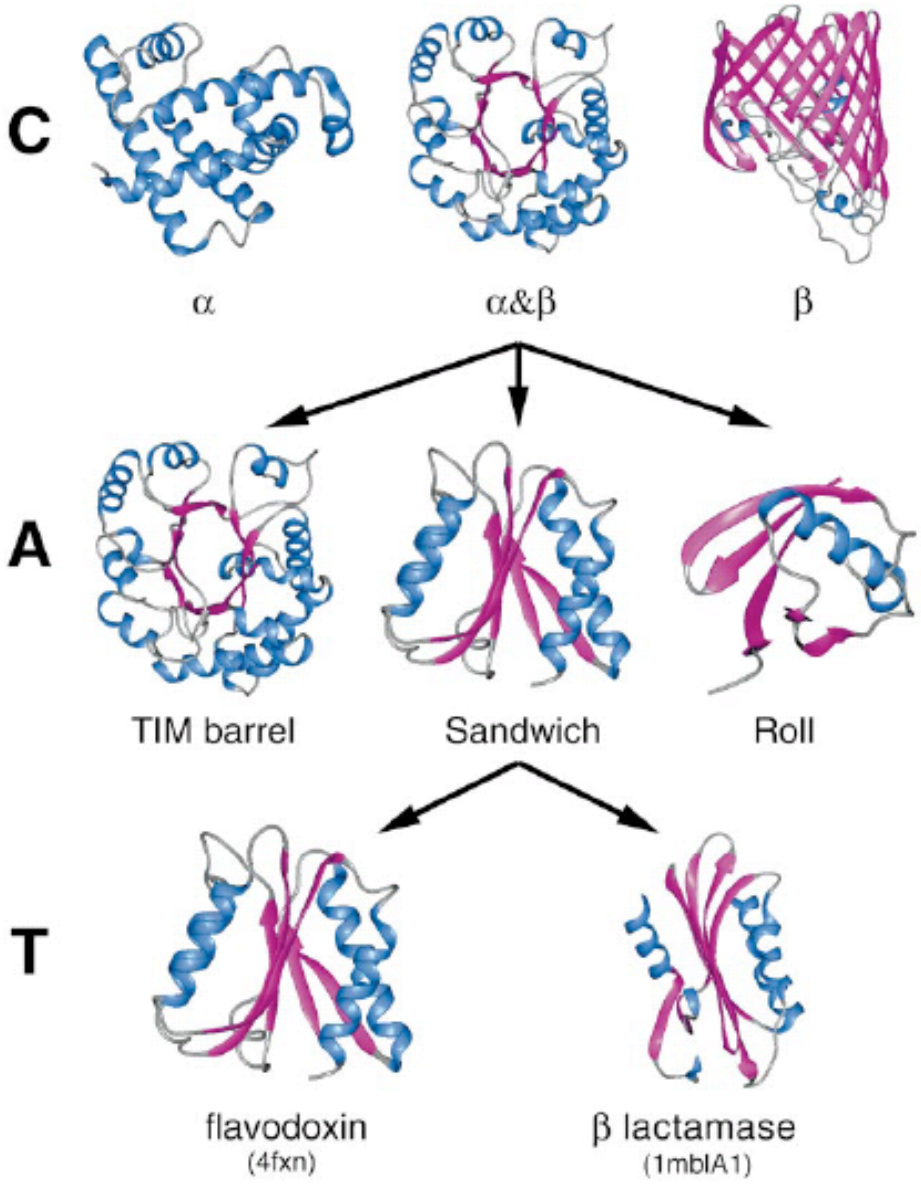

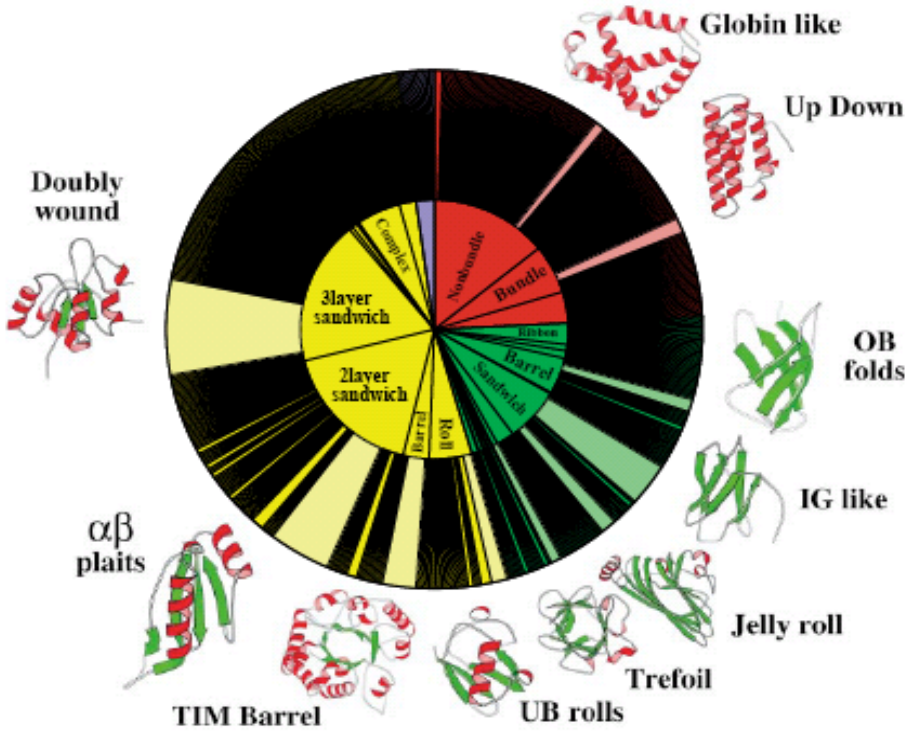

'CATHerine wheel' plot showing the distribution of non-homologous structures (i.e. a single representative from each homologous superfamily at the H-level in CATH) amongst the different classes (C), architectures (A) and fold families (T) in the CATH database. Protein classes are shown coloured as red (mainly α), green (mainly β) and yellow (α–β). Within each class, the angle subtended for a given segment reflects the proportion of structures within the identified architectures (inner circle) or fold families (outer circle). The superfold families are indicated in paler colours and illustrated with a MOLSCRIPT drawing of a representative from the family.

87. ONE-TO-MANY SIGNALING OF p53

Uversky Int. J. Biochem. Cell Biol. 43, 1093, 2011

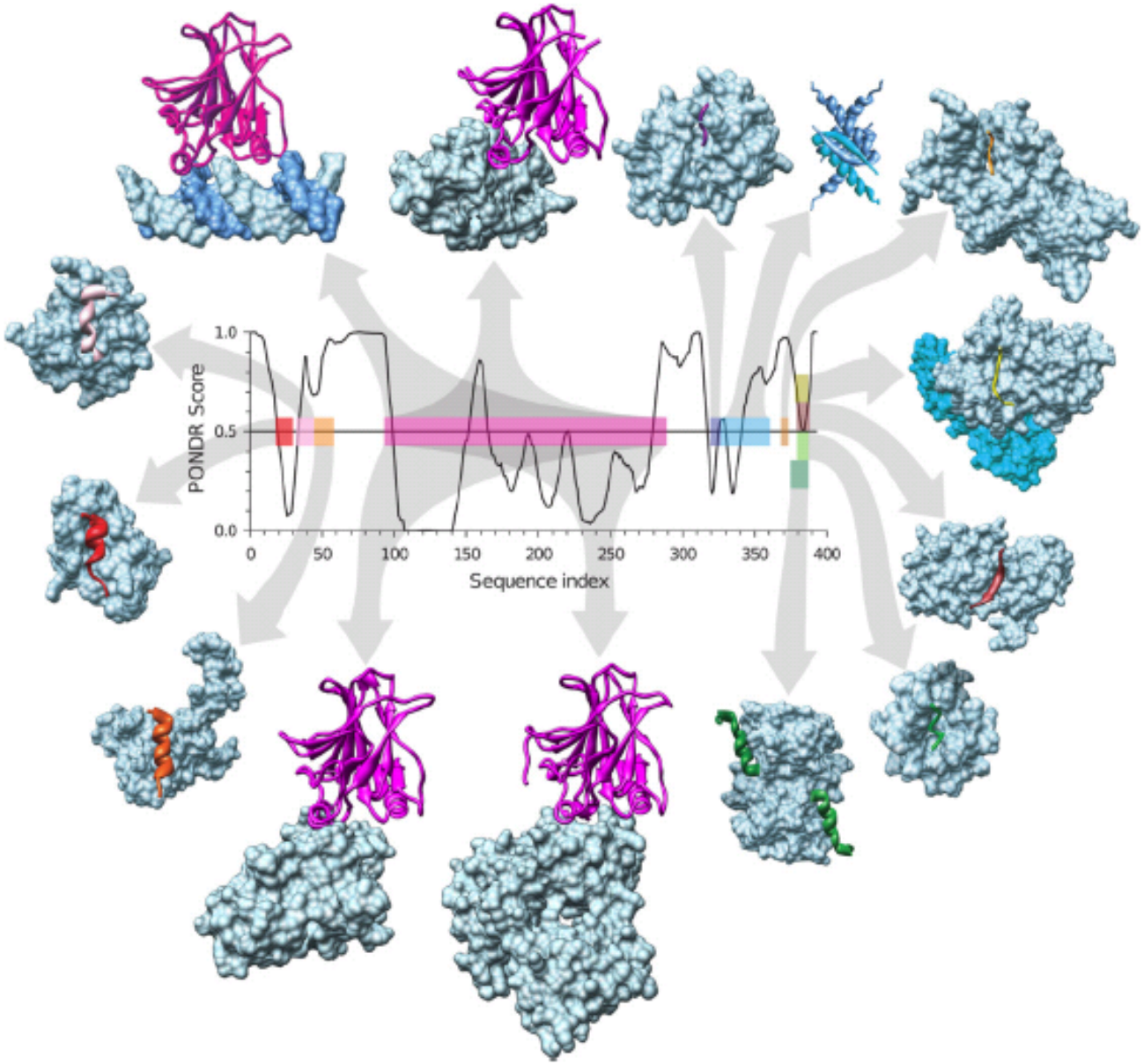

88. NUCLEAR MAGNETIC RESONANCE (NMR)

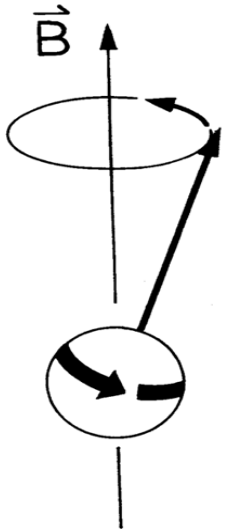

$\vec{\mu} = \gamma\hbar\vec{I}$

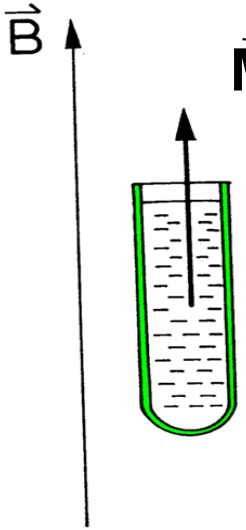

$\vec{M} = \sum_i \vec{\mu}_i$ Total nuclear magnetization

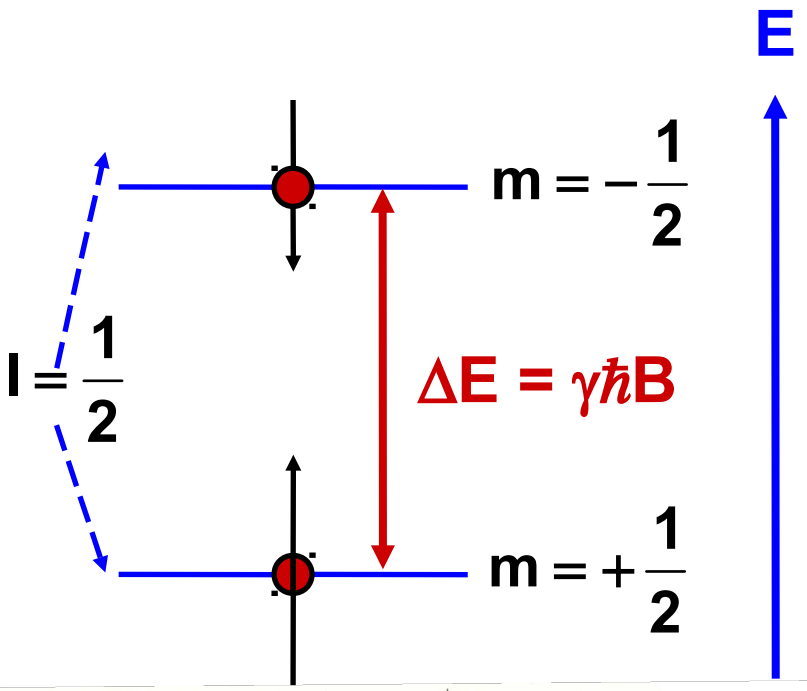

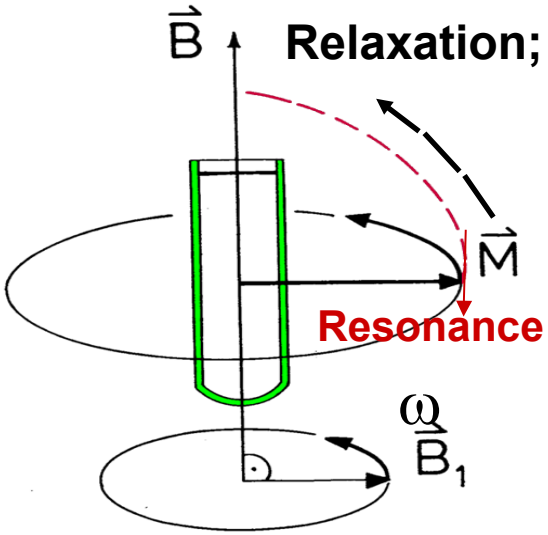

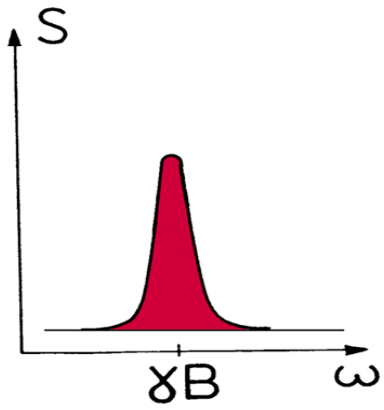

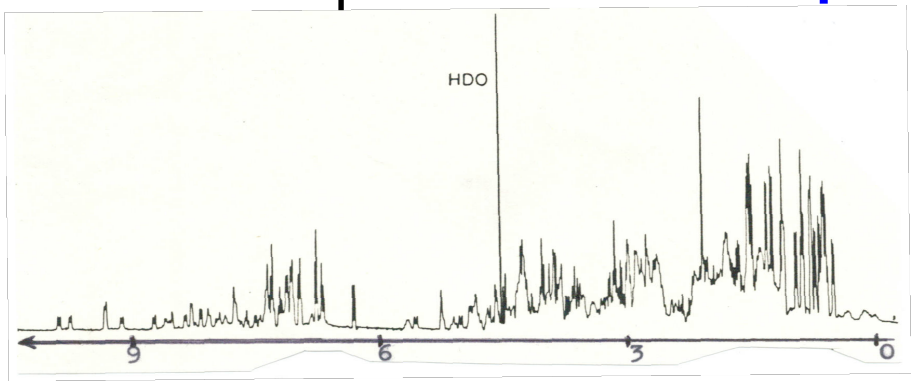

Resonance frequency (γ·B)

89. PRODUCT OPERATOR FORMALISM: BASIC IDEAS

LIOUVLLE-VON NEUMAN'S EQUATION:

$$i\hbar(d\sigma/dt) = [H, \sigma(t)]$$

$$\hbar^{-1}H = \sum_{k=1}^{N}\Omega_k I_{zk} + \sum_{k<l}\pi J_{kl}(2I_{zk}I_{zl}) + \sum_{k=1}^{N}\frac{1}{t_p}\phi I_{vk} \quad v = x, y$$

ϕ - rotation angle of M after B_1 pulse of duration t_p

$M_x(t) = N\gamma\hbar Tr\{F_x\sigma(t)\}$ $M_y(t) = N\gamma\hbar Tr\{F_y\sigma(t)\}$ $F_v = \sum_{k=1}^{N} I_{kv}$

$M_{xy} = M_x + iM_y \xrightarrow{\text{Fourier transform}}$ SPECTRUM

$$\sigma(t) \xrightarrow{H_1\tau_1} \sigma(t+\tau_1) \xrightarrow{H_2\tau_2} \sigma(t+\tau_1+\tau_2) \xrightarrow{H_3\tau_3} \sigma(t+\tau_1+\tau_2+\tau_3)$$

$$\sigma(t+\tau_1+\ldots+\tau_S) = \prod_{k=1}^{s}\exp\{-iH_k\tau_k\}\sigma(t)\prod_{k=1}^{s}\exp\{+iH_k\tau_k\}$$

$$\sigma(t) = \sum_s b_s(t)B_s \quad \text{basic operators } B_s = 2^{(q-1)}\prod_{k=1}^{s}(I_{vk})^{a_{sk}}$$

$a_{sk} = 1$ for q nuclei, $a_{sk} = 0$ for N – q nuclei

example N = 2: $B_s = \frac{1}{2}E$, $I_{x1},.., I_{z2}$, $2I_{x1}I_{x2},.., 2I_{z1}I_{z2}$

propagators $\exp\{H\tau\}$ $H\tau = \alpha B_r = \Omega_k\tau I_{zk}$, $\pi J_{kl}\tau(2I_{zk}I_{zl})$, ϕI_{vk}

σ evolution: $\exp\{-i\alpha B_r\}B_s\exp\{+i\alpha B_r\} = \sum_n b_{ns}(r,\alpha)B_n$

MATRIX REPRESENTATION OF σ

wave function of a nucleus j in a macroscopic ensamble N:

$$\psi_j = a_1^j\alpha + a_2^j\beta$$

$|1> = |1/2, 1/2>$ $I_{zj}|1> = (1/2)|1>$

$|2> = |1/2,-1/2>$ $I_{zj}|2> = -(1/2)|2>$

in the representation of I_{zj} eigenfunctions $\sigma_{mn} = <n|\sigma|m> =$

$$= (1/N)\sum_j (a_m^j)^* a_n^j = \overline{a_m^* a_n}$$

$$a_n = |a_n|\exp(i\alpha)$$

$$\sigma_{mn} = \overline{|a_m^*||a_n|}\cdot\overline{\exp\{i(\alpha_n - \alpha_m)\}}$$

$\sigma_{11} = p^+$ population of α state

$\sigma_{22} = p^-$ population of β state

$\sigma_{12} = \sigma_{21} = 0$ equilibrium (no B_1 pulse)

$\sigma_{12} \neq 0$ $\alpha_2 = \alpha_1$ resonance (phase coherence)

90. PRODUCT OPERATOR FORMALISM: OBSERVABLES

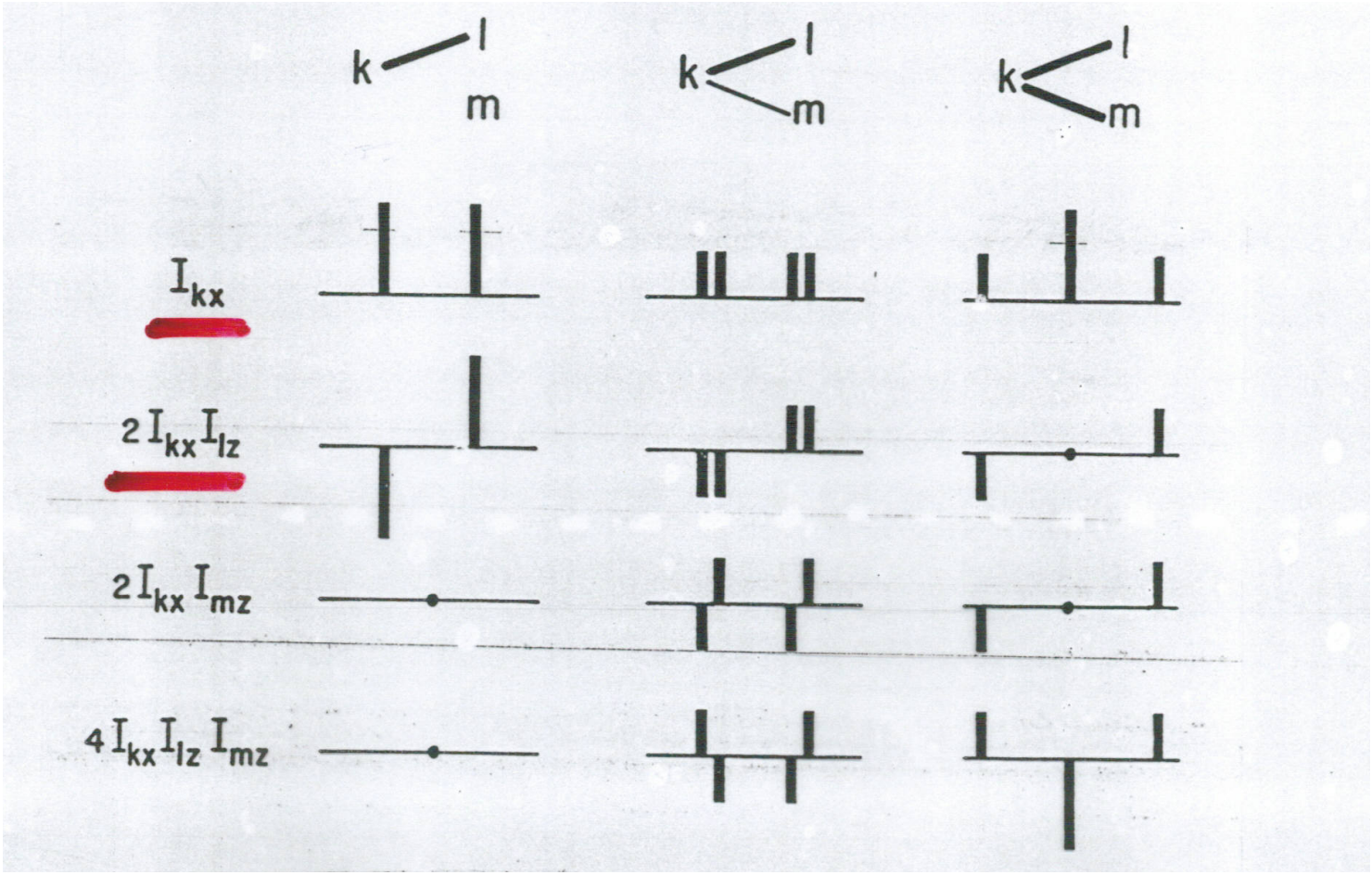

$$2I_{kx}I_{lz} \xrightarrow{\Omega_k \tau I_{kz}} \xrightarrow{\Omega_l \tau I_{lz}} \xrightarrow{\pi J_{kl} \tau \, 2I_{kz}I_{lz}}$$

$$\longrightarrow I_{ky} \sin(\pi J_{kl}\tau)\cos(\Omega_k \tau) - I_{kx} \sin(\pi J_{kl}\tau)\sin(\Omega_k \tau)$$

91. DETERMINATION OF STRUCTURAL AND DYNAMICAL PARAMETERS OF BIOPOLIMERS

Assignment of NMR signals on the basis of
chemical shifts δ(j) and coupling constants J(i,j)

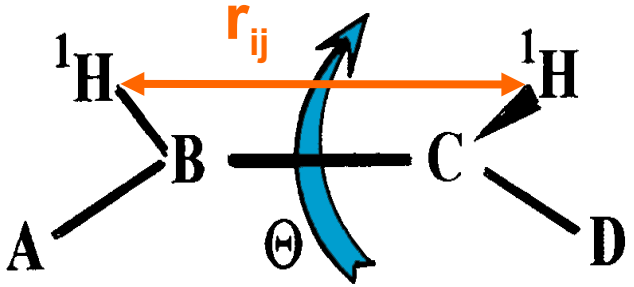

STRUCTURE

local

- **scalar coupling constants J(i,j)** → **dihedral angles Θ in four-atom fragments**
- **intensity of the dipolar interaction (nuclear Overhausera effect NOE)** → **distances r_{ij} between the nuclei in a molecule**

global

- **residual dipolar coupling RDC** → **mutual orientation of the molecular fragments**

DYNAMICS: relaxation times T_1, T_2 → **correlation times τ_c**

92. ^1H, ^1H - 2D NMR EXPERIMENT

Pulse sequence ^1H,^1H-NOESY

Signal:

$$S(\omega_1\omega_2) = \iint M_{xy}(t_1t_2)\exp(-i\omega_1t_1)\exp(-i\omega_2t_2)dt_1dt_2$$

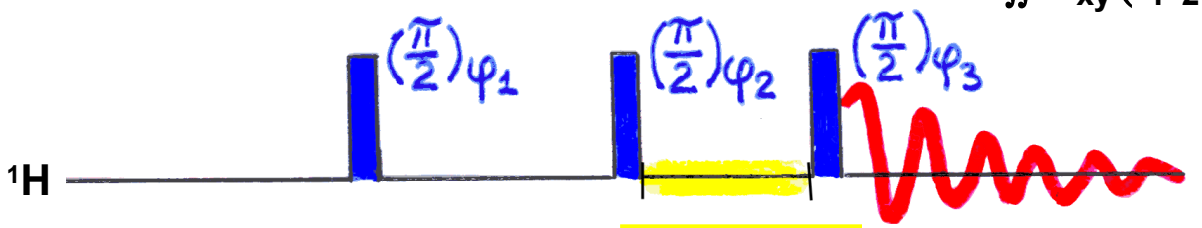

incremented t_1 **mixing t_m** acquisition t_2

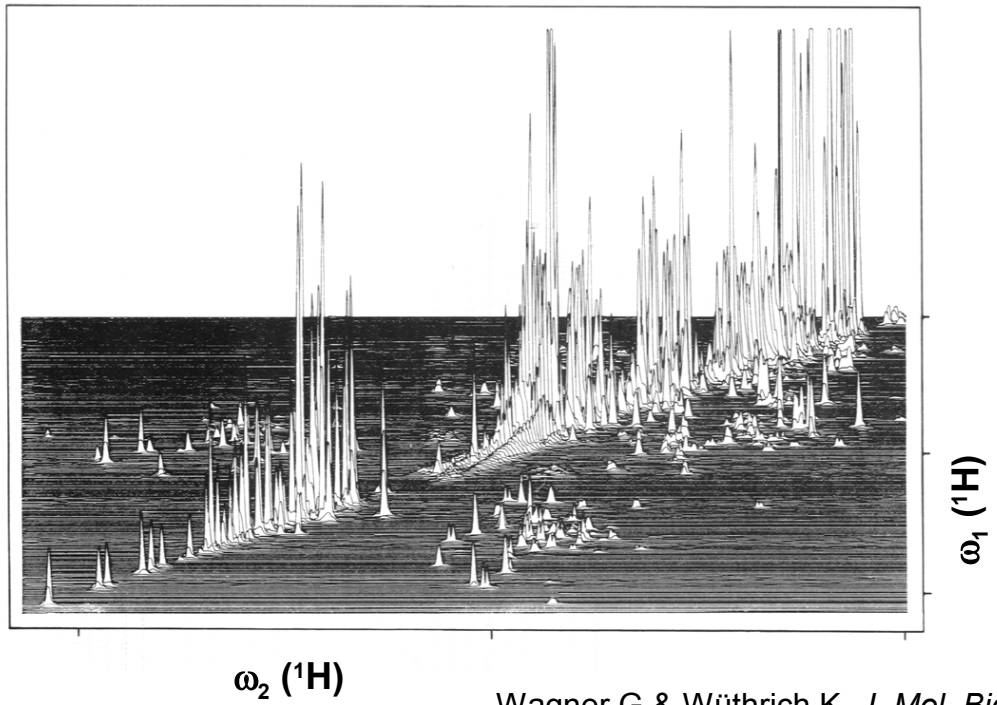

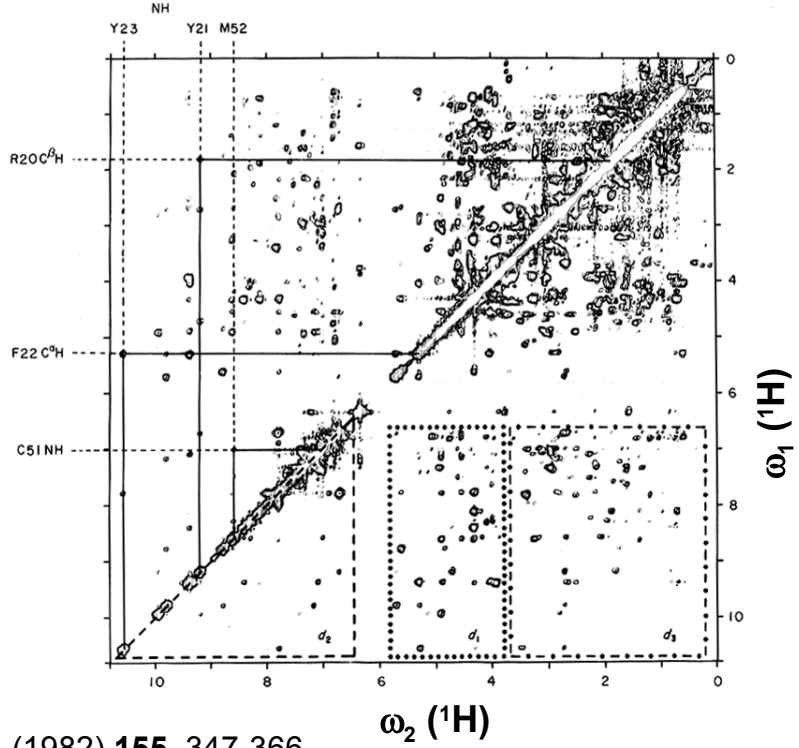

Wagner G & Wüthrich K, *J. Mol. Biol.* (1982) **155**, 347-366

93. HETERONUCLEAR 3D NMR EXPERIMENT

Pulse sequence ($^{15}N/^{13}C,^{1}H,^{1}H$-HMQC-COSY)

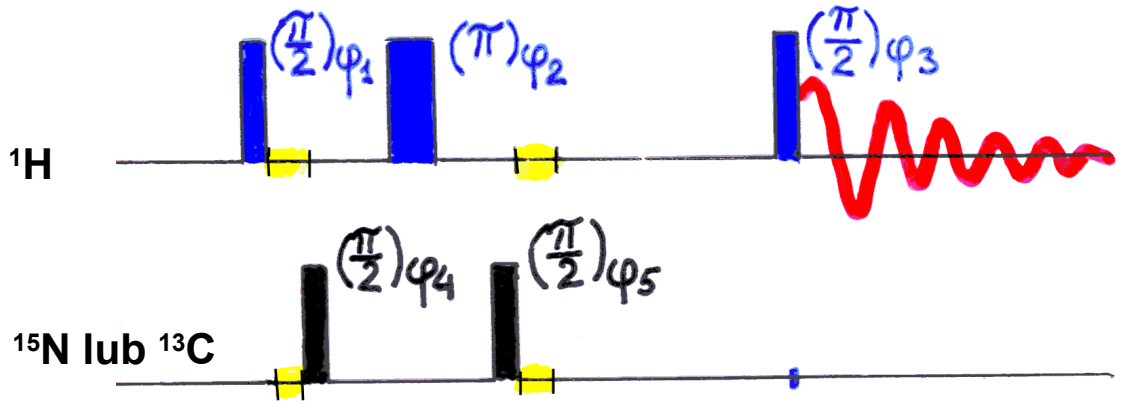

equilibrium incremented t_1 incremented t_2 acquisition t_3

constant τ constant τ

3D spectrum and its 2D section

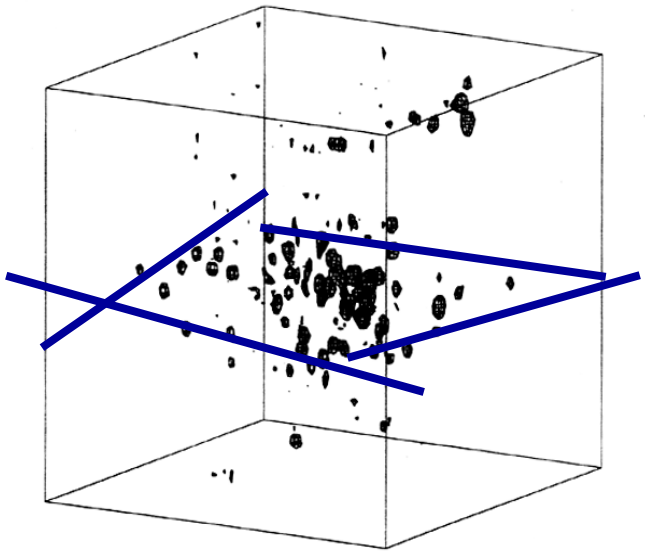

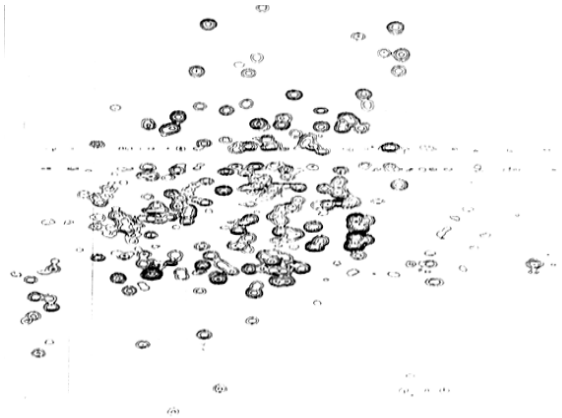

Signal:

$$S(\omega_1\omega_2\omega_3) =$$

$$= \iiint M_{xy}(t_1t_2t_3)\exp(-i\omega_1t_1)\exp(-i\omega_2t_2)\exp(-i\omega_3t_3)dt_1dt_2dt_3$$

Oschkinat H. et al., *Angew. Chem. Int. Ed. Engl.* (1994) **33**, 277-293

94. SEPARATION OF THE OVERLAPPING SIGNALS IN $^{15}N/^{13}C$- LABELLED MOLECULES BY 3D NMR

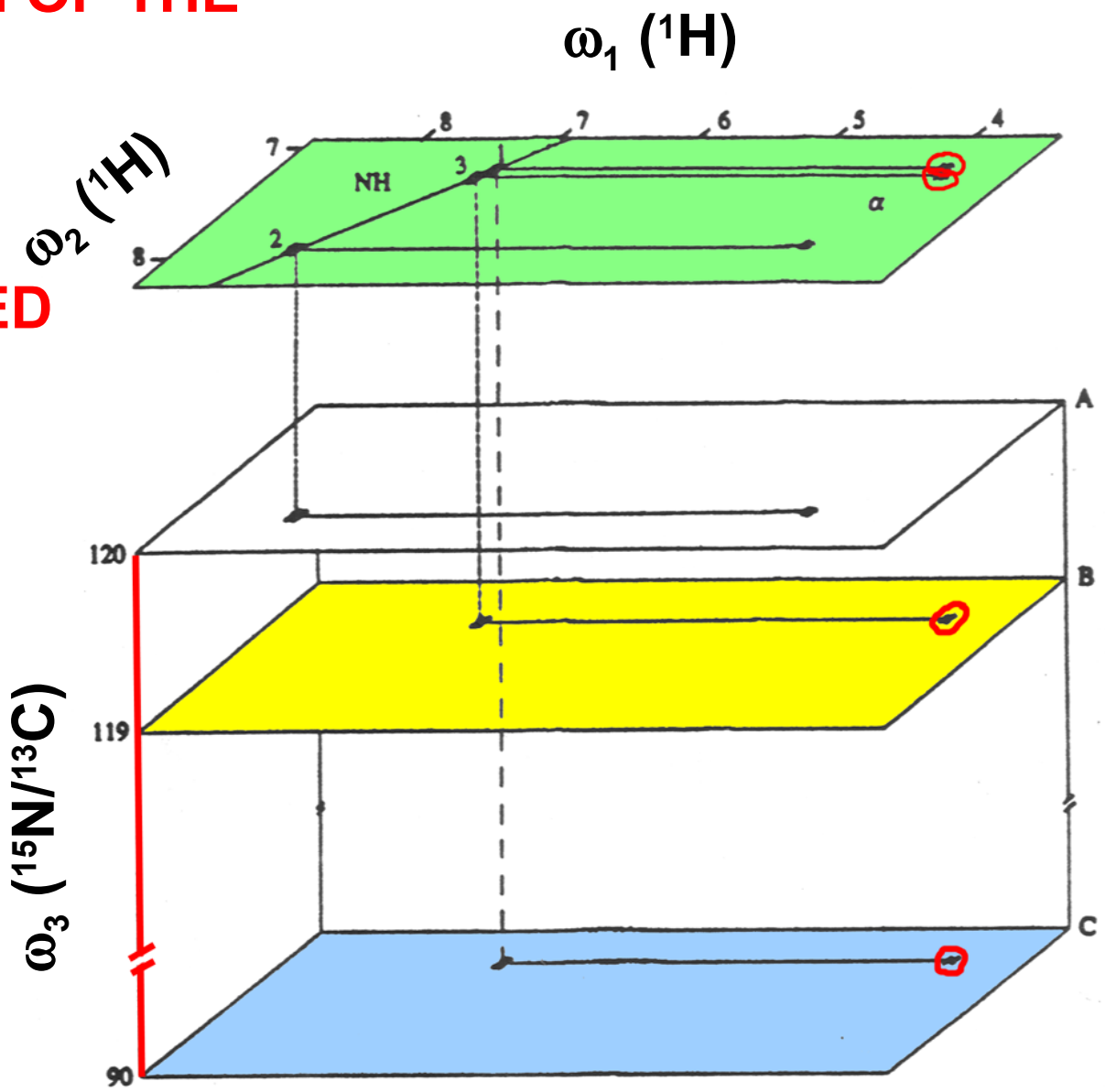

95. SEQUENCE AND 3D STRUCTURE OF V210I PrP MUTANT

Biljan et al. Int. J. Mol. Biol. 412, 660, 2011

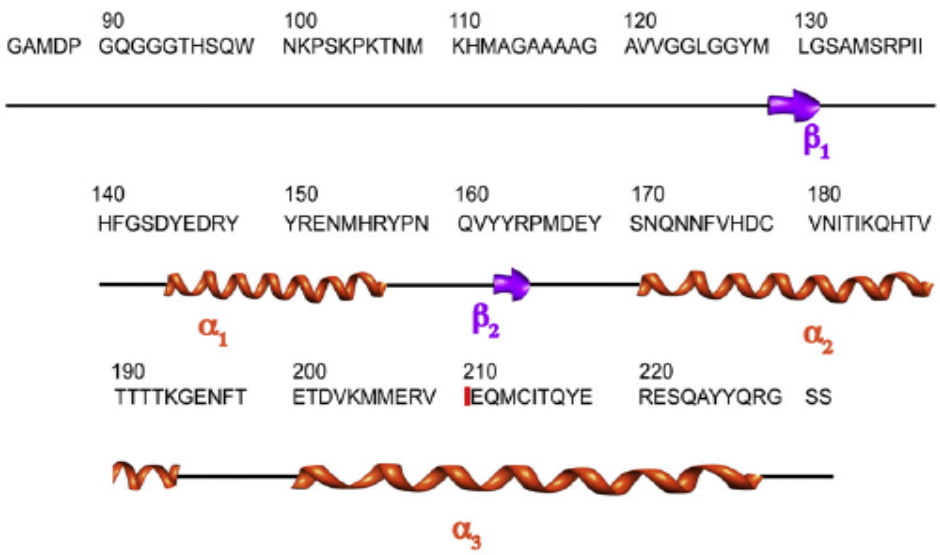

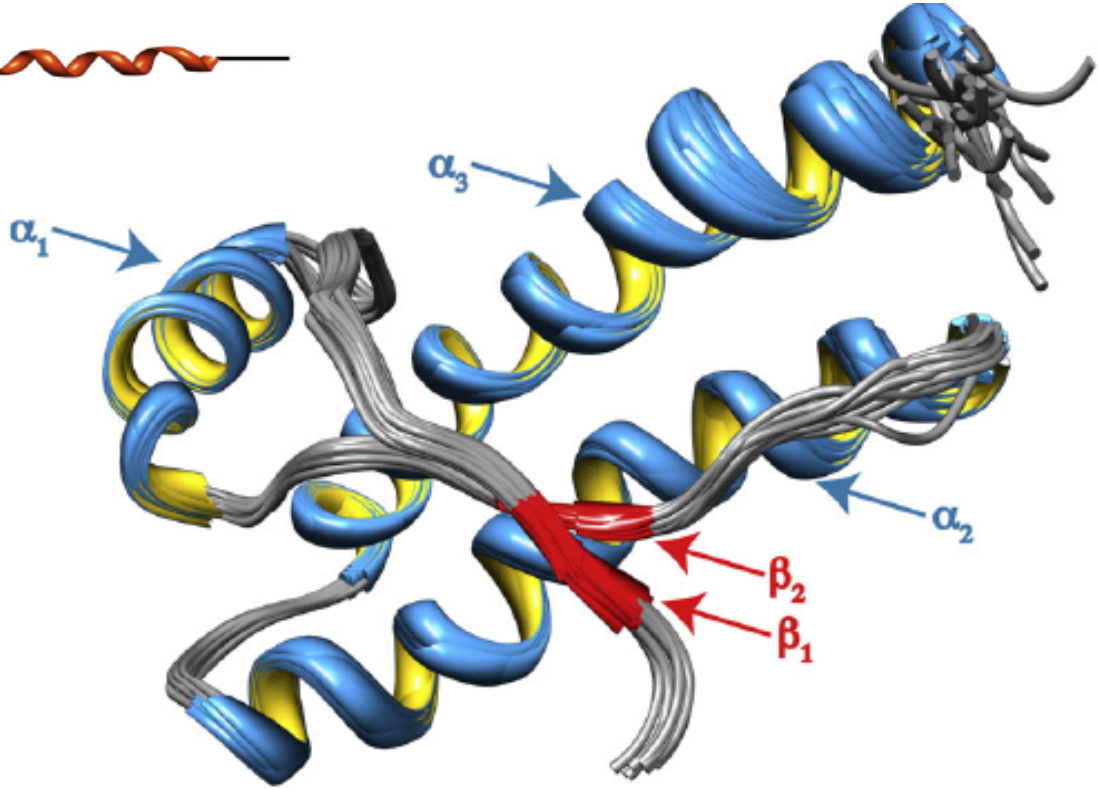

96. PSEUDOPOTENTIALS IN rMD SIMULATIONS

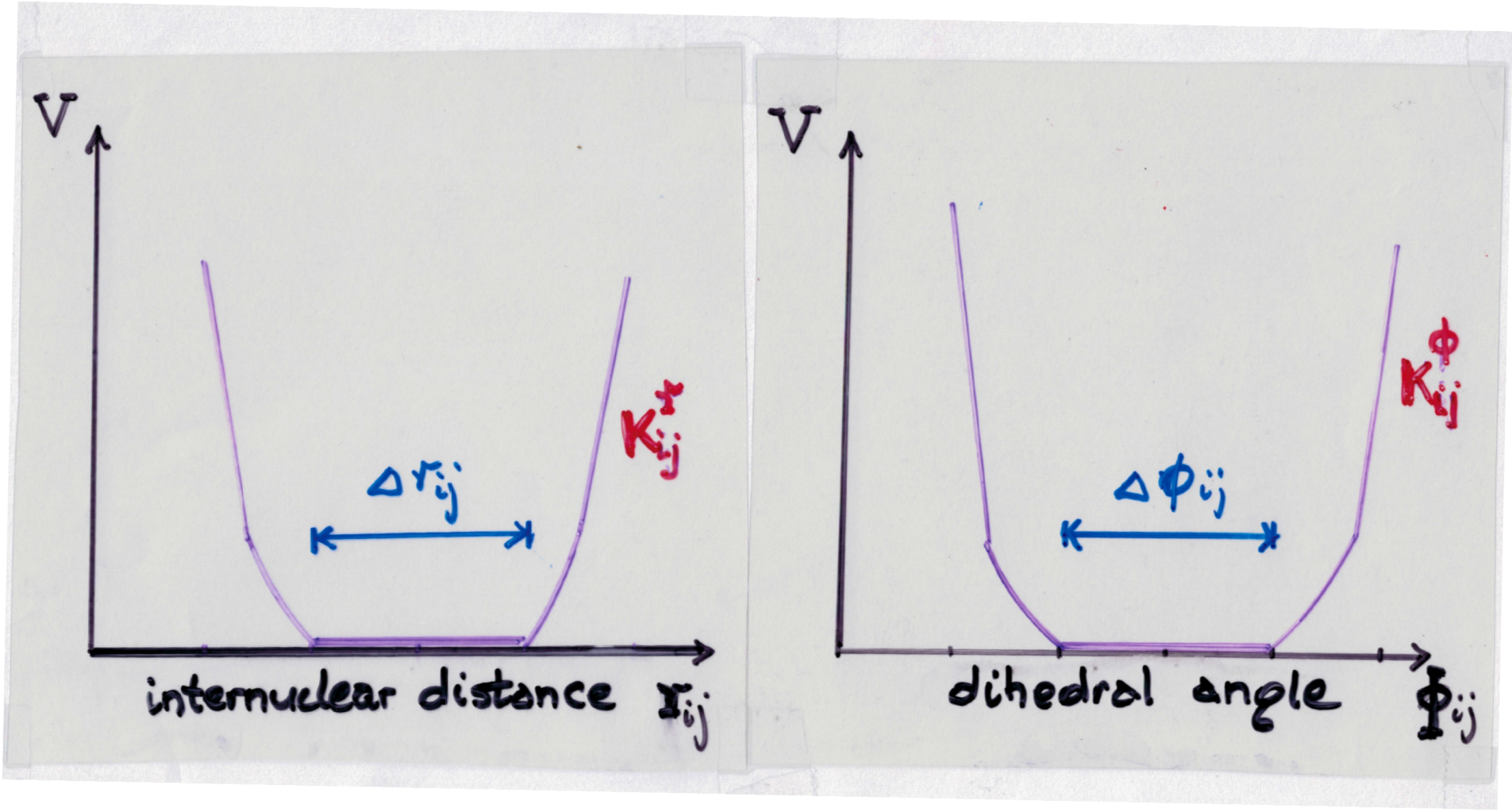

97. SEQUENTIAL ASSIGNMENTS IN PROTEIN 2D ^{1}H NMR

Wagner & Wütrich J. Mol. Biol. 155, 347, 1982

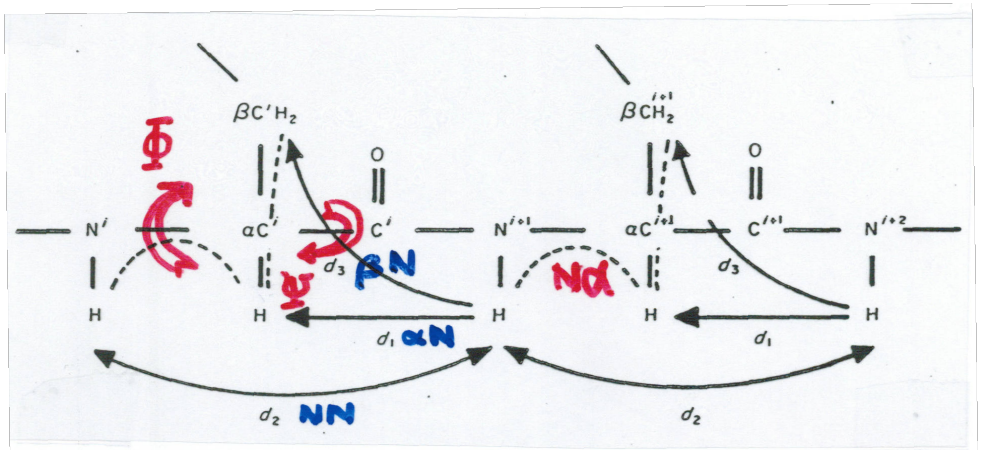

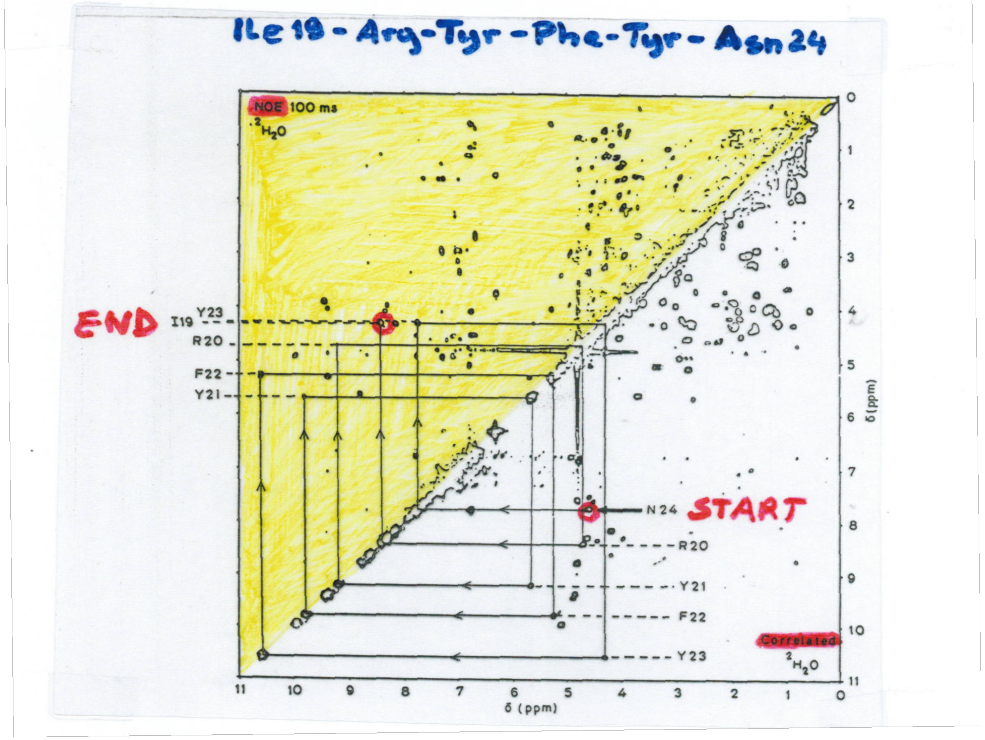

98. SEQUENTIAL ASSIGNMENTS IN PROTEIN 3D NMR

Ikura et al. Biochemistry 29, 4659, 1990

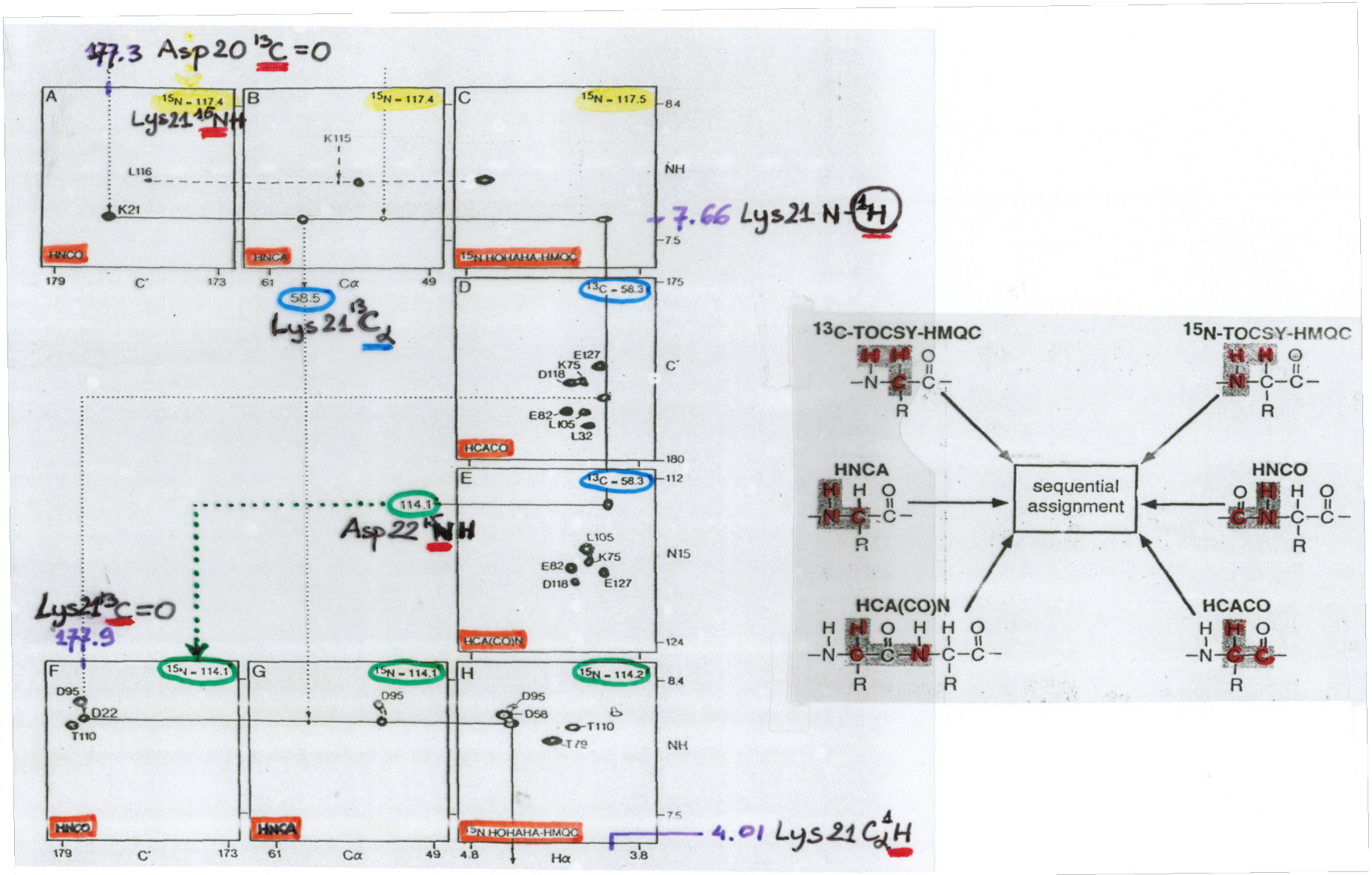

99. ANALYSIS OF 3D NMR TRIPLE RESONANCE SPECTRA

Zukov Ph. D. Thesis, 2001

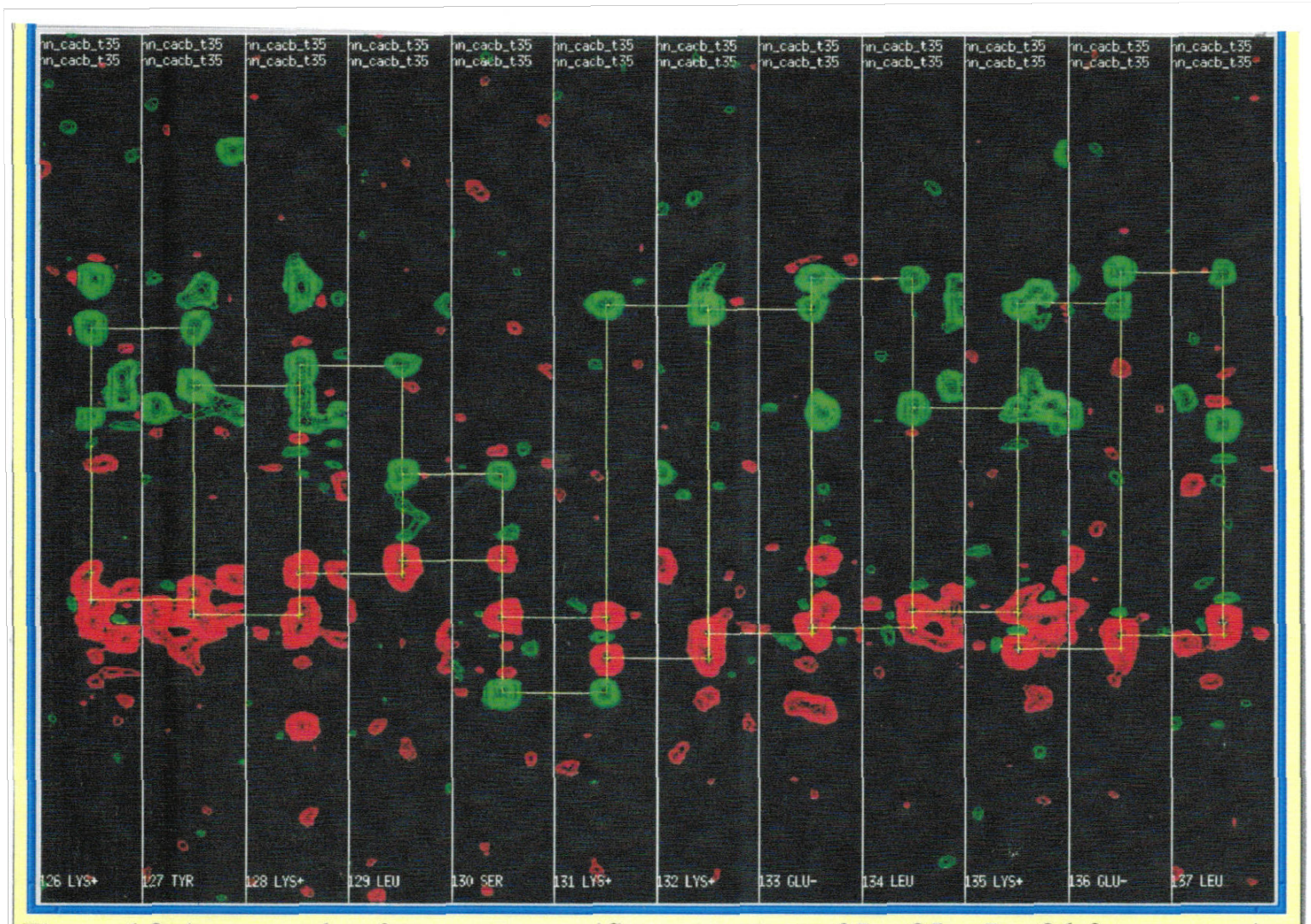

Figure 6.2 An example of sequence specific assignment of Lys25 – Leu36 fragment using HNCACB spectrum. Strips extending over the entire spectral width of ^{13}C dimension are defined for the amide groups of the residues indicated in each strip.

100. $^{1}H,^{15}N$-HMQC FINGERPRINT OF 269 AA PROTEASE

Remerowski et al. J. Biomol. NMR 4, 257, 1994

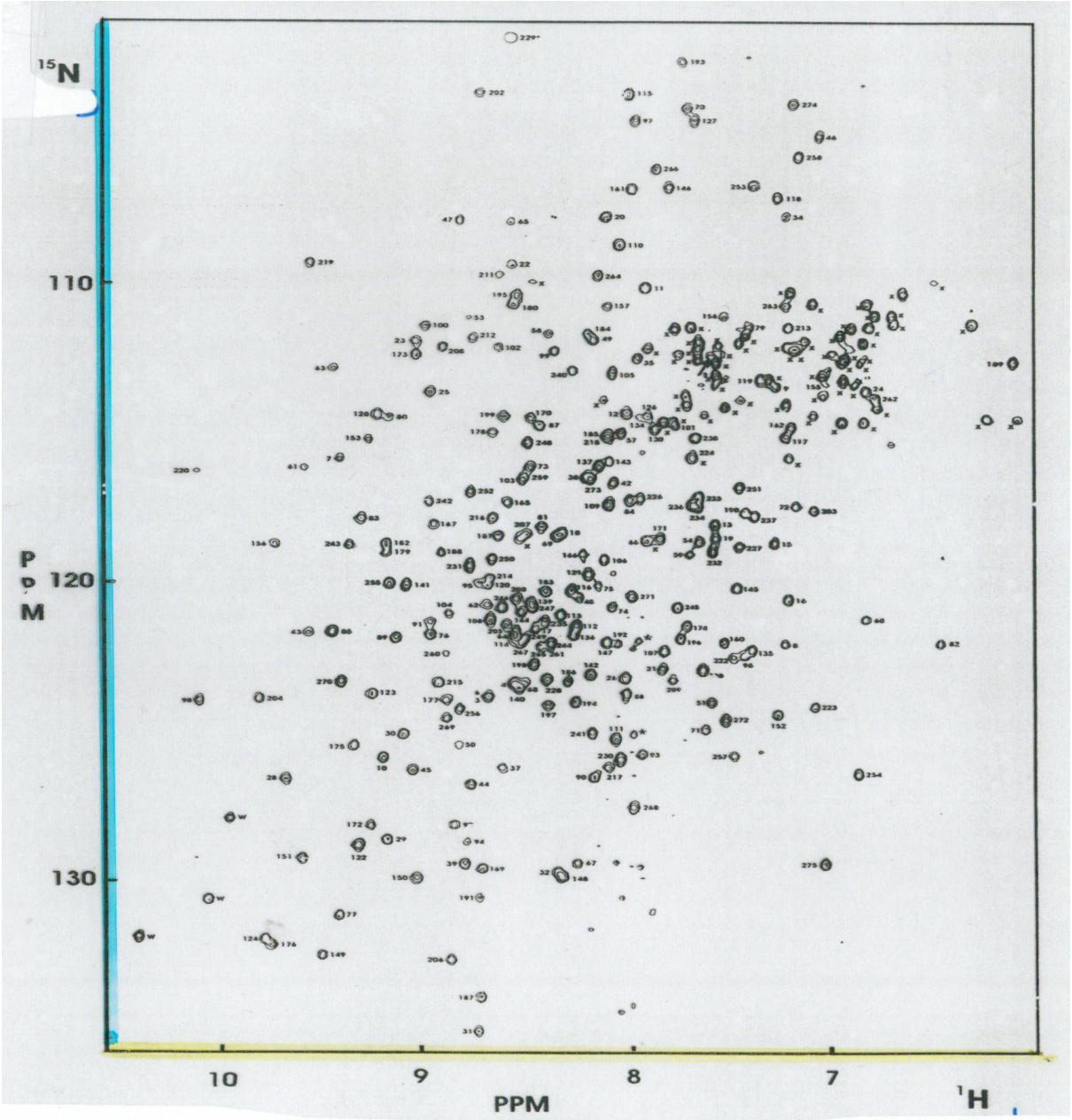

101. HCCH EXPERIMENTS FOR ASSIGNING SIDE CHAINS

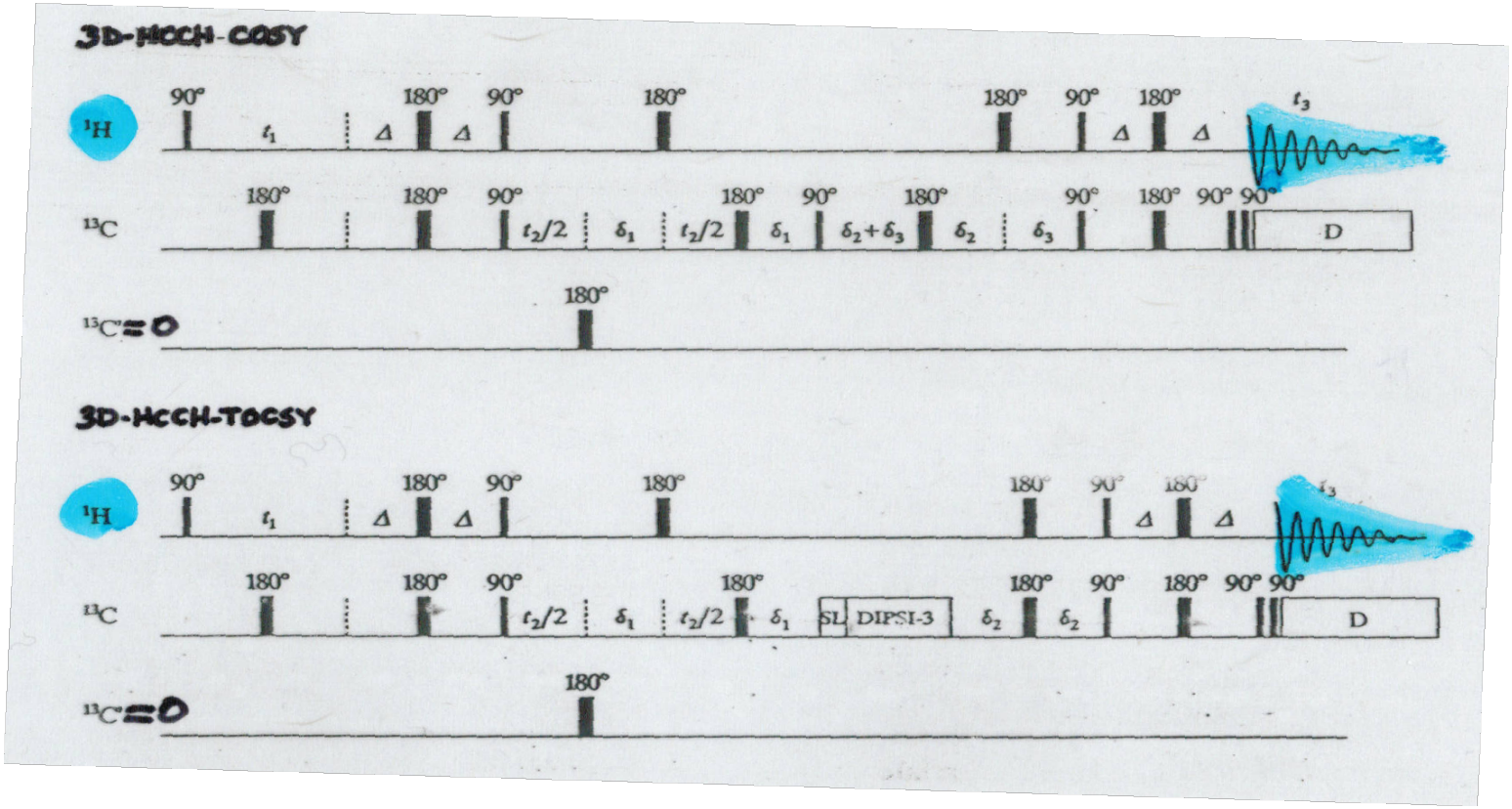

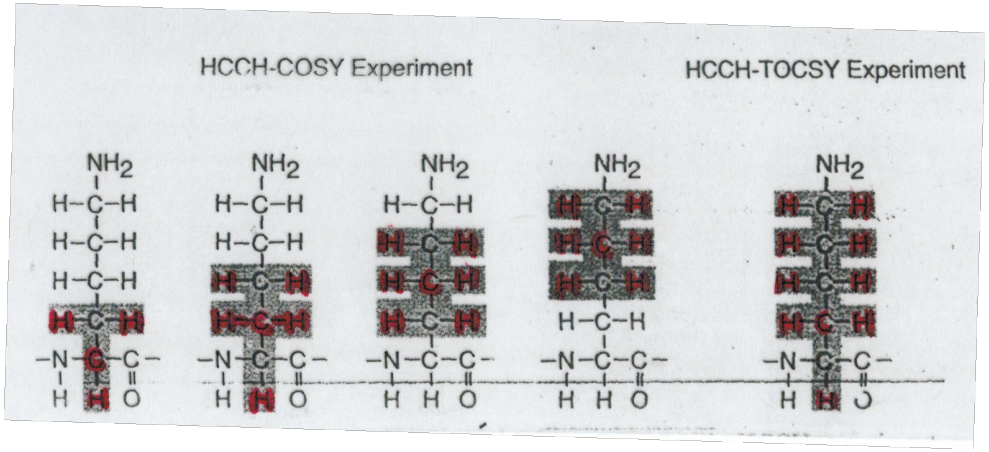

102. TROSY EXPRERIMENT

Pervushin et al. Proc. Natl. Acad. Sci USA 94, 12366, 1997

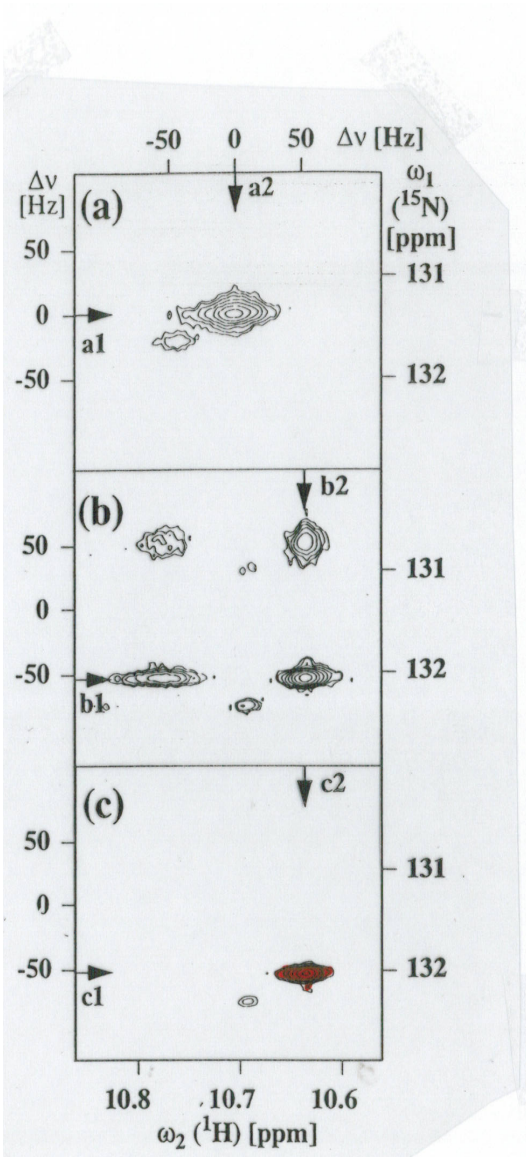

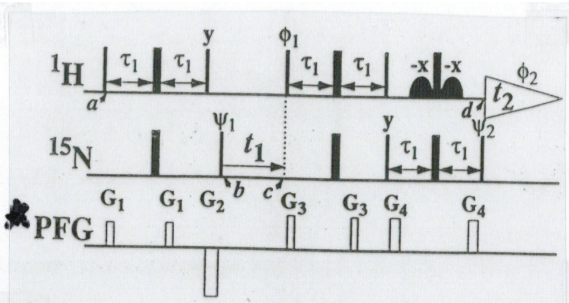

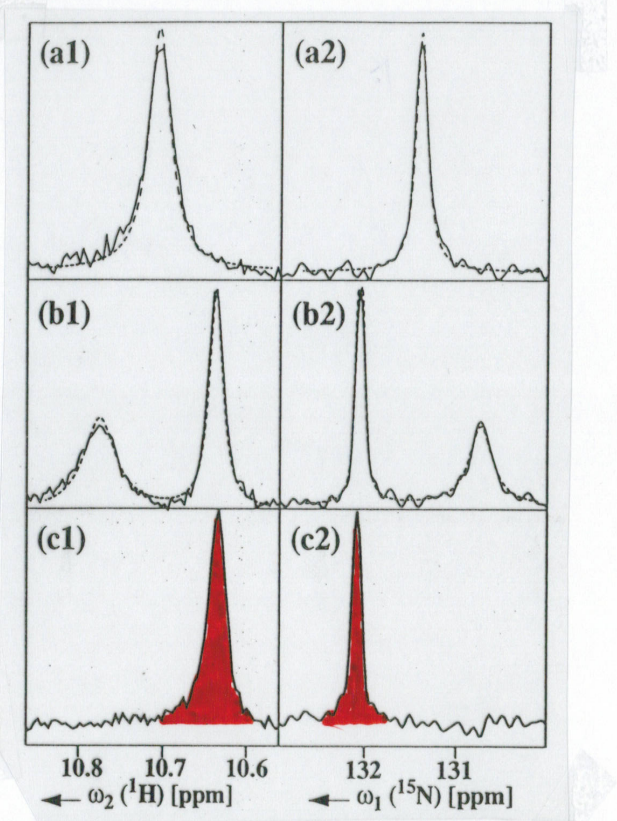

* Pulse Field Gradient

103. MUTUAL CANCELLATION OF DD AND CSA IN TROSY

RELAXATION RATES FOR $1 \leftrightarrow 2$ i $3 \leftrightarrow 4$ OF S'

$$R_{1212} = (p-\delta_S)^2[J(0)+3J(\omega_S)]+p^2[J(\omega_I-\omega_S)+3J(\omega_I)+6J(\omega_I+\omega_S)]+ + 3\delta_I^2 J(\omega_I)$$

$$R_{3434} = (p+\delta_S)^2[J(0)+3J(\omega_S)]+p^2[J(\omega_I-\omega_S)+3J(\omega_I)+6J(\omega_I+\omega_S)]+ + 3\delta_I^2 J(\omega_I)$$

RELAXATION RATES R_{1313} AND R_{2424} OF I FOR $1 \leftrightarrow 3$ i $2 \leftrightarrow 4$ ANALOGOUSLY AFTER CHANGES: $2 \leftrightarrow 3$ AND $I \leftrightarrow S'$

$$J(\omega) = \frac{2}{5}\cdot\frac{\tau_c}{1+\omega^2\tau_c^2} \qquad p = \frac{1}{2\sqrt{2}}\gamma_I\gamma_S\hbar r_{IS}^{-3}$$

$$\delta_S = \frac{1}{3\sqrt{2}}\gamma_S B_0 \Delta\sigma_S \qquad \delta_I = \frac{1}{3\sqrt{2}}\gamma_I B_0 \Delta\sigma_I \qquad \Delta\sigma_S \sim 160\,ppm \quad \Delta\sigma_I \sim 16\,ppm$$

$\Delta\sigma_S, \Delta\sigma_I$ -

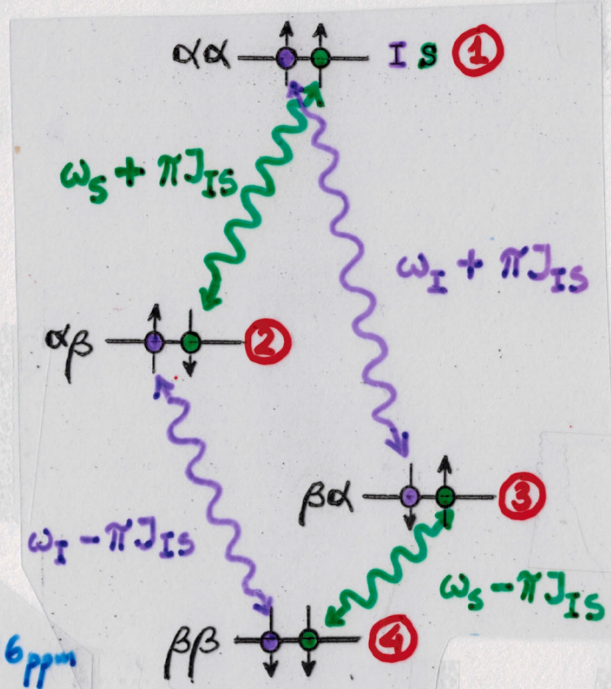

TOTAL COMPENSATION OF DD AND CSA

$p - \delta_S \cong 0$ $\quad p - \delta_I \cong 0$

FOR $^{15}N - ^1H$ AT 1100 MHz

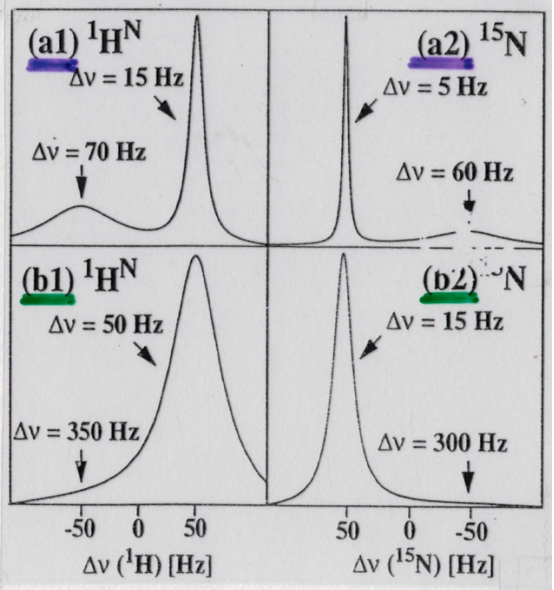

104. NUCLEAR OVERHAUSER EFECT (NOE)

$$\frac{d\bar{M}}{dt} = \hat{R}\bar{M} \qquad \bar{M} = (M_1, M_2, \ldots, M_g) \qquad M_k = M_z^k - \frac{n_k}{N} M_0$$

$$N = \sum_{k=1}^{g} n_k \qquad M_0 - \text{equilibrium magnetization}$$

relaxation matrix: $\hat{R} = [R_{ij}]_{i,j=1,2,\ldots,g}$

$$R_{ii} = \frac{2}{10}\gamma_H^4 \hbar^2 (n_i - 1)\tau_c r_{ii}^{-6}\left[\frac{1.5}{1+\omega_H^2\tau_c^2} + \frac{6}{1+4\omega_H^2\tau_c^2}\right] +$$

$$\frac{1}{10}\gamma_H^4 \hbar^2 \tau_c \sum_{j\neq i} n_j r_{ij}^{-6}\left[1 + \frac{3}{1+\omega_H^2\tau_c^2} + \frac{6}{1+4\omega_H^2\tau_c^2}\right] + R_i^{\text{NO-DD}}$$

$$R_{ij} = \frac{1}{10}\gamma_H^4 \hbar^2 n_i \tau_c r_{ij}^{-6}\left[\frac{6}{1+4\omega_H^2\tau_c^2} - 1\right]$$

SOLUTION:

$$\bar{M}(t_m) = \hat{a}(t_m)\bar{M}(0) = e^{-\hat{R}t_m}\bar{M}(0)$$

$$\bar{M}(0) = \frac{M_0}{N}(n_1, n_2, \ldots, n_g)$$

Intensities of cross-peaks NOESY:

$$a_{ij} = \left(\hat{\chi}^{-1}\begin{bmatrix} e^{-\Lambda_1 t_m} & & \\ & e^{-\Lambda_2 t_m} & \\ & & \ddots \end{bmatrix}\chi\right)_{ij} \qquad \hat{\chi}^{-1} = \chi^T$$

$\hat{\chi}$ - matrix of eigenvectors $\hat{R}$: $\hat{R} = \chi\hat{\Lambda}\chi^T$

$\hat{\Lambda}$ - matrix of eigenvalues $\hat{R}$: $\hat{\Lambda} = [\Lambda_{ij}]$

$$\Lambda_{ij} = \Lambda_i \delta_{ij}$$

$$\hat{R} = -\frac{1}{t_m}\ln\left[\frac{\hat{a}(t_m)}{\hat{a}(0)}\right] = -\frac{1}{t_m}\hat{\chi}(\ln\hat{\lambda})\hat{\chi}^T$$

$\hat{\lambda}$ - matrix of $\hat{a}$ eigenvalues (scaled)

t_m - mixing time
ω_H - proton resonance frequency
γ_H - proton magnetogiric ratio
$\hbar$ - Planck constant
τ_c - correlation time (rotational diffusion of a rigid sphere)
r_{ij} - interproton distance

105. SPIN DIFFUSION IN NOE (BPTI PROTEIN)

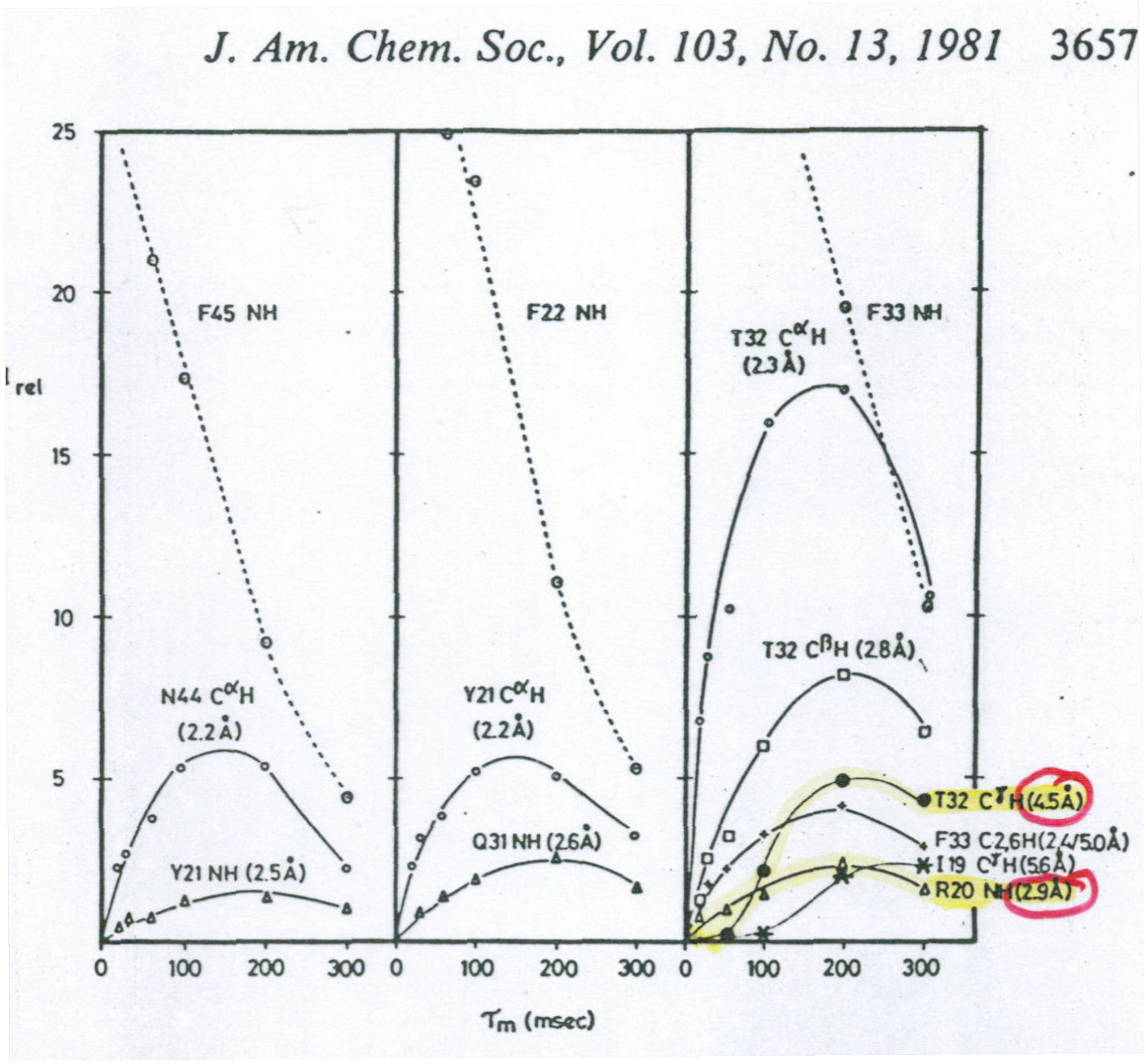

106. RESIDUAL DIPOLAR COUPLING (RDC)

RESIDUAL DIPOLAR COUPLING

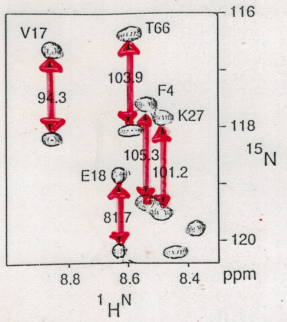

Fig. 3. Small region of the ^{15}N-^{1}H^N HSQC spectrum of human ubiquitin (pH 6.8, 38 °C, 0.3 mM, 5% w/v lipid), recorded without ^{1}H decoupling in the t_1 dimension. The $^1J_{NH} + {}^1D_{NH}$ splittings (Hz) are indicated.

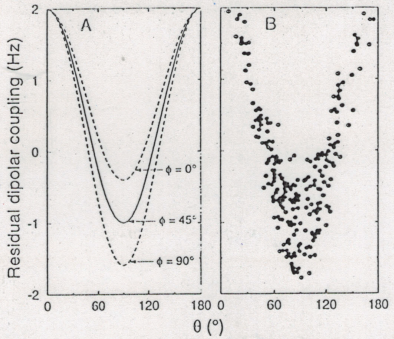



FIG. 1. Effect of the rhombicity R of the magnetic susceptibility tensor on residual dipolar couplings. (A) Theoretical dependence on the angles θ and ϕ. The solid line corresponds to the fully symmetric case and the dashed lines correspond to the fully asymmetric case for a value of 1 Hz for D_a and a rhombicity ($R = D_r/D_a$) of 0.4. (B) Distribution of the residual ^{1}H–^{15}N dipolar couplings as a function of the angle θ calculated for the N-terminal domain of Enzyme I (259 residues) with a random error of ±0.1 Hz, and values of 1 Hz and 0.4 for D_a and R, respectively. (C) Ribbon diagram of the N-terminal domain of Enzyme I (*19*) together with the coordinate frame of the magnetic susceptibility tensor employed to calculate the ^{1}H–^{15}N residual dipolar couplings in (B). The random error of ±0.1 Hz in the model dipolar couplings was chosen to represent typical experimental error in the residual dipolar couplings extracted from a series of J-modulated ^{1}H–^{15}N HSQC spectra (*15, 16*).

$$D_{ij}(\theta,\phi) = D_a^{ij}\{(3\cos^2\theta - 1) + \tfrac{3}{2}R(\sin^2\theta\cos 2\phi)\}$$

$$R = D_r^{ij}/D_a^{ij}$$

$$D_a^{ij} = \tfrac{1}{3}[D_{zz}^{ij} - (D_{xx}^{ij} + D_{yy}^{ij})/2]$$

$$D_r^{ij} = \tfrac{1}{3}[D_{xx}^{ij} - D_{yy}^{ij}]$$

$$|D_{zz}^{ij}| > |D_{yy}^{ij}| \geq |D_{xx}^{ij}|$$

$$D_a^{ij} = -\frac{\mu_0 h}{16\pi^3} S\gamma_i\gamma_j\langle r_{ij}^{-3}\rangle A_a^{ij}$$

$\hat{A}$ - molecular alignment tensor

S - order parameter

~3% DMPC/DHPC = 1:3 in H_2O

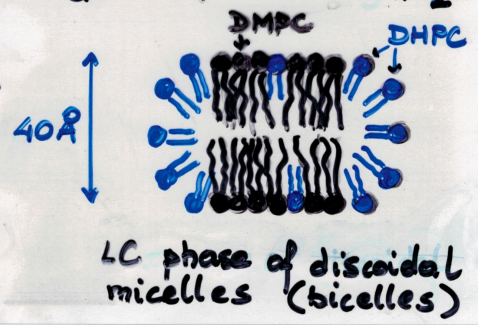

LC phase of discoidal micelles (bicelles)

107. SYSTEMS FOR NMR OF MEMBRANE PROTEINS

Raschle et al. Curr. Op. Struct. Biol. 20, 471, 2010

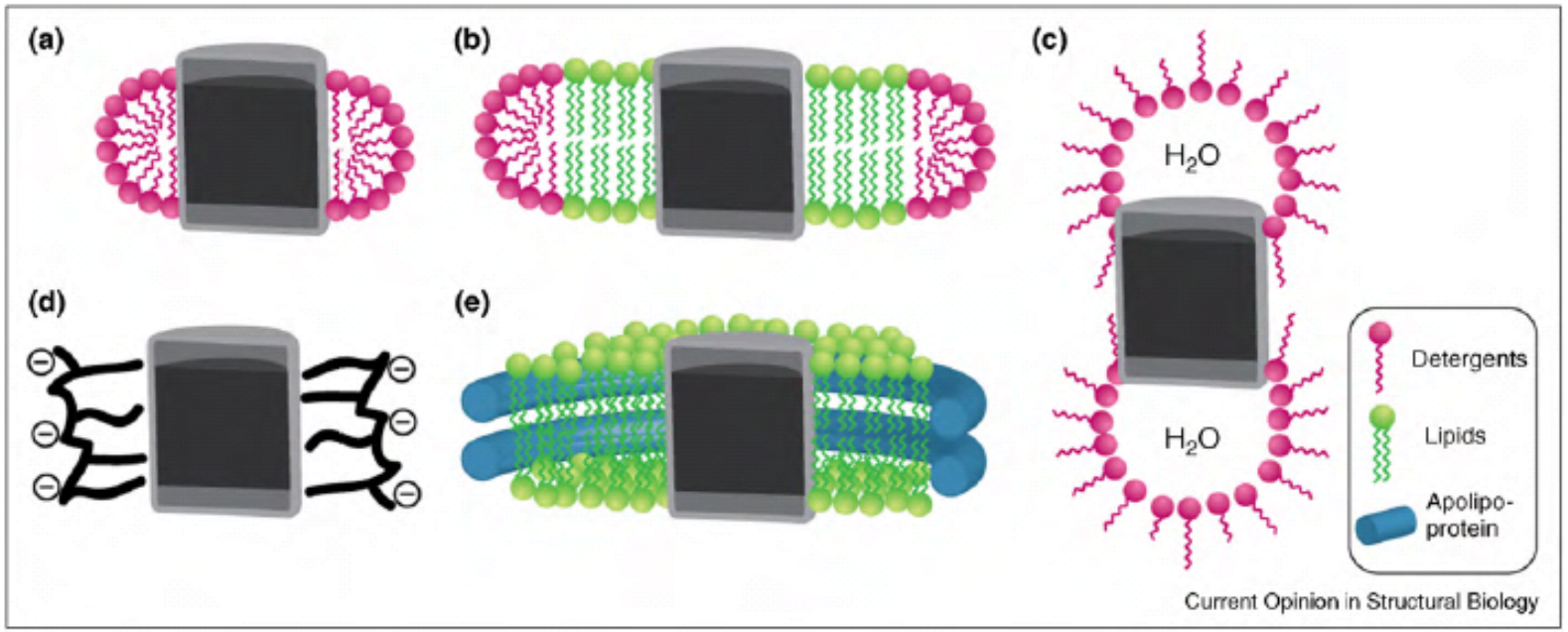

Schematic representation of different solubilization methods for integral membrane proteins. Micelle (a), bicelle (b), reverse micelle (c), amphipol (d), and nanolipoprotein particles (NLP; e). Shown are cartoons depicting each solubilization system. The membrane protein is depicted in gray, with its

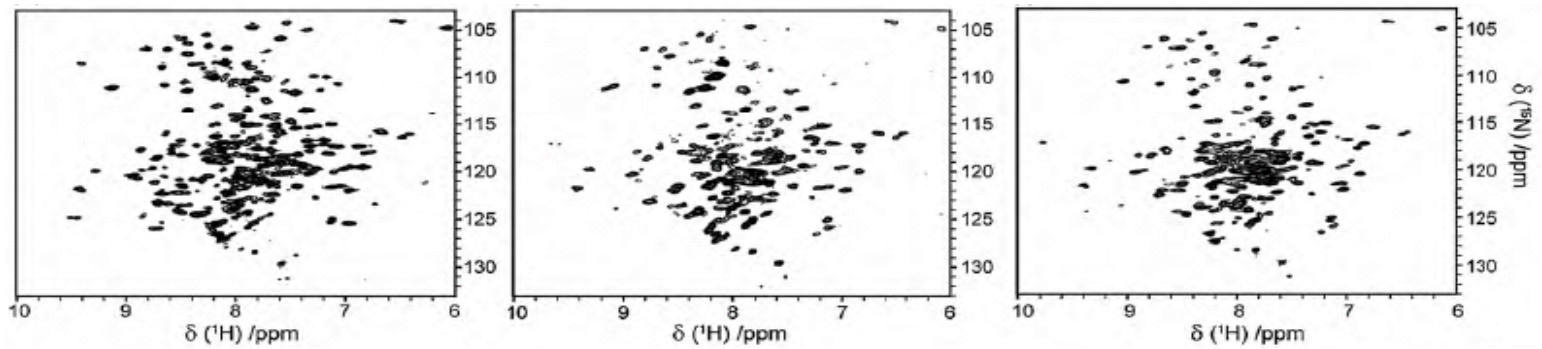

^{15}N,^{1}H-TROSY of bacteriorodopsin in: micelles, NPL, and amphipols

108. SOLID STATE NMR (SSNMR)

Judge & Watts Curr. Op. Chem. Biol. 15, 690, 2011

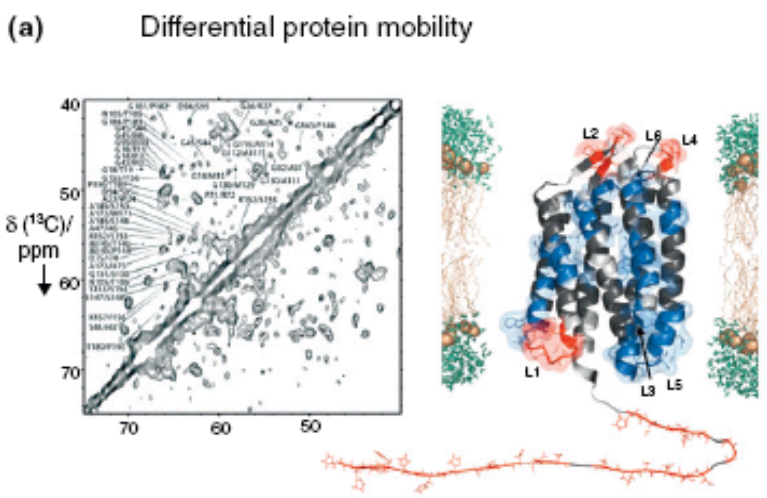

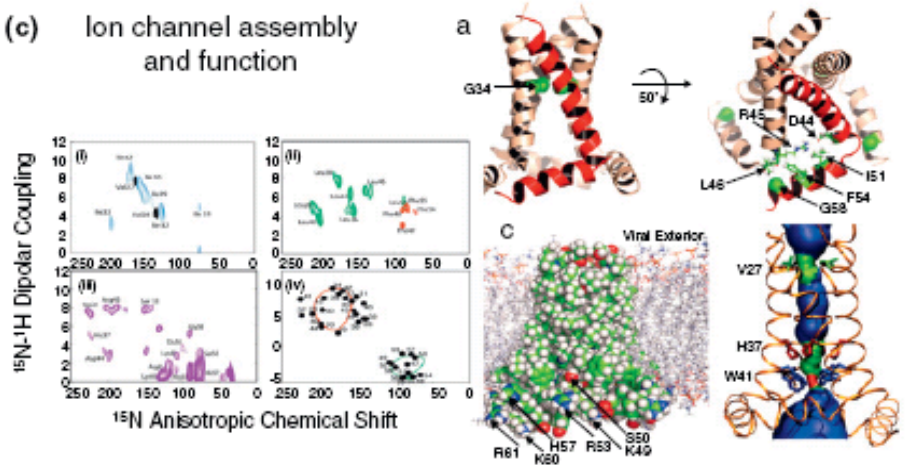

Solid state and wide line NMR for structural and functional studies of membrane-embedded proteins

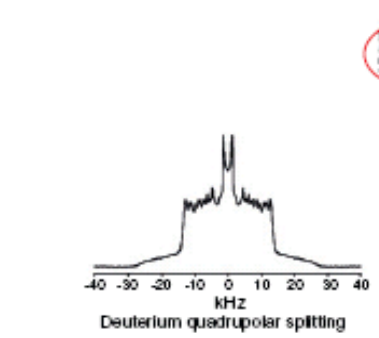

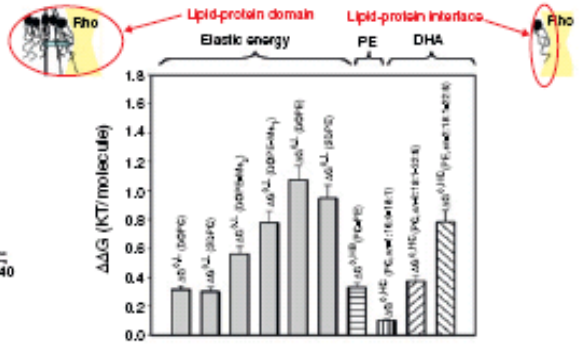

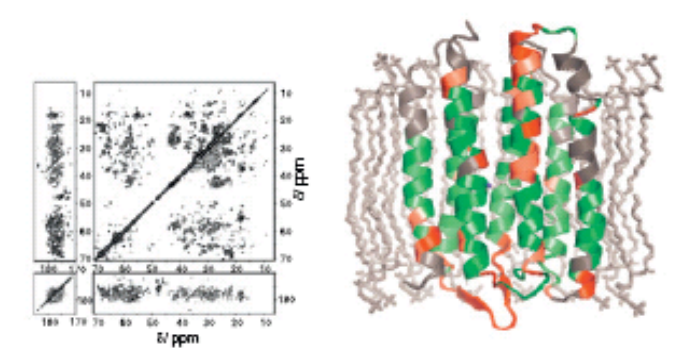

109. MAGIC ANGLE SPINNING (MAS)

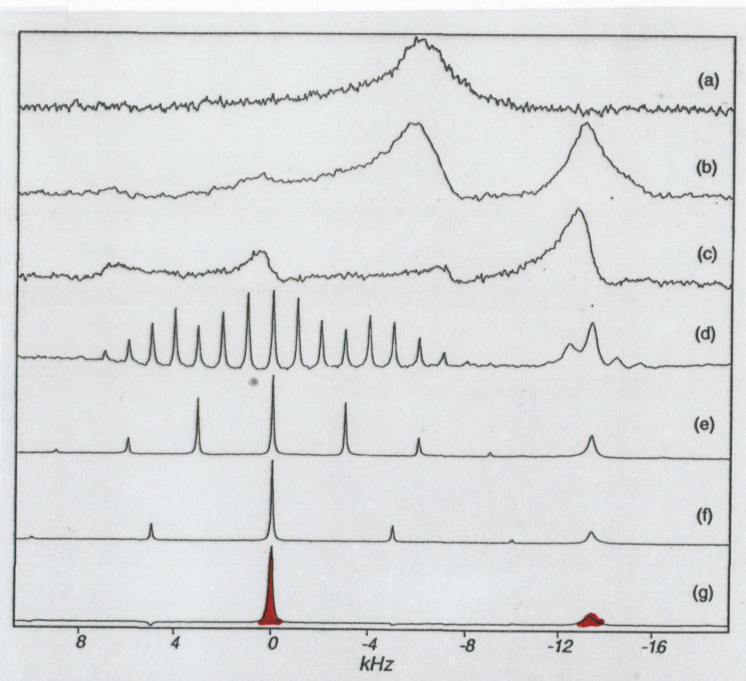

Fig. 1.40 ^{13}C NMR spectra of crystalline glycine: (a) without proton decoupling; (b) with proton decoupling; (c) with proton decoupling and cross-polarization; (d) CPMAS ($\nu_R = 1$ kHz); (e) CPMAS ($\nu_R = 3$ kHz); (f) CPMAS ($\nu_R = 5$ kHz); (g) CPMAS ($\nu_R = 5$ kHz) plus sideband suppression (TOSS).

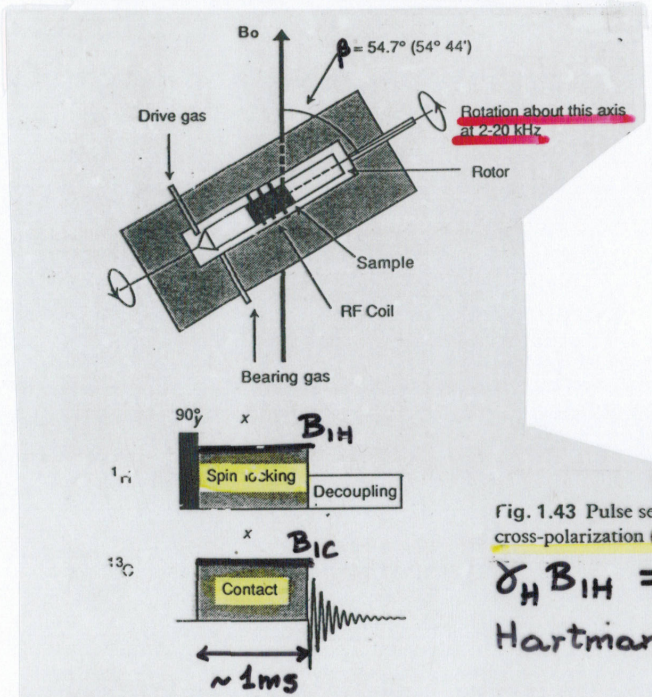

Fig. 1.43 Pulse sequence for cross-polarization (CP).

$\gamma_H B_{1H} = \gamma_C B_{1C}$

Hartmann - Hahn condition

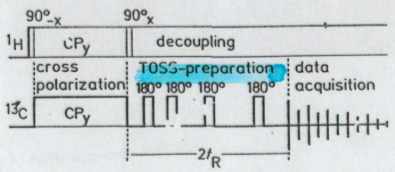

Fig. 3. Excitation scheme for TOSS and cross polarization. By means of cross polarization, transverse magnetization is transferred from the protons to the ^{13}C nuclei (see Figure 4 and caption). In order to prevent cross-polarization effects during the TOSS pulses, the transverse proton magnetization is rotated back to the z-direction by a 90° pulse at the beginning of the TOSS preparation period [47].

110. ASSIGNMENT BY NCOCA; KcsA FRAGMENT

McDermott Annu. Rev. Biophys. 38, 385, 2009

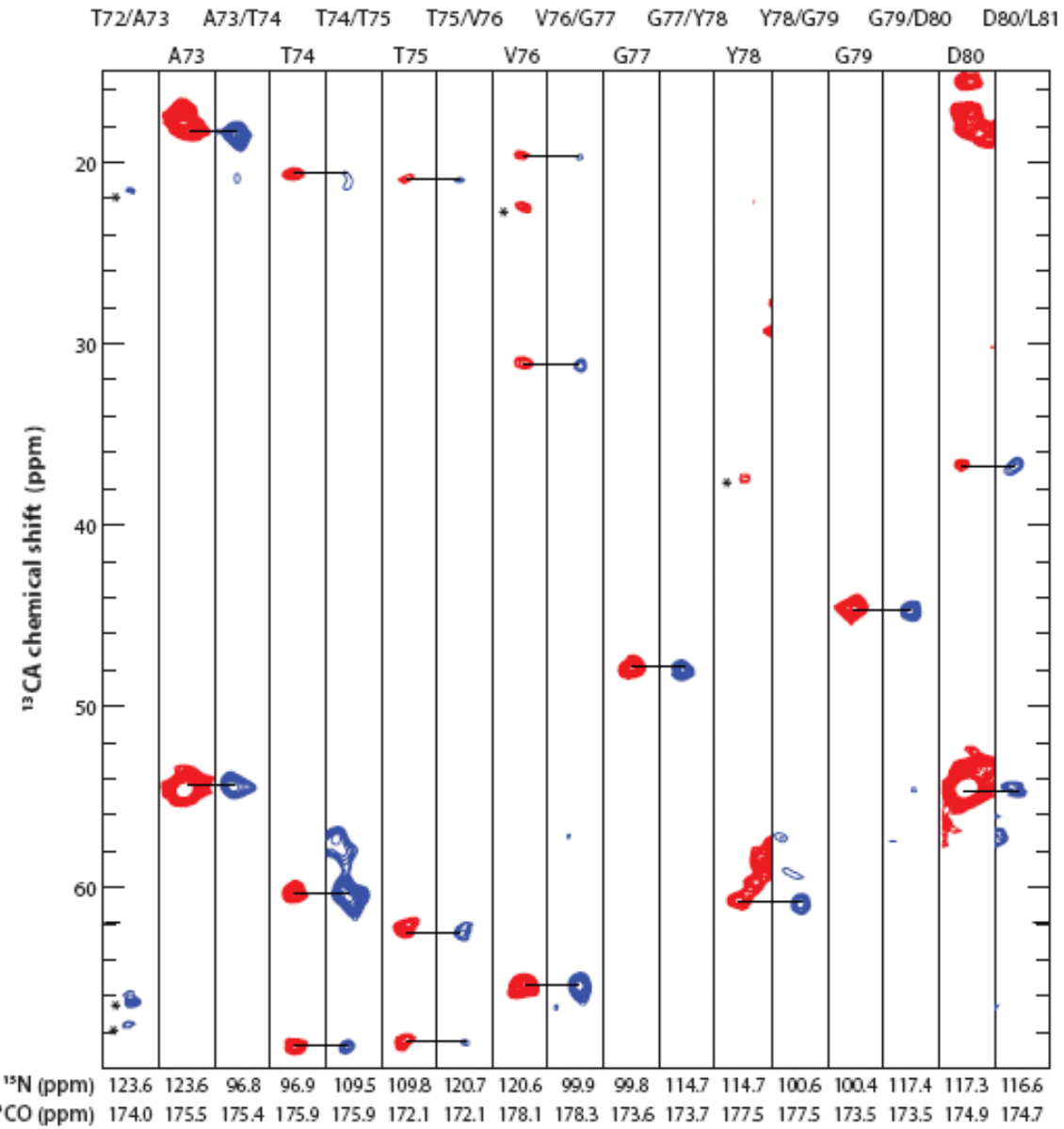

111. MAS SSNMR DEUTERATED BACTERIORODOPSYN

Reif J. Magn. Reson. 216, 1, 2012

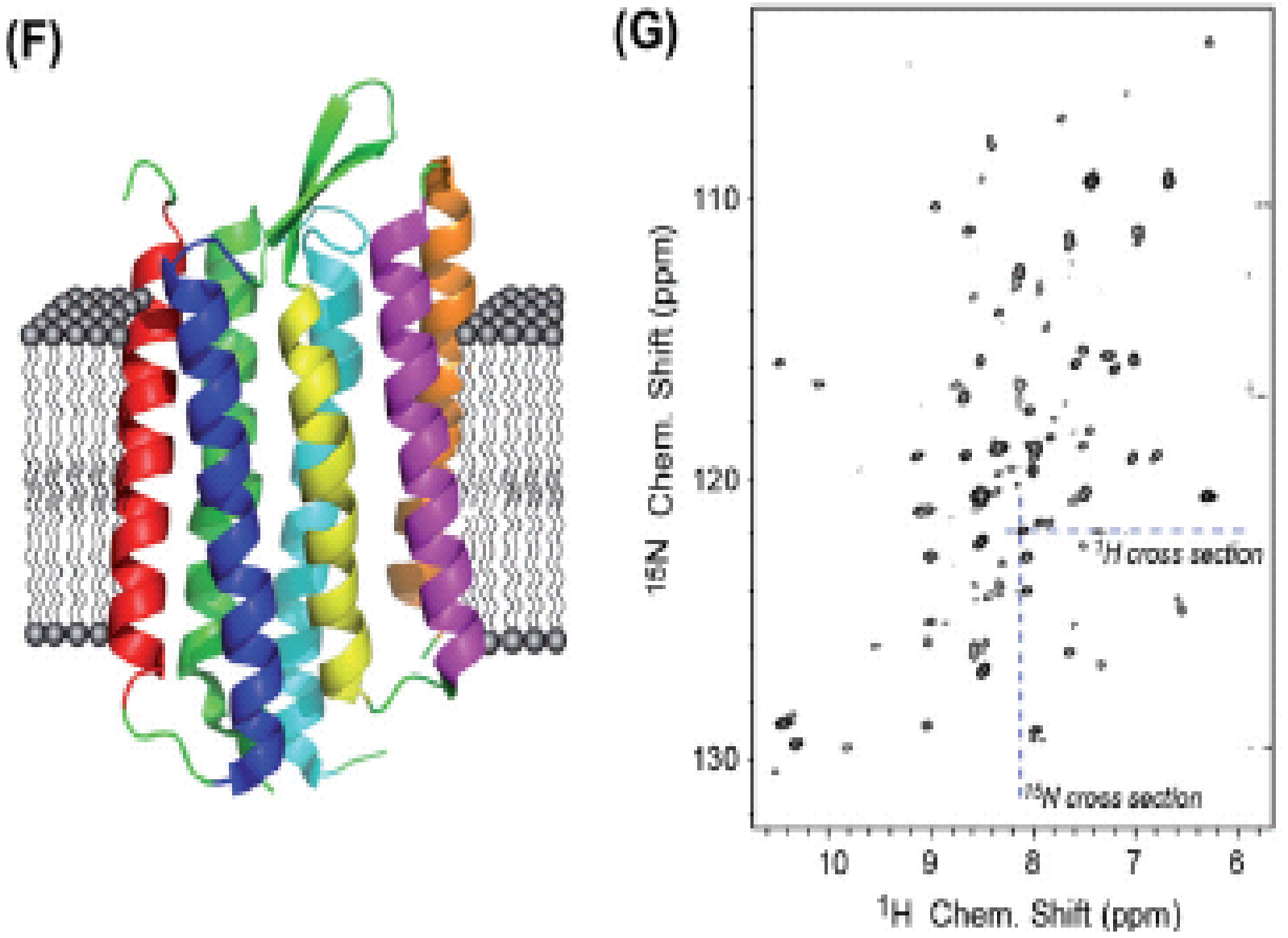

112. MODEL-FREE APPROACH IN PROTEIN DYNAMICS

TEORETICAL ASPECTS

$$G(\tau) = G_0(\tau) G_I(\tau)$$

$$J(\omega) = \int G(\tau) \exp(-i\omega\tau)\, d\tau$$

$$J(\omega) = \sum_{k=1}^{3} A_k(\alpha)\, J_{MFA}(S, \tau_k, \tau_{i,k}; \omega)$$

$$A_1 = 0{,}75 \sin^4\alpha$$

$$A_2 = 3(\sin^2\alpha)(\cos^2\alpha)$$

$$A_3 = 0{,}25(3\cos^2\alpha - 1)$$

$$\tau_1 = 1/(4D_{\parallel} + 2D_{\perp})$$

$$\tau_2 = 1/(D_{\parallel} + 5D_{\perp})$$

$$\tau_3 = 1/(6D_{\perp})$$

$$\tau_{i,k}^{-1} = \tau_k^{-1} + \tau_{int}^{-1}$$

$$J(\omega) = \frac{2}{5}\left[\frac{S^2\tau_R}{1+(\omega\tau_R)^2} + \frac{(1-S^2)\tau}{1+(\omega\tau)^2}\right]$$

$$\tau^{-1} = \tau_R^{-1} + \tau_{int}^{-1}$$

MEASUREMENTS

$$R_1 = \frac{1}{4} D^2 [J(\omega_H - \omega_N) + 3J(\omega_N) + 6J(\omega_H + \omega_N)] + \frac{1}{3} C^2 J(\omega_N)$$

$$R_2 = \frac{1}{8} D^2 [4J(0) + J(\omega_H - \omega_N) + 3J(\omega_N) + 6J(\omega_H) + 6(\omega_H + \omega_N)] + \frac{1}{18} C^2 [4J(0) + 3J(\omega_N)] + R_{ex}$$

$$NOE = 1 + \left(\frac{\gamma_H}{\gamma_N}\right) \frac{D^2}{4R_1} [6J(\omega_H + \omega_N) - J(\omega_H - \omega_N)]$$

$$D = \frac{\mu_0}{4\pi} \gamma_N \gamma_H \hbar \langle r_{NH}^3 \rangle^{-1}$$

$$C = \omega_N \Delta\sigma \qquad \Delta\sigma = -170 \text{ ppm}$$

$$r_{NH} = 1{,}04 \text{ Å}$$

$$R_{ex} = \Phi\, \omega_N^2$$

$S^2 = 1$ restricted internal motion (rigid molecule)

$S^2 = 0$ free internal motion

113. NANOSECOND DYNAMICS OF *E. Coli* Yfia

Zukov et al. Acta Biochim. Polon. 54, 769, 2007

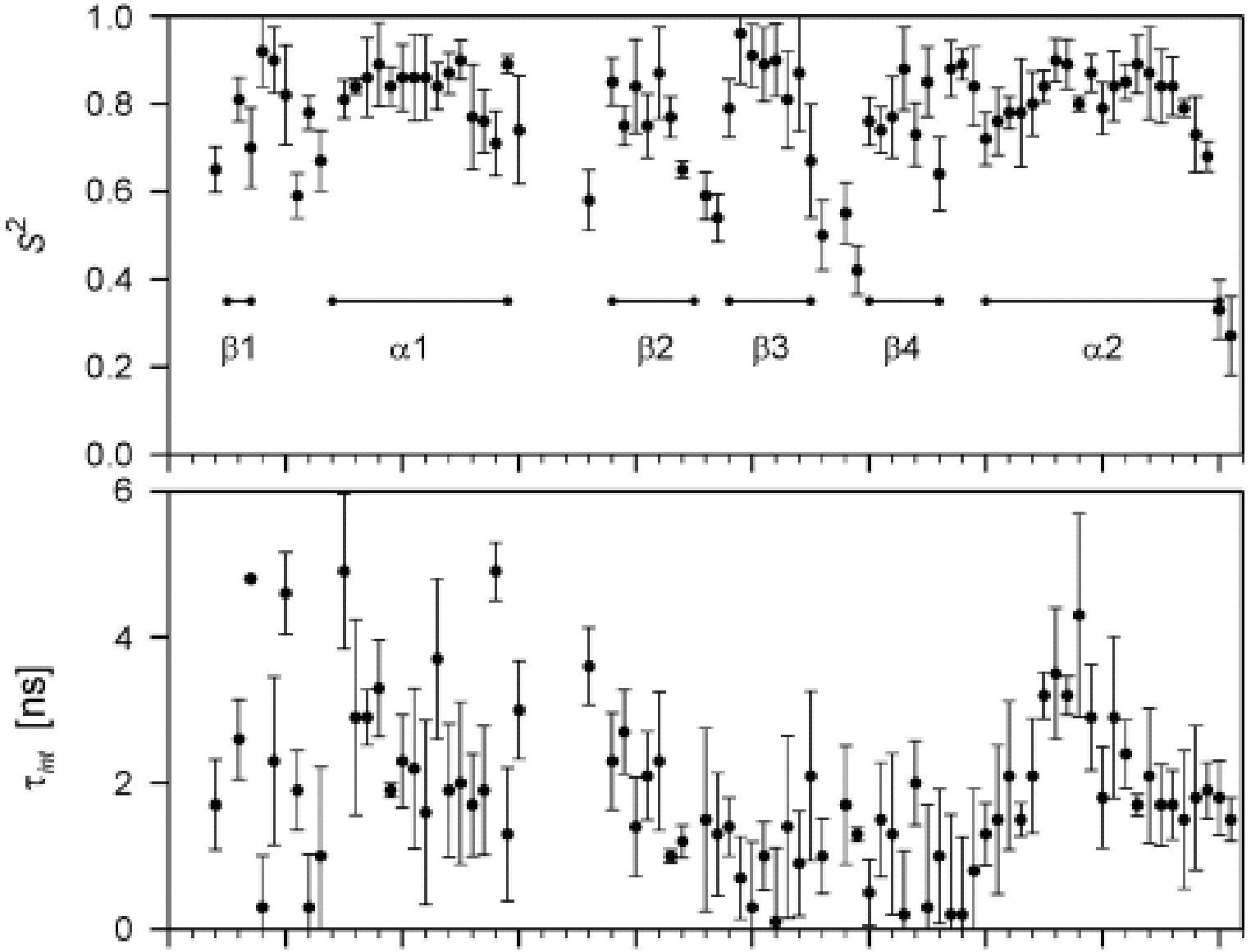

114. EWALD CONSTRUCTIONS

MONOCHROMATIC METHOD

LAUE METHOD

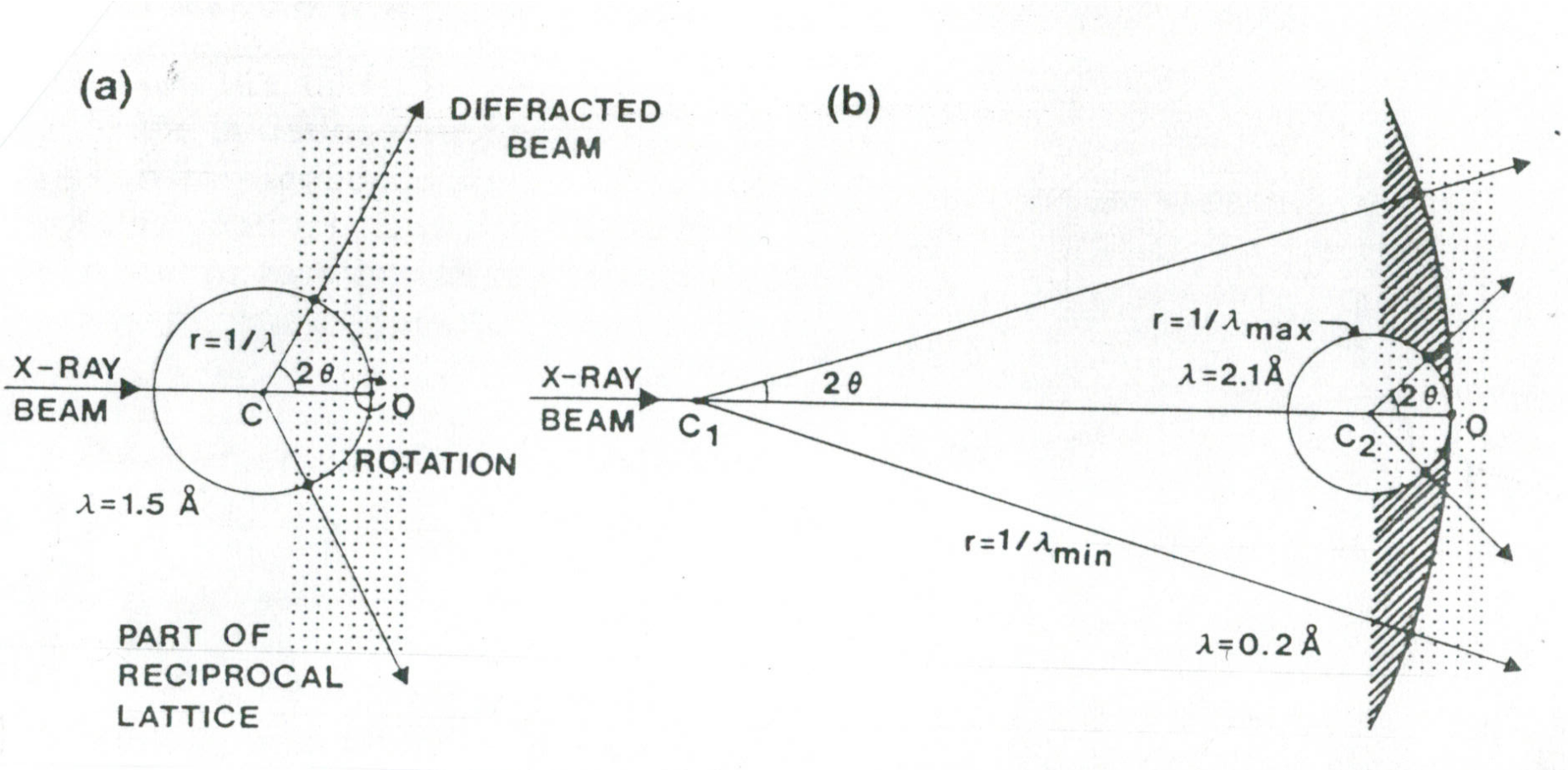

115.LAUE DIFFRACTION OF ISOCITRATE DEHYDROGENASE

Bolduc et al. Science 268. 1312. 1995

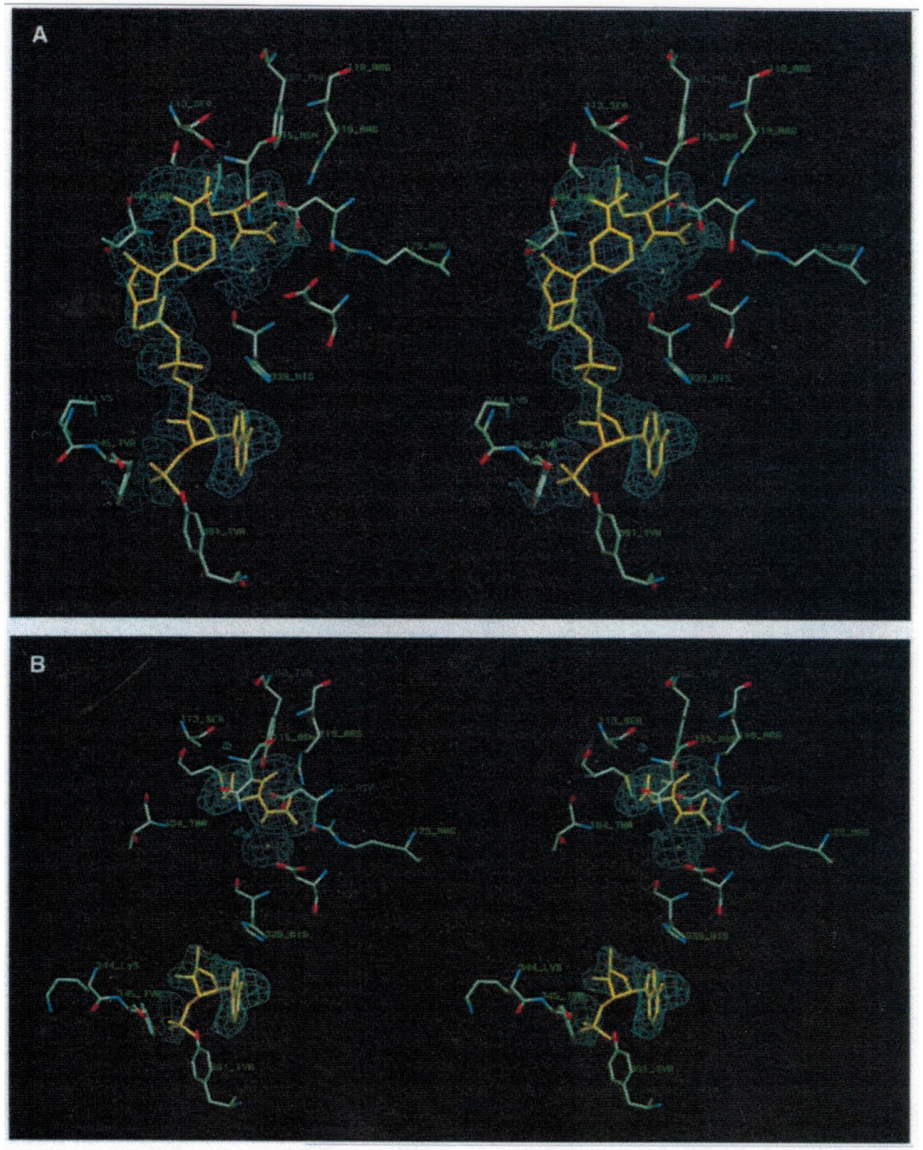

Fig. 1. Crystallographic structure of the rate-limited substrate-enzyme complexes for isocitrate dehydrogenase [(**A**) Y160F; and (**B**) K230M] at 2.5 Å resolution. These two difference maps indicate rate-limited complexes that correspond to species 4 and 5, respectively, in Eq. 1. Experimental difference maps of the active sites of both kinetic mutants were calculated with Fourier coefficients [F_o (60 seconds after substrate) − F_o (before substrate presentation)] α_{calc}.